ISSN: 1847-9286
Open Access Journal
www.jese-online.org

JESE

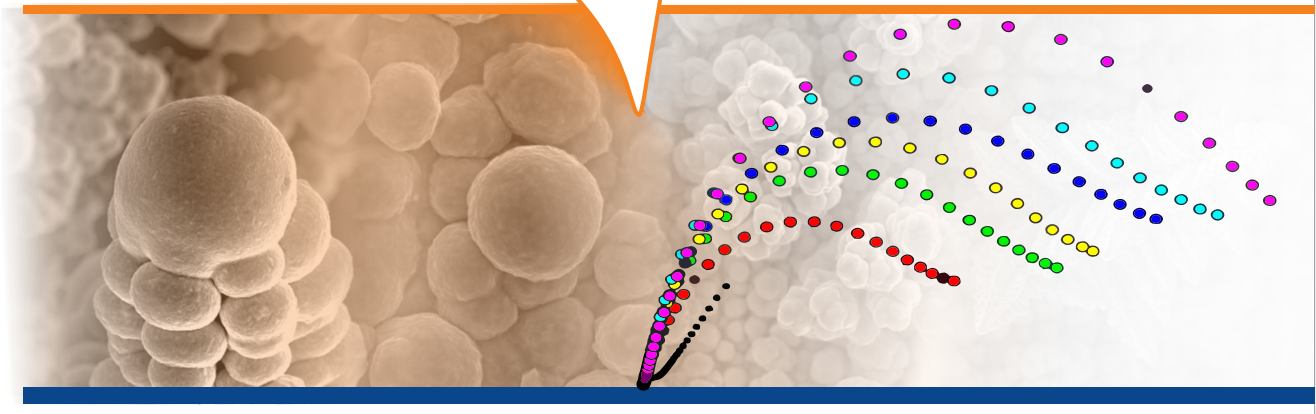

Journal of Electrochemical Science and Engineering

J. Electrochem. Sci. Eng. **1**(**1**) 2011, 1-73

IAPC Publishing

J. Electrochem. Sci. Eng. **1(1)** (2011) 1-26; doi: **10.5599/jese.2011.0003**

Open Access : : ISSN 1847-9286
www.jESE-online.org

Review

On the stability of perchlorate ions against reductive attacks in electrochemical systems and in the environment

MÁRIA UJVÁRI✉ and GYŐZŐ G. LÁNG

Eötvös Loránd University, Institute of Chemistry, Department of Physical Chemistry, Laboratory of Electrochemistry and Electroanalytical Chemistry, PO Box 32, Budapest 112, H-1518, Hungary

✉marcsi@chem.elte.hu

Received: June 16, 2011; Published: August 20, 2011

Abstract

The problems related to the electrochemical/electrocatalytic stability of perchlorate ions are reviewed in the light of recent experimental results. The electrocatalytic, catalytic, and electrochemical reduction processes are presented and the links between them are outlined. Some possible mechanisms of the complicated reduction processes are discussed. Various methods for the detection of reduction process are presented, e.g. voltammetry, impedance spectroscopy, and radiotracer methods. Environmental aspects and some methods for perchlorate removal and wastewater treatment are briefly summarized.

Keywords

Perchlorate ions; Environmental contamination; Waste water treatment; Electrocatalytic reduction; Reduction mechanism; Noble metals; Corrosion

1. Introduction

Based on the thermodynamic data presented in Table 1, ClO_4^- should be instable against reductive attacks in acidic medium in a wide potential range. In contrast, in the electrochemical literature ClO_4^- are often considered to be very stable anions.

Therefore, perchlorate containing solutions are widely used as supporting electrolytes in electrochemical studies with various electrodes. Among these investigations reports concerning dissolution, deposition, and corrosion of metals can also be found.

In such studies, it is tacitly assumed that the reduction of the ClO_4^- is not taking place under the actual experimental conditions. However, evidence for the occurrence of the reduction process has been reported for Rh [1-5], Pt [6-9], WC [10], Al [11], Ti [12], Ir [13], Ru [14], Re [15], Tc [16],

and Sn [17] electrodes. A survey of the literature can be found in recent reviews [18-21]. These observations prompt us to keep in mind the possibility of the occurrence of the reduction process at any electrode used in an aqueous acid medium containing perchlorate ions.

Table 1. *Standard potential values of reaction steps potentially involved in the reduction of* ClO_4^- ***

Reaction	E^o / V
$ClO_2 + e = ClO_2^-$	0.93
$ClO_3^- + 2H^+ + e = ClO_2 + H_2O$	1.15
$ClO_4^- + 2H^+ + 2e = ClO_3^- + H_2O$	1.19
$ClO_2 + H^+ + e = HClO_2$	1.27
$HClO + H^+ + 2e = Cl^- + H_2O$	1.50
$HClO_2 + 2H^+ + 2e = HClO + H_2O$	1.64

* Selected constants. Charlot, G.; Collumeau, A.; Marchon, M.J.C. Oxidation-Reduction Potentials of Inorganic Substances in Aqueous Solution, Butterworths, London, 1971.

Besides the significance of perchlorate reduction for the fundamental electrochemistry today, a very practical reason, the so-called perchlorate contamination challenge, came into foreground directing the attention towards the reductive elimination of perchlorate ions.

Perchlorates are used as an oxidizer component and primary ingredient in solid propellants for rockets, missiles, and fireworks. Therefore, dissolved ammonium, potassium, magnesium, or sodium salts are present as contaminants in groundwater and surface waters originating from improper disposal of the solid propellants and from the wastewaters of the manufacturing plants. As the sorption or natural chemical reduction of perchlorate in the environment is not significant, perchlorates are exceedingly mobile in aqueous systems and can persist for many decades under typical ground and surface water conditions. According to different reports [22-27], a large number of water sources in the United States have been contaminated with perchlorate. However, the perchlorate problem is not located to the US only. This type of contamination constitutes a major problem in China [28-30] and many other countries in the world [31-33]. For example, in Israel, an ammonium-perchlorate manufacturing plant that had been disposing untreated wastewater in four unlined ponds for 25 years caused extensive perchlorate contamination in the underlying aquifer. The perchlorate migration in the deep vadose zone has been found very low under natural recharge conditions in the semiarid region [34].

One of the main health hazards is connected with the very fact that perchlorate interferes with iodide uptake in the thyroid gland [35,36]. In large doses, it has been linked to anemia and fetal brain damage [30,35].

Several technologies have been studied for the treatment of perchlorate contaminated water, such as chemical precipitation and reduction, bioreduction, anion exchanges, electroreduction, membrane filtration, electrodialysis, and photocatalytic reduction. Even though some of these have been adopted for drinking water treatment, the optimization of cost, selectivity, and effective treatment is still a serious problem [37-39]. The electrochemical treatment method is one of the methods [20] considered applicable for solving the perchlorate contamination [24-26]. The elaboration of a treatment technology with dissolved complexes is significantly hindered by its high cost and significant difficulties with the regeneration or treatment of their end products. Some recent results in waste water treatment are presented below.

The electrochemical and electrophotocatalytic reduction of the perchlorate ion to the chloride ion were assessed at laboratory scale [40]. The study was carried out in two-chambered batch reactor systems in which the cathodic and anodic compartments were separated by an ion exchange membrane. Electrodes consisted of titanium coated with a thin film of small TiO_2 particles. Test water systems were buffered to an acid pH and background electrolyte was added. For photolytic systems, concentrations ranged from 5×10^{-2} mol dm^{-3} to 5×10^{-7} mol dm^{-3}. Reduction initially proceeded rapidly but slowed with time. The percentage of perchlorate electrochemically reduced after 2 h was found to range from less than 1% at the highest concentration to 30-35 % at lower concentrations. The extent of photocatalytic reduction at high perchlorate concentrations was approximately five times greater than the extent of electrochemical reduction at the same concentrations. An additional fourfold improvement in reduction percentage was observed when the electrode was doped with vanadium. A mathematical model suggested that the limiting factor in perchlorate reduction was the competition among anions for active sites on the electrode surface.

An electrically controlled anion-exchange process has been proposed to remove perchlorate ions from the industrial wastewaters [41]. A nanostructured conducting copolymer poly(aniline-co-o-aminophenol) (PANOA) was electrochemically synthesized on a glassy carbon (GC) electrode and its redox and anion exchange properties for perchlorate removal were investigated by cyclic voltammetry, FTIR, and X-ray photoelectron spectroscopy (XPS). FTIR spectra demonstrated that ClO_4^- were immobilized in the copolymer film after its oxidation in a solution containing NaCl and $NaClO_4$. The result of XPS spectra showed that the copolymer films oxidized in a solution containing 0.10 mol dm^{-3} NaCl and 0.010 mol dm^{-3} $NaClO_4$ at pH 5.7 and 9.0 had ClO_4^-/Cl^- molar ratio of 0.53 and 0.31, respectively, which were significantly higher than the 0.10 ratio in the tested aqueous solution.

New, potentially green, and efficient synthetic routes for the remediation and/or re-use of perchlorate-based energetic materials have been suggested in two other studies [42,43]. Four simple organic imidazolium- and phosphonium-based perchlorate salts/ionic liquids have been synthesized by simple, inexpensive, and nonhazardous methods, using ammonium perchlorate as the perchlorate source. By appropriate choice of the cation, perchlorate can be incorporated into an ionic liquid, which serves as its own electrolyte for the electrochemical reduction of the perchlorate anion. The electrochemical degradation of the hazardous perchlorate ion and its conversion to harmless chloride during electrolysis was studied using IR and Cl-35 NMR spectroscopies.

Bioelectrochemical systems (BESs) including microbial fuel cells (MFCs) and microbial electrolysis cells (MECs) integrate three important wastewater treatment options, namely, biological treatment, electrolytic dissolution, and electrochemical oxidation/reduction and are regarded as new sustainable and effective strategies for wastewater processing. An up-to-date review is provided on recent research and development in BESs-based recalcitrant wastes treatment [44]. Recently, the reduction of perchlorate in the cathode compartment of a BES has been described [45]. The authors were able to isolate one of the organisms (Dechlorospirillum strain VDY) responsible for the perchlorate reduction. At a potential of -500 mV *vs*. Ag/AgCl reference electrode, the organism was capable of reducing perchlorate without the addition of a redox mediator. The results of these studies demonstrate that biological perchlorate remediation can be facilitated through the use of an electrode as the primary electron donor, and that continuous treatment in such a system approaches current industry standards. An MFC with a

denitrifying biocathode for perchlorate reduction has been investigated to identify putative biocathode-utilizing perchlorate-reducing bacteria (PCRB), which can utilize a cathode as an electron donor, and this process can be harnessed to treat perchlorate while producing usable electrical power [46].

Perchlorate reduction has been observed with certain transition metal complexes and metal chelates, but the reactions are generally sluggish. A swift-oxo transfer reaction of perchlorate by rhenium oxazalin and thiazoline complexes has been reported quite recently [47,48]. The characteristic features of the new family of these molecular oxotransferases are their rapid kinetics and their ability in catalysing the very difficult reduction of perchlorate by atom transfer.

New (Re-Pd) bimetallic heterogeneous catalysts [49,50] for the reduction of perchlorate in water with dihydrogen have been prepared in two ways: (1) by impregnating 5 wt % Pd on activated carbon powder with one of the complexes trans-[ReO_2(py-X)(4)](+) (py-X = 4-substituted pyridine; X = H, Me, OMe, NMe_2) or (2) by adsorbing perrhenate onto the Pd/C powder in the presence of the pyridine ligand under a hydrogen atmosphere. Both sets of catalysts are highly active at pH 2.7-3.0 (HCl), with observed rates increasing with varying X in the order H < Me < OMe < NMe_2, which supports a rate-determining oxygen atom transfer reaction involving the Re(V) centers [51].

Granular activated carbon (GAC) coated with iron compounds (ICs) [52] or cetyltrimethyl ammonium bromide (CTAB) [53] were synthesized to remove perchlorate from water via adsorption. Laboratory-scale batch experiments were performed to study the factors affecting the perchlorate adsorption. In case of ICs/GAC, 97 % of the perchlorate ions were removed within 10 h at 90 °C. The experimental results also showed that $FeOHSO_4$ and Fe_2O_3 nanoparticles have the function of perchlorate adsorption and play important roles in ClO_4^- removal. In case of CTAB/GAC, the optimal adsorption occurred at pH 2-3, and the mechanisms were associated with surface complexation, electrostatic interaction, and ion exchange.

Studies in heterogeneous reaction of dissolved perchlorate ions with metals open a new possible pathway for new approaches in the technology. In recent years, the possible application of iron has been investigated [54], including the rate and extent of perchlorate reduction on several types of iron metal in batch and column reactors. Mass balances performed on the batch experiments indicate that perchlorate is initially sorbed to the iron surface, which is followed by a reduction to chloride. Perchlorate removal was proportional to the iron dosage in the batch reactors, with up to 66 % removal in the period of 336 h in the highest dosage system (1.25 g ml^{-1}). The most significant perchlorate removal occurred in solutions with slightly acidic or near-neutral initial pH values. Elevated soluble chloride concentrations significantly inhibited perchlorate reduction, and lower removal rates were observed for iron samples with higher amounts of background chloride contamination. The reactive iron phase is neither pure zero-valent iron nor the mixed oxide alone. A mixed valence iron hydr(oxide) coating or a sorbed Fe^{2+} surface complex represent the most likely sites for the reaction. The use of zero-valent iron for treating wastewaters containing RDX (cyclotrimethylene trinitramine) and perchlorate from an army ammunition plant (AAP) in the USA at elevated temperatures and moderately elevated temperature with chemical addition was evaluated in batch and column experiments [55].

The interaction of a metal with dissolved perchlorate ions should be considered as a corrosion process, *i.e.* the overall transformation is composed of at least two or three reactions:

$$Me+2H^+ \rightarrow Me^{2+}+H_2 \qquad (1.1)$$

$$4Me+ClO_4^-+8H^+ \rightarrow Cl^-+4Me^{2+}+4H_2O \quad (1.2)$$

From the electrochemical point of view, this formulation involves three charge transfer processes:

$$Me \rightarrow Me^{2+}+2e^- \quad (1.3)$$

$$H^++e^- \rightarrow \frac{1}{2}H_2 \quad (1.4)$$

$$ClO_4^-+8H^++8e^- \rightarrow Cl^-+4H_2O \quad (1.5)$$

This last step should be a very complex one composed of several elementary steps. The equations given above involve the coupling of the anodic dissolution of the metal with two cathodic processes: discharge of protons and reduction of ClO_4^-.

In principle, the reduction of ClO_4^- could occur through a "catalytic mechanism" via the interaction with hydrogen atoms adsorbed on the metal surface.

It follows from these considerations that the problem of perchlorate reduction constitutes an intersection of several branches of sciences: electrochemistry (anodic dissolution of metals, discharge of protons); corrosion science (coupling of cathodic and anodic processes); catalysis (electrocatalysis); and heterogeneous chemical processes. In this paper, we present the historical background of the relevant topics in the light of recent developments and some new results obtained from the studies of direct interaction of perchlorate ions with various metals.

2. Heterogeneous catalytic/electrocatalytic aspects of perchlorate reduction

In 1971, Butula and Butula [56] found that $HClO_4$ could be reduced if $Pd/BaSO_4$ and Rh/C catalyst was used in acetic acid at 60 °C. In the same decade, the hydrogenation of perchlorate ions was studied at different temperatures and different perchlorate and hydrogen ion concentrations [20].

It was demonstrated that ClO_4^- dissolved in acidic aqueous solutions could be reduced to Cl^- by molecular hydrogen in the presence of powdered platinum black catalyst [9]. Considering the link between the liquid (aqueous) phase heterogeneous catalytic hydrogenation and electrocatalytic reduction, it was easy to draw the conclusion that electrocatalytic/electrochemical reduction of ClO_4^- could be performed at electrodes prepared from materials identical to the material of catalyst powders used in the catalytic hydrogenation [57].

Electrodes with "catalytic" properties, such as Pt, Rh, Pd, Ir, and Ru, have been in the focus of interest. There was, and perhaps still is, a general belief in the literature that perfect voltamograms reflecting H adsorption on these electrodes can be obtained in $HClO_4$ solution. Although in addition to Pt and Rh electrodes ClO_4^- reduction on Ir [13] and Ru [14] conveyed the warning to be cautious with noble metal electrodes when using $HClO_4$ supporting electrolyte, most electrochemists in their various studies [58-60] carried out in the presence of $HClO_4$ supporting electrolyte ignored the possible complications that should be ascribed to the occurrence of a reduction process involving ClO_4^-.

In 1990, it became evident that the contradictory results obtained during previous decades could be explained if it was assumed that the reduction of the ClO_4^- was characteristic not only for the rhodized surfaces, but also for smooth polycrystalline surfaces and well-defined crystal faces

[3-5]. By this approach, almost all difficulties encountered in the interpretation of various phenomena could be eliminated during the last few years.

Thus far, the majority of the published experimental results were obtained by using combined voltammetric, amperometric, EQCM, impinging jet, and radiotracer methods [1,3,4,13,19,20,61-65].

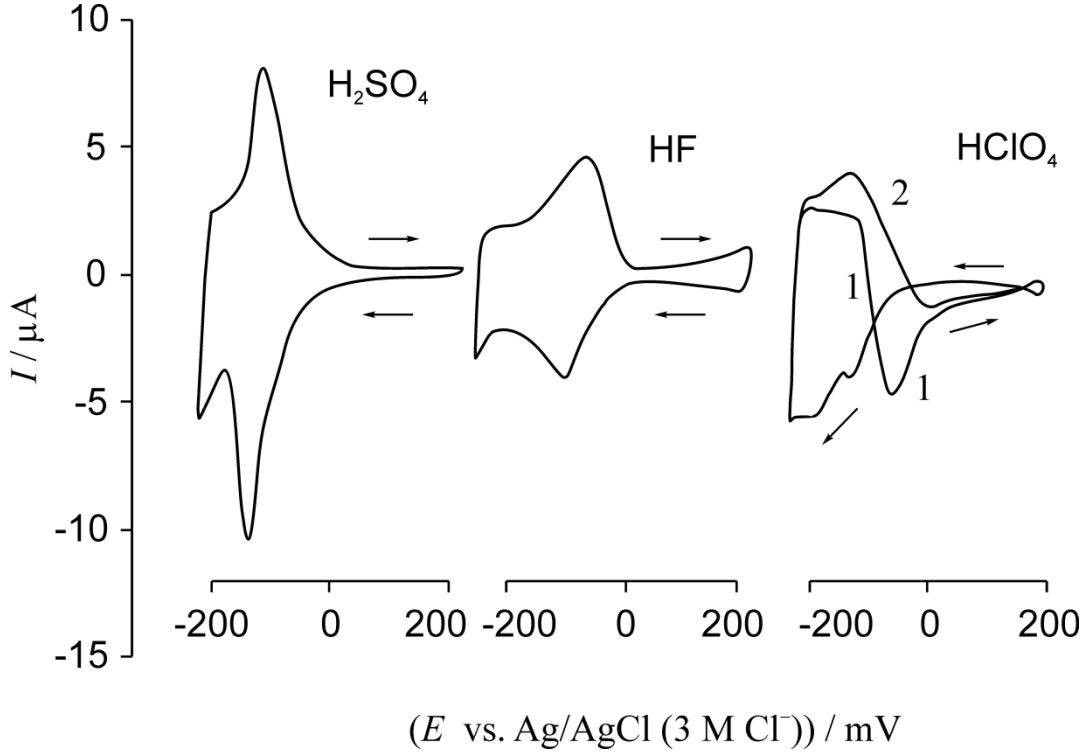

Figure 1. *Voltamograms obtained for rhodized electrodes in different electrolytes; acid concentration 1 mol dm^{-3}, sweep rate = 5 mV s^{-1}. Adapted from [61].*

The distortion of voltammetric curves in the presence of ClO_4^- is the firm evidence of the occurrence of the reduction process. Figure 1 shows the voltammetric curves obtained in 1 mol dm^{-3} H_2SO_4, HF and $HClO_4$ supporting electrolytes using rhodized electrodes [61]. In the case of H_2SO_4 and HF, despite some differences between them, the voltammetric curves behave "normally" as expected. In contrast, the voltammetric curve obtained in the presence of perchloric acid is distorted. The negative peak in the course of the positive sweep clearly indicates the occurrence of a cathodic process, namely, the reduction of perchlorate ions. Similar voltammetric curves were obtained with single- and polycrystalline smooth Rh [3,4] and platinized Pt [8] surfaces. Electrochemical behavior of Ir(100) in perchloric acid solutions has been characterized elsewhere [66]. The asymmetry of the cyclic voltammograms recorded in the double-layer region could be attributed to a slow reduction process, *e.g.* the reduction of perchlorate ions.

The characteristic features common to these systems are as follows:

(a) Nowadays, there is a general agreement that the rate of reduction of ClO_4^- at noble metal and catalytic electrodes should be very low at both ends of the potential scale; consequently the *I vs. E* curve should go through a minimum.

(b) The reduction process occurs almost exclusively during the positive sweep of the cyclic voltammogram.

(c) Generally, no reaction can be observed on the negative sweeps, but the shape, height, and position of the corresponding hydrogen peak differ significantly from those expected.

(d) The distortion of the anodic peak gradually disappears during subsequent cycles, but the anodic and cathodic peaks remain asymmetric.
(e) The only reduction product found in the solution was Cl^-.
(f) The very rapid decrease in the electrocatalytic activity with respect to ClO_4^- - reduction can be explained by self-inhibition, namely, by the inhibiting action of Cl^- formed during reduction and adsorbed on the electrode surface. The higher the Cl^- concentration, the more pronounced is its inhibitive effect.
(g) The desorption of Cl^- from the metal surface is a very slow process. For instance, no measurable desorption of Cl^- were detected until several minutes after switching the electrolyte solution from 1 mol dm^{-3} HF + 10^{-4} mol dm^{-3} HCl to 1 mol dm^{-3} HF [62,67].

According to the results presented in the literature, the rate of electrocatalytic reduction of perchlorates on Rh is relatively high. The reduction process leading to the formation of Cl^- should be a very complicated reaction as eight electrons are involved in the overall process. It is difficult to believe that it can be performed without the formation of any stable intermediates or products of side-reactions. Analogous to the reduction of perchlorate in homogeneous solution, the reduction of perchlorate at an electrode (or any surface) must involve oxygen atom transfer. Therefore, the controversy regarding the mechanism of the reduction of ClO_4^- on rhodium is not surprising. According to the "classical" view, the rate-determining step in the electrocatalytic process can be described as a reaction of adsorbed ClO_4^- species with adsorbed H atoms [1,13,19,61,62,67]. In contrast, the reduction process can be considered as a slow decomposition of ClO_4^- species on the surface followed by fast reduction steps [63]. The latter approach is based on the view that the reduction rate attains a measurable level at potentials where the surface concentration of H is very low; consequently, it is unlikely that it can play any role. Thus, it should be assumed that the rate-determining step is the decomposition of adsorbed ClO_4^- with the participation of a free adsorption site in its neighborhood.

In accordance with the above considerations, three fundamental types of possible mechanisms are distinguished for the electrocatalytic reduction of ClO_4^- [13,20,21,61-63,65,67], namely the mechanism (A) involving protons and/or adsorbed hydrogen, the serial mechanism (B) and the mechanism (C) involving free-metal sites.

Mechanism (A) can follow two alternative paths:

$$ClO_4^-(sol) \rightleftharpoons ClO_4^-(ads)$$

$$H^+(sol) + e^- \rightleftharpoons H(ads) \qquad \text{(A1)}$$

$$ClO_4^-(ads) + H(ads) \rightarrow \text{intermediates} \rightarrow Cl^-(ads) \rightarrow Cl^-(sol)$$

or

$$ClO_4^-(sol) \rightleftharpoons ClO_4^-(ads)$$

$$ClO_4^-(ads) + H^+ + e^- \rightarrow \text{intermediates} \rightarrow Cl^-(ads) \qquad \text{(A2)}$$

$$Cl^-(ads) \rightleftharpoons Cl^-(sol)$$

Mechanism (B):

$$ClO_4^- \rightleftharpoons ClO_4^-(ads)$$

$$ClO_4^-(ads) \rightarrow ClO_3^-(ads) + O(ads) \quad \text{(slow)}$$

$$O(ads) + 2H^+ + 2e^- \rightarrow H_2O \quad \text{(fast)}$$

$$ClO_3^-(ads) \rightarrow ClO_2^-(ads) + O(ads) \quad \text{(slow)}$$

$$O(ads) + 2H^+ + 2e^- \rightarrow H_2O \quad \text{(fast)}$$

$$ClO_2^-(ads) \rightarrow ClO^-(ads) + O(ads) \quad \text{(slow)}$$

$$O(ads) + 2H^+ + 2e^- \rightarrow H_2O \quad \text{(fast)}$$

$$ClO^-(ads) \rightarrow Cl^-(ads) + O(ads) \quad \text{(slow)}$$

$$O(ads) + 2H^+ + 2e^- \rightarrow H_2O \quad \text{(fast)}$$

where “(ads)” denotes that the species is adsorbed, while “(sol)” refers to components in the solution phase. According to this scheme, the whole process starting from perchlorate ion occurs on the surface and the role of desorption of intermediates can be neglected, *i.e.* their desorption rate is very low compared with the rate of the chemical transformation.

Mechanism (C):

According to this mechanism, it should be assumed that the rate-determining step is the decomposition of adsorbed perchlorate ion if a free "active" site $(\otimes)$ is in its neighborhood. This assumption is the same as that made in [64] in connection with the reduction of N_2O.

The decomposition reaction can be written as:

$$\otimes + ClO_4^- \rightarrow \text{intermediates} \rightarrow Cl^-$$

On the other hand, it can be assumed that the surface concentration of active sites is determined by the following reactions:

$$\otimes + H_2O \rightleftharpoons \otimes\text{-}OH + H^+ + e^-$$

or

$$\otimes + OH^- \rightleftharpoons \otimes\text{-}OH + e^-$$

In this case, the potential dependence of the surface concentration of free active sites plays an important role.

In the reaction schemes proposed in the literature, the adsorption of perchlorate ion is an elementary step in the overall reduction. The decomposition of the adsorbed perchlorate ion is assumed to be slow; however, there are only speculations about the rates of the subsequent steps. For instance, in the mechanism (B) all decomposition steps are assumed to be slow, but no rigorous investigation of this problem has yet been performed.

The electrochemical reduction of perchlorate ions on rhodium and ruthenium was investigated in a series of experiments (voltammetry, chronoamperometry, impedance spectroscopy) performed at different electrode potentials (*E*) and different temperatures (*T*).

Figure 2 shows cyclic voltammograms obtained for a Rh rotating disc electrode in contact with a 3 mol dm^3 $HClO_4$ solution [67].

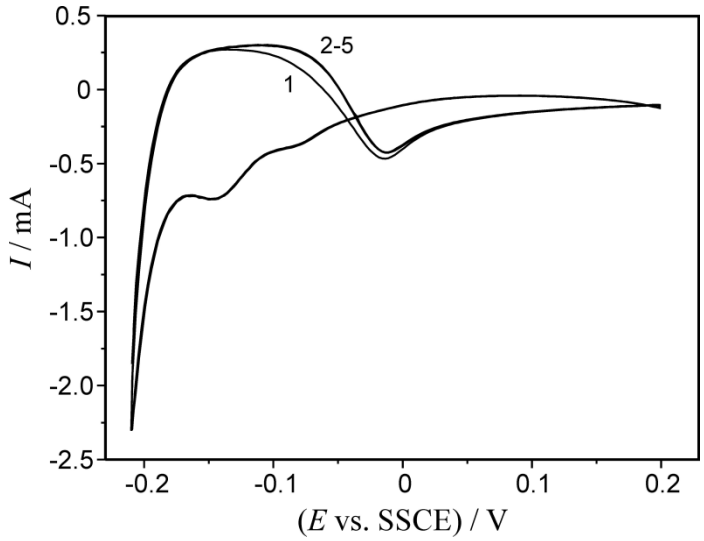

Figure 2. *Cyclic voltammograms obtained for a Rh rotating disc electrode in contact with a 3 mol dm^{-3} $HClO_4$ solution (geometric surface area of the electrode:* A *= 0.196 cm^2,rotation rate: ω_r= 950 rpm, temperature:* T *= 25.0 °C). Adapted from [67]. (SSCE: sodium saturated calomel electrode)*

There is a distinct difference between the curves recorded at stagnant electrodes and the curves obtained with the RDE. In case of stationary electrodes, the distortion of the anodic peak gradually disappears during subsequent potential cycles, *i.e.* the negative current during the positive sweep is continuously decreasing over the consecutive scans. In contrast, in case of rotating disc electrodes, the shape of the voltammogram does not change after the second or third cycle, and a negative current can be always observed during the positive sweep. It means that the desorption rate of Cl^- generated during the reduction process is significantly influenced by the hydrodynamic conditions, probably through desorption/diffusion coupling. This conception is supported by the results of chronoamperometric measurements carried out at different temperatures. The curves obtained at *T* = 45 °C are presented in Figure 3 [67].

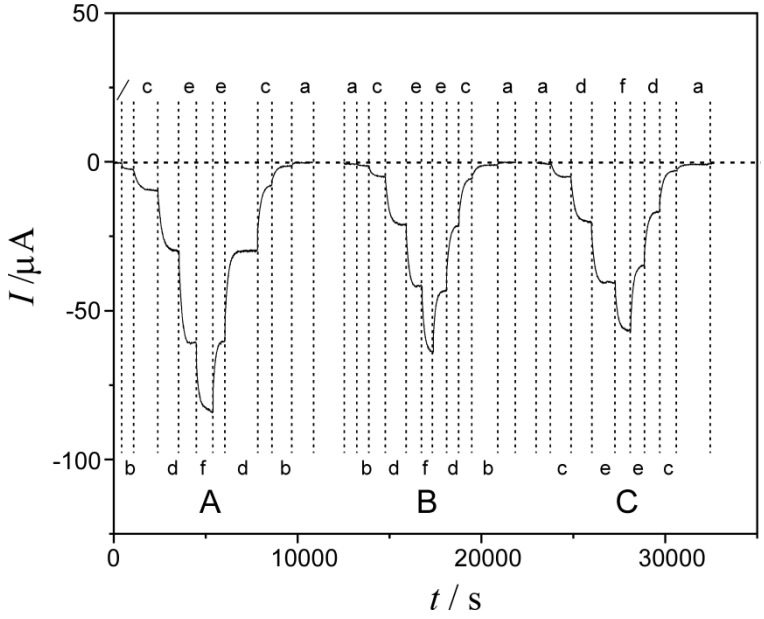

Figure 3. *Chronoamperometric measurements. The current (*I*) as a function of time (*t*) at constant electrode potentials and at different electrode rotation rates. Electrode potentials: A: 0.01 V vs. SSCE; B: 0.06 V vs. SSCE; C: 0.11 V* vs. *SSCE. Rotation rates (ω_r): a: 0 rpm; b: 500 rpm; c: 1000 rpm; d: 2000 rpm; e: 3000 rpm; f: 4000 rpm. (geometric surface area of the electrode:* A *= 0.196 cm^2, temperature:* T *= 45.0 °C) Adapted from [67].*

During these experiments the current was recorded as a function of time at constant electrode potentials and at different electrode rotation rates. Well-defined stationary currents were observed in all cases. The values of the stationary currents depend on the rotating rate of the RDE, the electrode potential, and the temperature.

It should be pointed out that the above measurements were carried out at potentials where the surface concentration of adsorbed H is very low, if existent. Consequently, it is unlikely that it can play any role. Thus, it should be assumed that the rate-determining step is the decomposition of adsorbed ClO_4^- with the participation of a free adsorption site.

Figure 4 shows impedance spectra of Ru (deposited on gold) in 1 mol dm^3 $HClO_4$ solution.

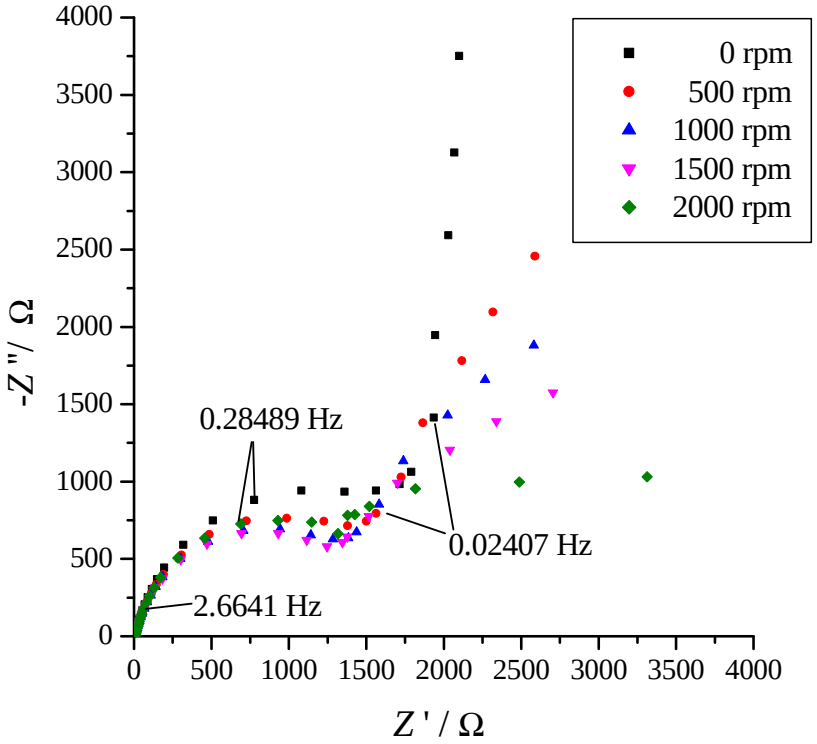

Figure 4. *Impedance spectra (complex plane plot) recorded on Ru in 1 mol dm^3 $HClO_4$ solution. The impedance of the electrode were measured at different rotating rates of the RDE at the electrode potential of* E *= -0.15 V* vs. *SSCE. (geometric surface area of the electrode:* A *= 0.196 cm^2, temperature:* T *= 25 °C). (Recent, unpublished results)*

The impedance of the electrode was measured at different rotating rates of the RDE at the electrode potential of E=-0.15 V *vs.* SSCE (T = 25 °C). The impedance measurements were started as soon as stationary conditions were reached (*e.g.* about 20 min after changing the rotation rate of the RDE). The first observation is that the plots are very similar to what is expected qualitatively for the case of a single charge transfer step coupled with diffusion [68].

For all the spectra obtained in this study, only one time constant can be identified in the high frequency range, which suggests that the measured impedance response is dominated by a single (rate determining) charge transfer step. In the case of the reduction of perchlorate ions, the assumption that the $ClO_4^- \rightarrow ClO_3^-$ transformation is the rate determining step seems to be a relevant and acceptable interpretation of the phenomena observed. Experiments with ClO_3^- strongly support this hypothesis.

Figure 5 shows cyclic voltammograms obtained for Rh in contact with a solution containing 0.49 mol dm^{-3} $NaClO_4$ + 0.01 mol dm^{-3} $HClO_4$, and for the same electrode in contact with a solution

containing 0.49 mol dm^{-3} $NaClO_3$ + 0.01 mol dm^{-3} $HClO_4$. It can be clearly seen from the figure that in this potential range, the negative current is at least 2 orders of magnitude higher in the presence of ClO_3^- than the current measured in the other solution. For comparison, the voltammetric curve obtained in 1 mol dm^{-3} $HClO_4$ solution is also given in the figure.

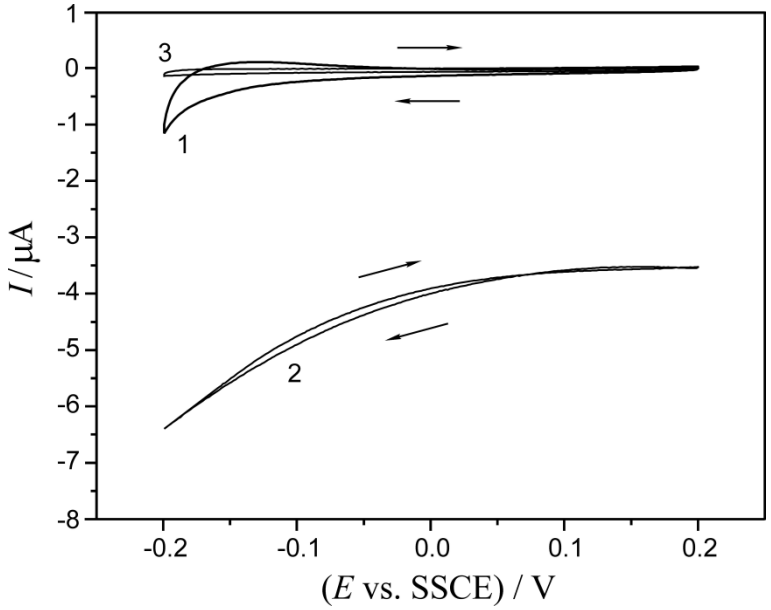

Figure 5. *Cyclic voltammograms obtained for Rh (1): in contact with a solution containing 0.49 mol dm^{-3} $NaClO_4$ + 0.01 mol dm^{-3} $HClO_4$, and (2): for the same electrode in contact with a solution containing 0.49 mol dm^{-3} $NaClO_3$ + 0.01 mol dm^{-3} $HClO_4$. (3): voltammetric curve obtained in 1 mol dm^{-3} $HClO_4$ solution. (geometric surface area of the electrode:* A *= 0.196 cm^2, temperature:* T *= 25.0 °C). Adapted from [67].*

Electrocatalytic activity in perchlorate reduction was found in the case of some non-noble metals, such as Tc [16], Re [15], Sn [17] and Ti [12,69]. Considering the very fact that Tc is an artificial element, emitting β-radiation, the coupled electrochemical and radiochemical study of electrodeposition of Tc species from $HClO_4$ supporting electrolyte gave an interesting insight in the reduction of ClO_4^-.

It was found that under potentiostatic conditions during the deposition of Tc species, the increase in the radiation intensity, i.e. the increase of the amount of deposited material, is accompanied by a continuous increase of a cathodic current as shown in Figures 6 and 7 (the amount of the electrodeposited Tc species was determined directly by the measurement of the intensity of the radiation coming from the electrodeposited layer).

So far, only the occurrence of ClO_4^- reduction has been suggested as acceptable explanation [16]. The voltammetric study of the system furnished unambiguous evidence proving the validity of this assumption (Figure 8).

It is well known [70] that the electrochemical behavior and properties of technetium and rhenium and those of their various ions are very similar.

Considering the similarity of Tc and Re, it was no wonder that the behavior found in the case of Tc can also be observed for Re and *vice versa*.

In contrast to the behavior of platinized platinum electrodes, the catalytic activity of “rhenized” electrodes can be observed under potentiostatic or galvanostatic conditions for relatively long periods of time, although no real steady state can be attained [15], as is shown in Figure 9 in the case of a potentiostatic experiment.

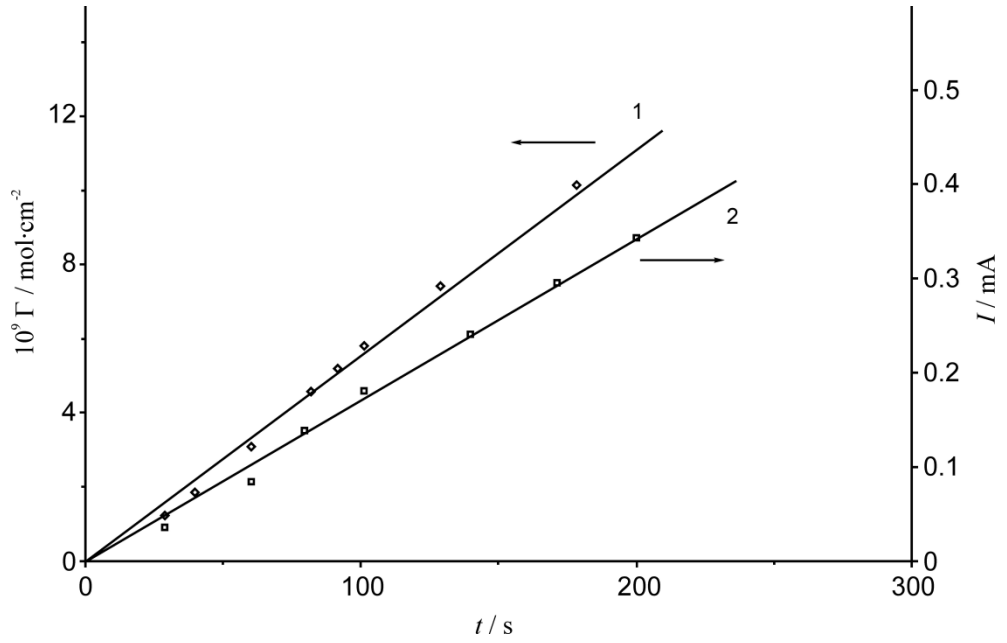

Figure 6. *Γ* vs. *time (1) and (absolute value) current* vs. *time (2) curves obtained in the course of a simultaneous radiometric and electrochemical measurement of the deposition of Tc species (*$c_{TcO_4^-}$ *=8×10^{-4} mol dm^{-3}) from a 1 mol dm^{-3} $HClO_4$ supporting electrolyte at* E *= 50 mV, (geometric surface area, 13 cm^2). Adapted from [20].*

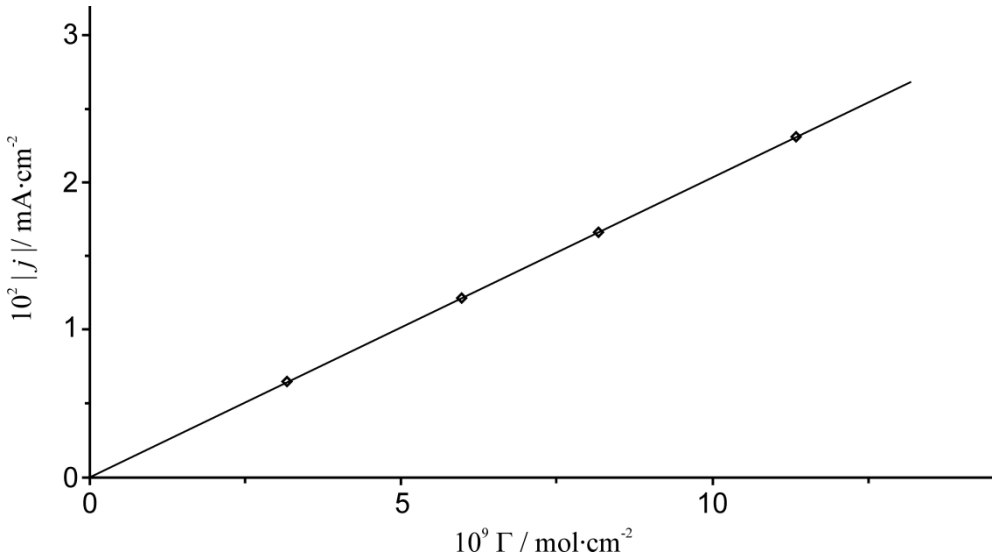

Figure 7. *The* $|j|$ *current density* vs. Γ *relationship obtained from data presented in Figure 6. Adapted from [20].*

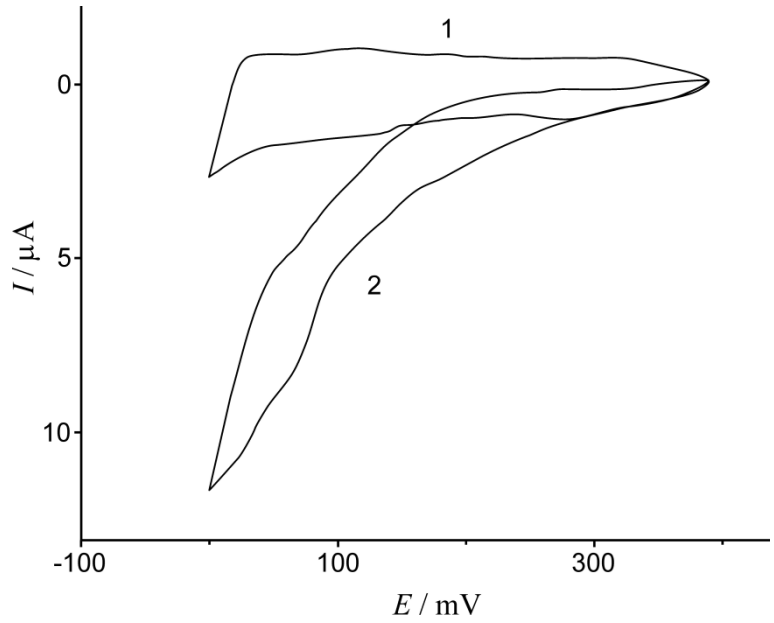

Figure 8. *Cyclic voltammetric curves at a Tc-covered surface (Γ = 2 × 10^{-8} mol cm^{-2}) in 1 mol dm^{-3} H_2SO_4 (1) and in 3 mol dm^{-3} $HClO_4$ (2). Sweep rate, 2.5 mV s^{-1} (geometric surface area, 13 cm^2). Adapted from [20].*

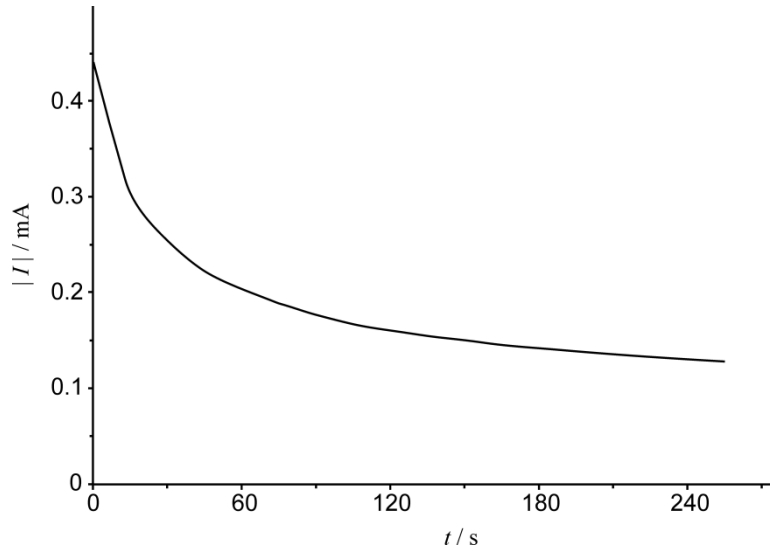

Figure 9. *Current* vs. *time curve obtained in 1 mol dm^{-3} $HClO_4$ solution, at 90 mV, at a rhenized electrode, (geometric surface area, 2 cm^2). Adapted from [15].*

The continuous decrease in the reduction current can be explained by two important effects:

i) the self-inhibition of the process by the adsorption of Cl^- formed in the reduction (the current efficiency with respect to the formation of Cl^- is above 90 %). The effect of Cl^- was demonstrated in separate experiments by adding HCl in low concentration to the solution phase in the course of the reduction [15], and

ii) deactivation of the electrode surface owing to the chemical transformation of the surface layer participating in the reaction.

The electrochemical behavior of tin in deaerated sodium perchlorate was studied using potentiodynamic and potentiostatic techniques [17]. The behavior of tin in sodium perchlorate was unexpectedly complicated by the reduction of the perchlorate anion. It was shown that the reduction process takes place within a potential region comprising the negative side of the double layer region and the positive side of the hydrogen region ($-0.7 \leq E \leq -1.3$ V). It was stated that the presence of oxide on the electrode surface favors the reduction reaction, which may occur in two steps: the formation of basic tin(II) chloride followed by its reduction, producing chloride.

Similar mechanistic conclusions were drawn in the case of titanium electrode. It was reported that perchlorate ion is electrochemically reduced to chloride ion at an active titanium electrode in aqueous 1.0 M $HClO_4$ [12]. It is assumed that the reduction occurs by direct reaction at the surface rather than a pathway involving catalysis by soluble titanium corrosion products. The reaction occurs by oxygen atom transfer to the titanium surface, and the implications of this mechanism for the surface composition of active titanium electrodes are discussed. Chlorate ion is also reduced at titanium, and the rate coefficient for chlorate reduction is at least 10^5 times greater than that for the perchlorate reduction.

In experiments with Ti in contact with perchlorate and nitrate solutions, Ti(III) or Ti(II) were generated by applying anodic current [69]. These multivalent Ti species are strong reducing agents and reduce perchlorate and nitrate. Kinetic experiments were carried out in synthetic perchlorate, nitrate solutions, and tap water media at different perchlorate and nitrate concentrations.

3. Reaction mechanisms and electrode impedance

In another study [67], the experimental results obtained for the electrochemical reduction of perchlorate ions on rhodium have been explained by the following reaction mechanism. After a potential step from a potential at which the adsorption of ClO_4^- does not occur, the reduction process starts with the adsorption of perchlorate ions at free active sites on the metal surface occupied, e.g. by OH^-.

$$ClO_4^-(sol) + OH^-(ads) \rightleftarrows ClO_4^-(ads) + OH^-(sol)$$

The decomposition reaction can be written as:

$$ClO_4^-(ads) \rightarrow \text{intermediates} \rightarrow Cl^-(ads) \rightleftarrows Cl^-(sol)$$

After the production of a certain amount of Cl^-, practically all active sites are occupied by Cl^- or ClO_4^-, and a well defined stationary state with constant current is established.

For the stationary state, the following reaction scheme can be suggested:

$$ClO_4^-(0) + Cl^-(ads) \rightleftarrows ClO_4^-(ads) + Cl^-(0) \qquad (3.S1)$$

$$ClO_4^-(ads) + 2H^+ + 2e^- \rightarrow ClO_3^-(ads) + H_2O \quad \text{(slow)} \qquad (3.S2)$$

$$ClO_3^-(ads) \rightarrow \text{intermediates} \rightarrow Cl^-(ads) \quad \text{(very fast)} \qquad (3.S3)$$

$$Cl^-(0) \rightleftarrows Cl^-(sol), \qquad (3.S4)$$

or in a generalized form:

$$A^-(0) + B^-(ads) \rightleftarrows A^-(ads) + B^-(0) \qquad (3.1)$$

$$A^- (ads) + nH^+ + ne^- \rightarrow B^- (ads) + \frac{n}{2} H_2O \quad (3.2)$$

$$B^- (0) \rightleftarrows B^- (sol) \quad (3.3)$$

where n is the number of electrons transferred from the metal phase to A^- in forming one B^- species, "(ads)" denotes here that the species is adsorbed on an active site, while "(0)" refers to components in the solution phase in the immediate vicinity of the electrode surface [71]. The rate of the first reaction (v_1) depends on the electrode potential (E), the concentration of A^- and B^- near to the electrode surface ($c_A(0)$ and $c_B(0)$), the surface concentration of adsorbed A^- and B^- ions (Γ_A and Γ_B), respectively,

$$v_1 = v_1 \left[E, c_A(0), c_B(0), \Gamma_A, \Gamma_B \right], \quad (3.4)$$

while the rate of the second reaction (v_2) depends on the electrode potential E, Γ_A and the concentration of H^+ ($c_H(0)$) adjacent to the electrode surface:

$$v_2 = v_2 \left[E, \Gamma_A, c_H(0) \right]. \quad (3.5)$$

According to the above considerations

$$\Gamma_A + \Gamma_B = \Gamma_T \quad (3.6)$$

where Γ_T is the total surface concentration of the active sites. It can be assumed, that Γ_T is constant at a given electrode potential.

Under steady-state conditions $\overline{v}_1 = \overline{v}_2$.

The transport equations for the (linear) diffusion of the species B^- can be written in the form:

$$\left(\frac{\partial c_B}{\partial t} \right)_x = D_B \left(\frac{\partial^2 c_B}{\partial x^2} \right)_t \quad (3.7)$$

where x is the distance from the electrode surface.

If the system is perturbed with a sinusoidal signal of low amplitude, the variables can be written in terms of a stationary and a fluctuating component:

$$\xi(x,t) = \overline{\xi}(x) + \Delta\xi(x) \exp(i\omega t), \quad (3.8)$$

where $\overline{\xi}(x)$ represents the steady-state quantity, $\Delta\xi(x)$ is the amplitude of the fluctuation, ω is the angular frequency of the perturbing signal, t is the time, and "i" is the imaginary unit. On making an appropriate Taylor series expansion of the reaction rates - with the plausible assumptions

Γ_T = constant, $\left(\frac{\partial v_1}{\partial c_A(0)} \right) \approx 0$ and $\left(\frac{\partial v_2}{\partial c_H(0)} \right) \approx 0$,

we obtain :

$$v_1 = \overline{v}_1 + \left(\frac{\partial v_1}{\partial E} \right)_{c_B, \Gamma_B} \Delta E \exp(i\omega t) + \left(\frac{\partial v_1}{\partial c_B(0)} \right)_{E, \Gamma_B} \Delta c_B(0) \exp(i\omega t) + \left(\frac{\partial v_1}{\partial \Gamma_B} \right)_{E, c_B} \Delta\Gamma_B \exp(i\omega t) = \quad (3.9)$$

$$= \overline{v}_1 + k_0 \Delta E \exp(i\omega t) + k_1 \Delta c_B(0) \exp(i\omega t) + k_2 \Delta\Gamma_B \exp(i\omega t)$$

$$v_2 = \bar{v}_2 + \left(\frac{\partial v_2}{\partial E}\right)_{\Gamma_B} \Delta E \exp(i\omega t) - \left(\frac{\partial v_2}{\partial \Gamma_B}\right)_E \Delta\Gamma_B \exp(i\omega t) = \bar{v}_2 + k_3 \Delta E \exp(i\omega t) - k_4 \Gamma_B \exp(i\omega t) \quad (3.10)$$

Each of the "rate constants" (k_0 - k_4) appearing in equations (3.9) and (3.10) represents a partial derivative. The "faradaic" current density related to the charge-transfer reaction is given by $i_F = nFv_2$. Thus the linearized form of i_F becomes

$$\Delta i_F = nF(k_3 \Delta E - k_4 \Delta\Gamma_B) \quad (3.11)$$

Since $\frac{\partial \Gamma_B}{\partial t} = v_2 - v_1$, thus

$$i\omega\Delta\Gamma_B = (k_3 - k_0)\Delta E - (k_2 + k_4)\Delta\Gamma_B - k_1 \Delta c_B . \quad (3.12)$$

The linearized form of eq.(7) is :

$$i\omega \Delta c_B(x) = D_B \frac{\partial^2 \Delta c_B(x)}{\partial x^2} . \quad (3.13)$$

The above set of linearized equations (3.9) to (3.12) and the differential equation, (3.13) can be solved analytically [68,72-74] by using the following boundary conditions:

at $x = 0$

$$\Delta J_B(0) = -D_B \frac{\partial \Delta c_B(0)}{\partial x} = \Delta v_1 = k_0 \Delta E + k_1 \Delta c_B + k_2 \Delta\Gamma_B \quad (3.14)$$

at $x = \delta$

$$\Delta c_B(x = \delta) = 0 \quad (3.15)$$

where δ represents the diffusion layer thickness, and J_B is the flux of species B^-.

The resulting expression for the "faradaic" admittance is quite complicated:

$$Y_F(\omega) = Y_1(\omega) + Y_2(\omega) = nFk_3\left(1 - \frac{k_4}{i\omega + k_2 + k_4 + \frac{k_1 k_2}{Q - k_1}}\right) + nFk_4 \frac{k_0 - \frac{k_1 k_0}{k_1 - Q}}{i\omega + k_2 + k_4 + \frac{k_1 k_2}{Q - k_1}} \quad (3.16)$$

with $Q = \frac{Ds\left[\exp(2s\delta) + 1\right]}{\exp(2s\delta) - 1}$ and $s = \sqrt{\frac{i\omega}{D_B}}$.

The first term of the right hand side of equation (3.16) can be rewritten as $Y_1(\omega) = 1/Z_1(\omega)$, where the impedance function $Z_1(\omega)$ can be expressed by

$$Z_1(\omega) = \frac{1}{nFk_3} + \frac{1}{\frac{1}{\frac{k_4}{nFk_3} i\omega} + \frac{1}{\frac{k_4}{nFk_2k_3} - \frac{k_1 k_4}{nFk_2k_3}\frac{\tanh(s\delta)}{D_B s}}} . \quad (3.17)$$

The second term can be written as $Y_2(\omega) = 1/Z_2(\omega)$, where

$$Z_2(\omega) = \frac{1}{nF}\frac{k_2 + k_4}{k_0 k_4} - \frac{k_1}{nFk_0}\frac{\tanh(s\delta)}{D_B s} - \frac{k_1 s}{nFk_0 k_4}\tanh(s\delta) . \quad (3.18)$$

Thus, the faradaic impedance of the electrode (Z_F) is given as

$$Z_F(\omega)=\frac{1}{1/Z_1(\omega)+1/Z_2(\omega)}. \tag{3.19}$$

In a general case, the impedance function completed by elements representing the ohmic resistance (R_u) of the electrolyte solution and the double layer capacitance (C_{dl}) can be written as:

$$Z_T(\omega)=R_u+\left[\frac{1}{Z_1(\omega)}+\frac{1}{Z_2(\omega)}+i\omega C_{dl}\right]^{-1}. \tag{3.20}$$

The impedance function of the double layer in such type of electrochemical systems can be well approximated by $Z_{dl}(\omega) = (i\omega A_{dl})^{-\beta}$, where $\beta \le 1$ (but it is close to 1) [75]. Thus,

$$Z_T(\omega)=R_u+\left[\frac{1}{Z_1(\omega)}+\frac{1}{Z_2(\omega)}+(i\omega A_{dl})^{\beta}\right]^{-1}, \tag{3.21}$$

In principle, it is possible to estimate the parameters of equation (3.21) from the measured impedance data by complex nonlinear fitting. However, the complete expression of the impedance (equation (3.20)) contains 10 free parameters, and the fitting in the case of such a high number of parameters is always a very difficult task. In addition, due to the mathematical structure of equation (3.21), the parameters are expected to be strongly correlated [76]. In order to overcome the difficulties concerning CNLS fitting, simplifications in the mathematical expressions should be introduced. It may be assumed that k_0 is very small, therefore $Z_2(\omega)$ can be neglected or approximated by an ohmic resistance: $Z_2(\omega) \approx R_k$.

On the other hand, by substituting

$R_{ct}=\frac{1}{nFk_3}$, $C_A=\frac{k_4}{nFk_3}$, $R_A=\frac{k_4}{nFk_2k_3}$, $P_1=-\frac{k_1k_4}{nFk_2k_3\sqrt{D_B}}$, and $P_0=\delta/\sqrt{D_B}$

into equation (17), we have

$$Z_1(\omega)=\frac{1}{R_{ct}}+\frac{1}{\frac{1}{i\omega C_A}+\frac{1}{R_A+P_1\frac{\tanh(P_0\sqrt{i\omega})}{\sqrt{i\omega}}}}=\frac{1}{R_{ct}}+\frac{1}{\frac{1}{i\omega C_A}+\frac{1}{R_A+Z_W}}. \tag{3.22}$$

The equivalent circuit analog [77] corresponding to the analytical expression given by equation (3.21) is presented in Figure 10.

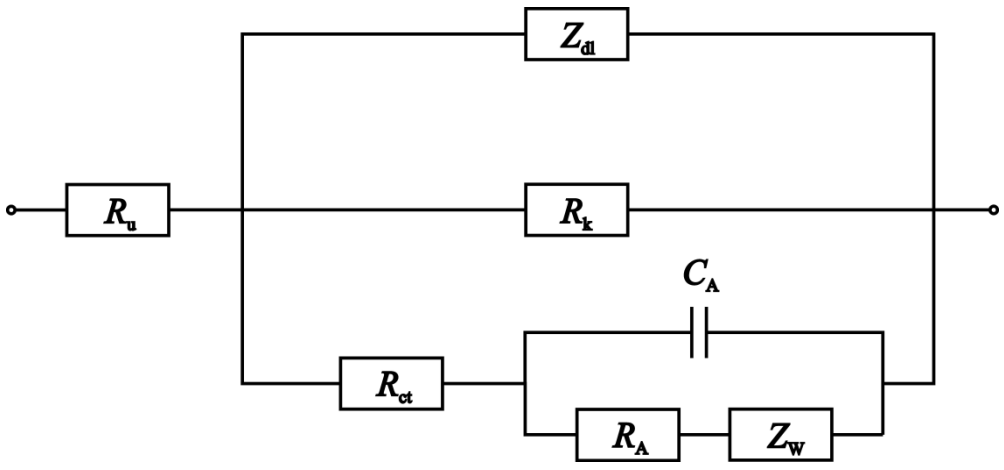

Figure 10. *The equivalent circuit analog.*

Detailed numeric results of the CNLS fittings are presented in the study by Ujvári et al [78]. Surprisingly, despite of the great number of adjustable parameters, many of them could be determined with a good statistics (for instance Ru, P_0, R_A, C_A, P_l, A_{dl}, β,), and reasonable estimated mean values have been obtained for the others.

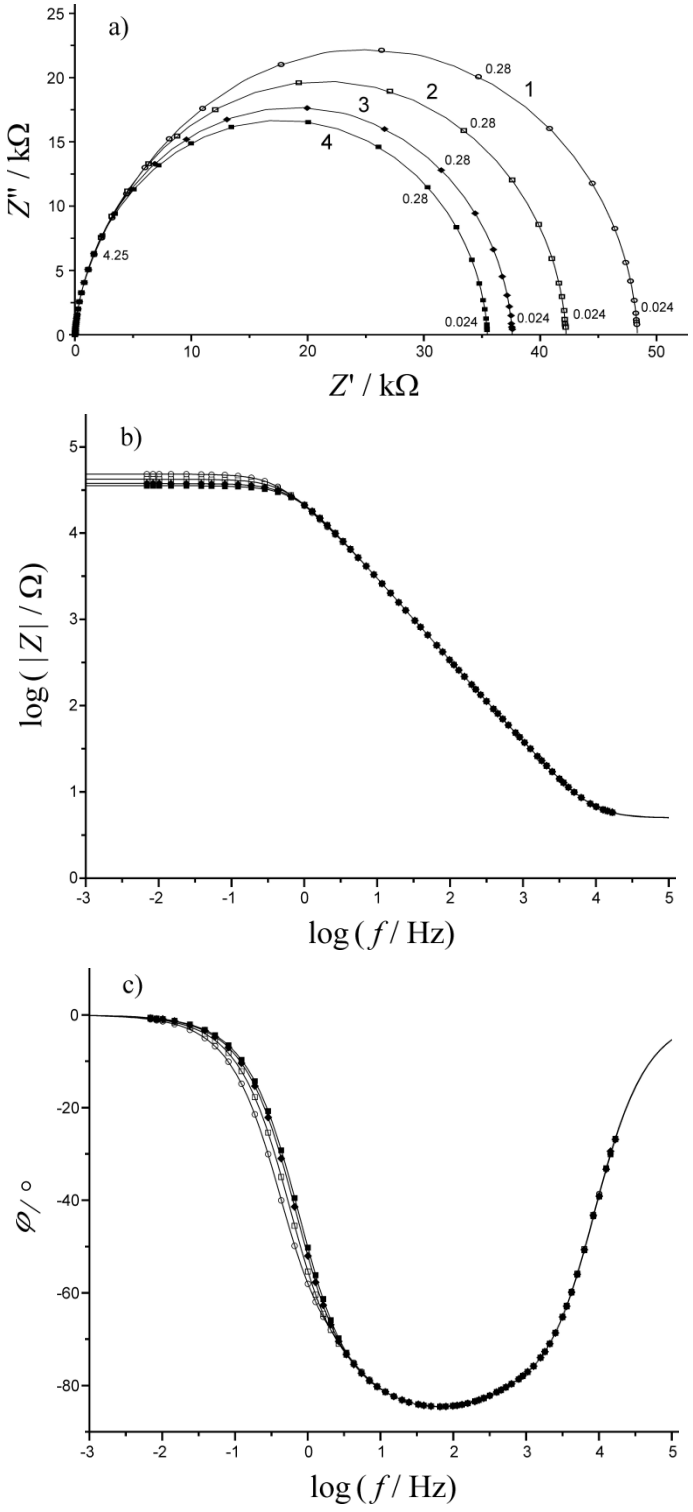

Figure 11. (a) *Impedance spectra (complex plane plots) recorded on Rh in 1 mol dm^3 $HClO_4$ solution. The impedance of the electrode were measured at different rotating rates of the RDE at the electrode potential of* E *= 0.01 V* vs. *SSCE. (*T *= 25.0 °C). Rotation rates (ω_r): 1(○): 500 rpm; 2 (□): 1000 rpm; 3 (♦): 2000 rpm; 4 (■): 3000 rpm.* ***(b) – (c)*** *Bode diagrams (log|Z| versus*

log f and φ versus log f *plots) at 4-4 different rotation rates of the RDE. Continuous lines: simulated curves calculated by using the optimized parameters. Adapted from [67].*

Figures 11b and 11c show the Bode diagrams (log|*Z*| versus log *f* and *φ* versus log *f* plots) at 4-4 different rotation rates of the RDE, respectively (*E*=0.01 V *vs.* SSCE, *T* = 25 °C). The Argand diagrams (complex impedance plane plots) are presented in Figure 11a. In Figures 11a-11c, beside the measured values (discrete points), the simulated curves calculated by using the optimized parameters are also displayed (continuous lines). The "visual" inspection of the transformed curves (Bode plots) supplies more valuable information concerning the goodness of a fit than that of the complex plane plot, since complex plane plots usually show a rather "good" fit, while the transformed curves reveal the problems. The physical reality of the parameters is perhaps the most important criterion in checking the correctness of a model. The variation of the appropriate fitting parameters with rotating rates of the RDE could be very informative. Particularly the changes observed in C_A and P_0 are of special interest. C_A increases monotonically with the rotation rate, as expected for decreasing concentration of chloride ions in the immediate vicinity of the electrode surface. The P_0 *vs.* $\omega_r^{-1/2}$ plot is linear.

4. Reduction of perchlorate ions in the course of anodic dissolution and corrosion of metals

Most studies concerning the basics of the anodic dissolution of metals focused on relatively simple systems [79]. "Simple systems" ideally consist of single-crystalline or polycrystalline, highly pure metals in acid aqueous solutions free of dissolved oxygen, surface-active substances, and complexing agents. The dissolution behavior in alkaline or neutral media, even in deaerated or aerated aqueous solutions free of surface-active and complexing substances, is difficult to study because of the easy formation and slow dissolution of protective layers. Also, the influence of surface-active substances on the dissolution kinetics and mechanisms of metals is better known in acid than in neutral or alkaline environments.

It is an almost general conclusion drawn from anodic dissolution studies that the nature of anions present in the electrolyte solutions affects the dissolution process to a more or less pronounced extent.

In most mechanistic considerations, this effect is explained by the role of the specific adsorption of anions. Accepting this assumption, and taking into consideration that the adsorbability of the anions on metals is very different depending on the nature of the anion, it would be important to study the dissolution process in the presence of anions with very low adsorbability in order to minimize the role of anion adsorption in the dissolution process, consequently, to obtain experimental data without the interference of anion specific adsorption. According to some very recent views, ClO_4^- are assumed to fulfill this requirement [80,81].

On the basis of the assumption of stability of ClO_4^- sophisticated electrochemical methods, such as EQCM and electrochemical impedance spectroscopy (EIS), were used for the study of anodic dissolution and corrosion of various metals in perchloric acid solutions, for instance, in the case of nickel [82] and iron [80,81].

Detailed mechanistic conclusions are drawn from such studies without taking into account the possible reduction of ClO_4^- under the conditions of the experiments.

In a series of communications [83-85], the authors pointed out that the reduction of ClO_4^- takes place during the corrosion of Cu, Al, Zn, Ni, and Fe in deoxygenated $HClO_4$ solutions and emphasized that, for the interpretation of the results of corrosion or anodic dissolution studies in the $HClO_4$/metal systems, this fact cannot be left out of consideration. Presence of chlorate and

perchlorate ions leads to passivity breakdown and pitting corrosion of iron in sulfuric acid solutions [86]. The origin of the pitting has been attributed to Cl^- produced via the reduction of ClO_3^- and ClO_4^- by Fe^{2+}. Similar results were obtained for Al in [87]. The XPS experiments detected perchlorate and chloride ions on the surface. Both of these ions may play role in the passivity breakdown.

Oscillatory electrodissolution of Al in perchloric acid solutions has been described [88]. According to the authors, current oscillations occurred over a large range of $HClO_4$ concentration and over a wide scale of applied potential. During the anodic dissolution of the Al electrode in $HClO_4$ solutions, perchlorate ions were reduced to chloride ions, which induced pitting corrosion.

The electrodeposition of Cu on Ru(0001) in perchlorate media has also been investigated [89]. XPS was used to determine surface composition. The spectra show that ClO_4^- dissociates into adsorbed Cl^- and ClO_x^- species.

The composition of the passive layers formed on Zn electrode in naturally aerated and de-aerated 0.1 M $KClO_4$ solution were studied using chronopotentiometry, electrochemical impedance, and X-ray photoelectron spectroscopic measurements (XPS). Cl^- from the perchlorate reduction reaction were detected in the solutions during electrode polarization [90,91].

5. Interaction of ClO_4^- with iron group metals in aqueous media

The dissolution kinetics and mechanism of iron-group metals has been investigated in a great number of studies [79-82,92].

The kinetics of the anodic dissolution of iron, cobalt, and nickel was found to be quite similar and a common mechanistic picture can be used for the interpretation of phenomena occurring with these metals.

In the 1960s, Göhr and Kruger investigated the behavior of cobalt in perchloric acid solution using measurements carried out under controlled potential and current [93,94]. The results were interpreted on the basis of thermodynamic data. It was concluded that at open circuit and at small polarizations cobalt corrodes exclusively with hydrogen evolution. The possibility of the reduction of ClO_4^- under these conditions was not considered as a physical reality.

Similar conclusions were drawn in case of other iron-group metals as presented in the survey article by Lorenz and Heusler devoted to the problems of the dissolution of iron-group metals [79]. On the other hand, it is an almost generally accepted view that the nature of the anions present in the solution phase in contact with the dissolving metal plays an important role in the kinetics and mechanism of the dissolution process.

It is assumed that the main factor determining the effect of anions in these reactions is the adsorbability of the anion, i.e. the direct interaction of anions with the metal surface. Generally, it is assumed that this interaction does not lead to the chemical transformation of the anion. It is also assumed that the adsorbability of ClO_4^- on iron-group metals is very low; thus, the adsorption of other anions can be studied in the presence of perchlorate supporting electrolyte without significant role of adsorption competition.

However, the validity of this assumption could be questioned in the light of some recent studies [20] and revisiting some results reported in the literature more than fifty years ago [95,96].

As mentioned above, the problem of perchlorate contamination of ground waters is nowadays an important environmental issue [24,37-39], and several methods were suggested and elaborated for reductive elimination of ClO_4^-. One of these methods, reported quite recently, is the reduction with metallic iron. The results obtained from these practical studies can be

considered convincing evidence of the reduction interaction of Fe with ClO_4^-. Results with Co prove that the rate and extent of the reduction process could also be very characteristic [97]. Under suitable chosen experimental conditions, even this process could be the predominant reaction in the dissolution of metallic cobalt in the presence of ClO_4^-.

In contrast to Fe and Co, a relatively slow reduction was found in the presence of Ni [83]. Nevertheless, it can be stated unambiguously that ClO_4^- dissolved in acidic aqueous solutions can be reduced with Ni [83], Fe [98], and Co [97] metals. According to [99], significant reduction of perchlorate to chloride ions occurred on the nickel cathode in a cell with a nickel working electrode and a platinum counter electrode in concentrated solutions of $HClO_4$. It has been shown that the mechanism of this process involves platinum deposited in small amounts on the cathode as a result of oxidation of the platinum anode in the perchloric acid solution. The reduction of perchlorate was accompanied by oxidation of the nickel cathode, which can be attributed to chlorate ions formed in the initial step of perchlorate reduction.

To estimate the relative role of ClO_4^- reduction in the overall dissolution process of Ni, Fe, and Co, we summarized some data obtained in previous studies of metal-perchlorate (perchloric acid) interaction (Table 2). It may be seen that the rate of the formation of Cl^- from ClO_4^- is relatively low in the case of Ni at ambient temperature, while for Fe and Co, depending on the experimental conditions, the reduction of ClO_4^- could play a substantial role in the overall process. Considering this situation, it could be expected that the results of the usual corrosion measurements carried out in the presence of acidic perchlorate solution should reflect this role in the case of Co and Fe.

Table 2. *Interaction of Ni, Fe, and Co with ClO_4^- at T = 25°C*

	Electrolyte		A	B		
	$HClO_4$/M	$NaClO_4$/M	Chemical amount corresponding to the mass of dissolved metal, mol	Chemical amount of Cl^- formed during the dissolution of metal, mol	B / A	Conversion* / %
Ni	3		3.57×10^{-2}	7.5×10^{-5}	2.1×10^{-3}	0.84
	1		1.26×10^{-2}	2.6×10^{-5}	2.0×10^{-3}	0.80
Fe	1	2	1.80×10^{-3}	8.6×10^{-5}	4.77×10^{-2}	19.6
	0.1	2.9	5.73×10^{-4}	4.56×10^{-5}	7.96×10^{-2}	31.8
	0.1	0.9	4.48×10^{-4}	2.92×10^{-5}	6.52×10^{-2}	26.1
	0.5	0	4.48×10^{-4}	2.96×10^{-5}	6.61×10^{-2}	26.4
	1	0	1.27×10^{-3}	5.75×10^{-5}	4.53×10^{-2}	18.1
Co	1	0	9.48×10^{-4}	4.95×10^{-5}	5.2×10^{-2}	20.1
	4	0	14.45×10^{-4}	15.74×10^{-5}	1.09×10^{-1}	43.5
	0.1	1.9	11.73×10^{-4}	9.54×10^{-5}	8.1×10^{-2}	32.5

* The percentage of dissolved metal involved in ClO_4^- reduction (see text).

The data presented in the Table 2 were obtained using metal powders. Thus, they should be considered as average values as during the dissolution process the parameters of the systems are changing continuously. Some of these factors are as follows:

i) The H^+ concentration is changing according to the following equation

$$c_{H^+} = c^0_{H^+} - 8c_{Cl^-} - 2\left(c_{Co^{2+}} - 4c_{Cl^-}\right) = c^0_{H^+} - 2c_{Co^{2+}} \quad (5.1)$$

ii) The surface area of the metal powder is changing in the course of the dissolution process [100].

The change in the H^+ concentration could be very important at low initial $HClO_4$ concentrations. For instance, taking into consideration the data reported in Table 2 for the dissolution of Co at 0.1 mol dm^{-3} $HClO_4$ concentration at 25 °C using 25 ml solution, the final H^+ concentration is

$$c_{H^+} = (0.10 - 0.094) = 6\times10^{-3}\text{mol dm}^{-3}. \quad (5.2)$$

This means that at the end of the dissolution experiment, the hydrogen ion concentration is more than one order of magnitude lower than that in the initial state.

Only in the case of high H^+ concentration (4 mol dm^{-3}) can be expected a practically constant acidity during the whole dissolution experiment. The problems caused by the H^+ consumption are well reflected in the temperature dependence of the conversion of ClO_4^- to Cl^- in the presence of Co powder.

At low $HClO_4$ concentrations (0.1 and 1 mol dm^{-3}), the scattering of the data is remarkable, while in the case of a solution of 4 mol dm^{-3} $HClO_4$, a monotonous increase can be observed.

The change in the pH influences not only the rate of the perchlorate reduction – metal dissolution, but also the adsorption of the produced Cl^-. The adsorption phenomena were studied on powdered metals [100]. The principle of the method used was the measurement of radiation intensity originating from labeled adsorbed species on a powdered metal layer sprinkled on a thin plastic foil that serves simultaneously as the window for radiation measurement. The measurements were carried out at ambient temperature in an Ar atmosphere. Radiotracer experiments at different H^+-ion concentrations can be seen in Figure 12. The adsorption of Cl^- decreases with the pH.

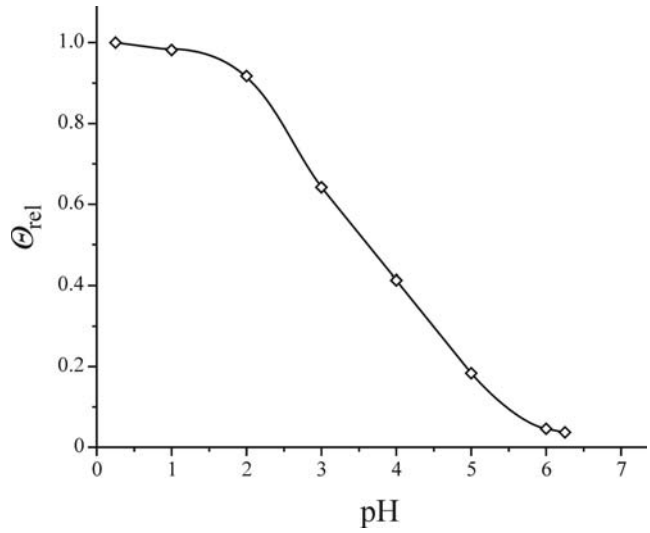

Figure 12. *The pH dependence of the adsorption of chloride ions (on relative scale) on Co.*

It should be noted, however, that attempting the study of the adsorption of labeled Cl^- on powdered Co in 0.5 M $NaClO_4$ solution at low pH values, for instance, pH ≈ 2 (by addition of $HClO_4$) the count-rate vs. time curves (curves 1, 2 and 3 in Figure 13) going through maximum were obtained.

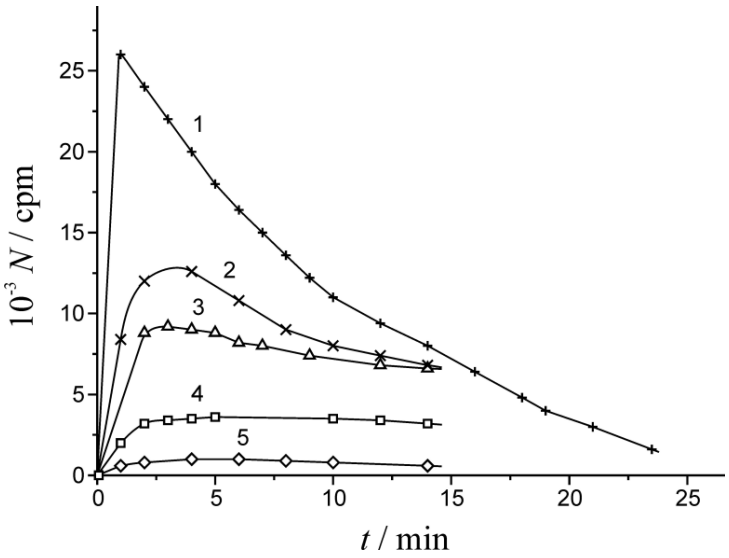

Figure 13. *Count-rate vs. time curves obtained following the addition of 0.25 ml 1 mol dm^{-3} $HClO_4$ to a solution of 0.5 mol dm^{-3} $NaClO_4$ + 1×10^{-4} mol dm^{-3} labeled Cl^- in contact with 0.5 g Co powder. (1) First run, (2) second run, (3) third run, (4) addition of 1×10^{-4} mol NaCl, (5) addition of 5×10^{-4} mol NaCl. Adapted from [98].*

The decrease in the count-rate means that no equilibrium or steady state is attained with respect to the surface concentration of the isotope emitting the radiation. This phenomenon can be explained by the production of inactive Cl^- (*i.e.* by the decrease of specific activity of Cl^- species). The displacement of the active species by non-active ones occurs immediately at the surface and this could be the very reason for the rapid decrease of the count-rate in the case of curve (1).

In the course of the corrosion, the pH also shifts from the initial pH ≈ 2 value to higher ones. In order to demonstrate that the decrease in the count-rate is mainly determined by the production of inactive Cl^-, $HClO_4$ was added again to the solution phase shifting the pH to the original value. The results of this procedure presented by curves 2 and 3 in Figure 13 show that the maximum in the count-rate is significantly lower than that for curve 1 and that the maxima are less pronounced in the two former cases. This observation is in agreement with the assumption of the production of Cl^-. It is evident that with decreasing specific activity the "isotopic dilution" caused by the production of further Cl^- becomes less and less pronounced and this is reflected by the position and shape of the maxima on curves 1, 2, and 3.

Curves 4 and 5 in Figure 13 were obtained following the addition of inactive NaCl to the solution phase. In this case, the "isotopic dilution" was carried by direct addition of inactive Cl^-. The effect observed is in accordance with the expectation. In the course of the corrosion of Co powder, Cl^- are formed from the ClO_4^-. Thus, the pH dependence presented in Figure 12 was determined starting from pH = 6 and measuring the radiation intensity only a short period following a shift of pH to a preselected value. For more details about anion adsorption see Ref. [101].

6. Conclusion

The experimental evidence collected during the previous decades unambiguously indicates that the electrochemical stability of perchlorate ions holds no promise. Starting from this statement, experimental data and theoretical considerations based on the concept of stability of ClO_4^- should be rigorously revised, given the large number of such publications in the electrochemical

literature. On the other hand, the electrochemical treatment method is one of the ways considered as applicable for solving the perchlorate contamination problem.

***Acknowledgements**: Financial support from Hungarian Scientific Research Fund (OTKA) is acknowledged (OTKA-67994/OMFB-01078/2007 and PD75445).*

References

[1] S. Ya. Vasina, O. A. Petrii, *Elektrokhim.* **6** (1970) 242-246.
[2] G. Horányi, E. M. Rizmayer, *J. Electroanal. Chem*. **198** (1986) 379-391.
[3] C. K. Rhee, M. Wasberg, G. Horányi, A. Wieckowski, *J. Electroanal. Chem.* **291** (1990) 281-287.
[4] C. K. Rhee, M. Wasberg, P. Zelenay, A. Wieckowski, *Catal. Lett.* **10** (1991) 149-164.
[5] J. Clavilier, M. Wasberg, M. Petit, L. H. Klein, *J. Electroanal. Chem*. **374** (1994) 123-131.
[6] I. Bakos, G. Horányi, *J. Electroanal. Chem*. **332** (1992) 147-154.
[7] G. Horányi, I. Bakos, React. *Kinet. Catal.* L. **46** (1992) 139-144.
[8] G. Horányi, I. Bakos, *J. Electroanal. Chem*. **331** (1992) 727-737.
[9] G. Horányi, G. Vértes, *J. Electroanal. Chem*. **64** (1975) 252-254.
[10] G. Horányi, G. Vértes, *Inorg. Nucl. Chem. Lett.* **10** (1974) 767-770.
[11] J. Paoinot, J. Augustynski, *Electrochim*. *Acta* **20** (1975) 747-752.
[12] G. M. Brown, *J*. *Electroanal*. *Chem*. **198** (1986) 319-330.
[13] M. Sanches Cruz, M. J. Gonzalez Tejera, M. C. Villamanan, *Electrochim*. *Acta* **30** (1985) 1563-1569.
[14] F. Colom, M. J. Gonzalez Tejera, *J. Electroanal. Chem*. **190** (1985) 243-255.
[15] I. Bakos, G. Horányi, S. Szabó, E. M. Rizmayer, *J. Electroanal. Chem.* **359** (1993) 241-252.
[16] G. Horányi, I. Bakos, *J. Appl. Electrochem*. 23 (1993) 547-552.
[17] C. M. V. B. Almeida, B. F. Giannetti, T. Rabockai, *J. Electroanal. Chem*. **422** (1997) 185-189.
[18] G. Horányi, I. Bakos, *ACH-Models Chem*. **131** (1994) 25-41.
[19] G. Horányi, in *Catalysis; A Specialist Periodical Report* (J. J. Spivey, Ed.) The Royal Society of Chemistry, Cambridge, GB. 1996; Vol. **12**, pp. 254-301.
[20] G. G. Láng, G. Horányi, *J. Electroanal. Chem.* **552** (2003) 197-211.
[21] G. M. Brown, B. Gu, in *Perchlorate, Environmental Occurence, Interactions and Treatment*, (B. Gu, J.D. Coates Eds.) Springer Publishers, 2006, pp.17-47.
[22] U.S. Environmental Protection Agency (US EPA), *EPA report, Perchlorate Environmental Contamination: Toxicological Review and Risk Characterization*, 2002.
[23] I. H. Yoon, X. Meng, C. Wang, K.W. Kim, S. Bang, E. Choe, L. Lippincott, *J. Hazard. Mater.* **164** (2009) 87–94.
[24] E. T. Urbansky, *Perchlorate in the Environment*, Kluwer Academic Publisher, Dordrecht, 2001.
[25] E. T. Urbansky, *Environ. Sci. Pollut.* R. **9** (2002) 187-192.
[26] E. T. Urbansky, M.R. Schock, *J. Environ. Manage.* **56** (1999) 79-95.
[27] C. Steinmaus, M. D. Miller, A. H. Smith, *J. Occup. Environ. Med.* **52** (2010) 1217-1224.
[28] Y. Cai, Y. Shi, P. Zhang, S. Mou, G. Jiang, *Prog*. *Chem*. **18** (2006) 1554-1564.
[29] Y. Shi, P. Zhang, Y. Wang, J. Shi, Y. Cai, S. Mou, G. Jiang, *Environ. Int.* **33** (2007) 955-962.
[30] L. Lu, Y. Wang, J. He, *Chin. J. Geochem*. **25** (2006) (Suppl. 1), 255.
[31] Z. Wang, D. Forsyth, B. P.-Y. Lau, L. Pelletier, R. Bronson, D. Gaertner, *J. Agr. Food Chem*. **57** (2009) 9250–9255.
[32] T. R. Tellez, C. P. Michaud, A. C. Reyes, B. C. Blount, C. B. Van Landingham, K. S. Crump, J. P. Gibbs, *Thyroid* **15** (2005) 963–975.

[33] J. V. Dyke, K. Ito, T. Obitsu, Y. Hisamatsu, P. K. Dasgupta, B. C. Blount, *Environ. Sci. Technol*. **41** (2007) 88–92.
[34] H. Gal, N. Weisbrod, O. Dahan, Z. Ronen, R. Nativ, *J. Hydrol.* **378** (2009) 142–149.
[35] P. K. Dasgupta, A. B. Kirk, J. V. Dyke, S. I. Ohira, *Environ. Sci. Technol.* **42** (2008) 8115-8121.
[36] B. C. Blount, K. U. Alwis, R. B. Jain, B. L. Solomon, J. C. Morrow, W. A. Jackson, *Environ. Sci. Technol*. **44** (2010) 9564-9570.
[37] R. Srinivasan, G. Sorial, *Sep. Purif. Technol* **69** (2009) 7-21.
[38] R. Srinivasan, G. Sorial, E. Sahle-Demessie, *Environ. Eng. Sci.* **26** (2009) 1661-1671.
[39] E. Kociolek-Balawejder, L. J. Wilk, *Przem*. *Chem*. **88** (2009) 1221-1228.
[40] T. L. Theis, A. K. Zander, X. Li, J. Sene, M. A. Anderson, *J. Water Supply Res. T.* **51** (2002) 367-374.
[41] Y. Zhang, S. Mu, B. Deng, J. Zheng, *J. Electroanal. Chem*. **641** (2010) 1-6.
[42] D. B. Cordes, M. Smiglak, C. C. Hines, N. J. Bridges, M. Dilip, G. Srinivasan, A. Metlen, R. D. Rogers, *Chem. Eur. J.* **15** (2009) 13441-13448.
[43] X. D. Wang, W. Y. Wu, G. F. Tu, K. X. Jiang, *T. Nonferr. Metal. Soc.* **20** (2010) 2032-2036.
[44] L. Huang, S. Cheng, G. Chen, *J. Chem. Technol. Biot.* **86** (2011) 481-491.
[45] J. C. Thrash, J. I. Van Trump, K. A. Weber, E. Miller, L. A. Achenbach, J.D. Coates, *Environ*. *Sci. Technol*. **41** (2007) 1740-1746.
[46] C. S. Butler, P. Clauwaert, S. J. Green, W. Verstraete, R. Nerenberg, *Environ. Sci. Technol.* **44** (2010) 4685-4691.
[47] M. M. Abu-Omar, *Chem. Commun*. **17** (2003) 2102-2111.
[48] M. M. Abu-Omar, *Comment. Inorg. Chem*. **24** (2003) 15-37.
[49] K. D. Hurley, J. R. Shapley, *Environ. Sci. Technol*. **41** (2007) 2044-2049.
[50] Y. Zhang, K. D. Hurley, J. R. Shapley, *Inorg. Chem.* **50** (2011) 1534-1543.
[51] K. D. Hurley, Y. Zhang, J. R. Shapley, *J. Amer. Chem. Soc.* **131** (2009) 14172-14173.
[52] J. H. Xu, N. Y. Gao, Y. L. Tang, Y. Deng, M. H. Sui, *J. Environ. Sci.-China* **22** (2010) 1807-1813.
[53] J. H. Xu, N. Y. Gao, Y. Deng, M. H. Sui, Y. L. Tang, *J. Colloid Interf. Sci.* **357** (2011) 474-479.
[54] A. M. Moore, C. H. de Leon, T. M. Young, *Environ. Sci. Technol*. **37** (2003) 3189-3198.
[55] S. Y. Oh, D. K. Cha, P. C. Chiu, B. J. Kim, *Water Sci. Technol.* **54** (2006) 47-53.
[56] L. Butula, I. Butula, *Croat. Chem. Acta* **43** (1971) 131.
[57] G. Horányi, *Catal. Today* **19** (1994) 285-311.
[58] S. A. Bilmes, N. R. De Tacconi, A. J. Arvia, *J. Electroanal. Chem.* **143** (1983) 179-194.
[59] M. Hourani, A. Wieckowski, *J. Electroanal. Chem.* **244** (1988) 147-161.
[60] N. Kizhekevariam, M. J. Weaver, *Surf. Sci.* **277** (1992) 21-30.
[61] M. Wasberg, G. Horányi, *J. Electroanal. Chem*. **381** (1995) 151-158.
[62] M. Wasberg, G. Horányi, *J. Electroanal. Chem*. **385** (1995) 63-70.
[63] A. Ahmadi, R. W. Evans, G. Attard, *J. Electroanal. Chem.* **350** (1993) 279-295.
[64] A. Ahmadi, E. Bracey, R. W. Evans, G. Attard, *J. Electroanal. Chem.* **350** (1993) 297-316.
[65] M. Wasberg, J. Bácskai, G. Inzelt, G. Horányi, *J. Electroanal. Chem.* **418** (1996) 195-198.
[66] T. Pajkossy, L. A. Kibler, D. M. Kolb, *J. Electroanal. Chem*. **600** (2007) 113–118.
[67] G. G. Láng, N. S. Sas, M. Ujvári, G. Horányi, *Electrochim. Acta*, **53** (2008) 7436–7444.
[68] G. Láng, L. Péter, *ACH-Models Chem.* **131** (1994) 137-153.
[69] D. M. Wang, H. Y. Lin, S. Ismat Shah, C. Y. Ni, C. P. Huang, *Sep. Purif. Technol* **67** (2009) 127-134.
[70] R. J. Magee, T. J. Cardwell in *Encyclopedia of Electrochemistry of the Elements,* (A. J. Bard Ed.) Marcel Dekker, New York, 1974, Vol. **2**.
[71] L. Kiss, *Kinetics of Electrochemical Metal Dissolution* (*Studies in Physical and Theoretical Chemistry*, Vol. **47**) Elsevier, Amsterdam, 1988.
[72] G. Láng, G.Inzelt, *Electrochim. Acta* **44** (1999) 2037-2051.

[73] G. Láng, J. Bácskai, G. Inzelt, *Electrochim. Acta* **38** (1993) 773-780.
[74] V. Torma, G. Láng, *Magy. Kém. Foly.* **104** (1998) 265-276.
[75] J-B. Jorcin, M. E. Orazem, N. Pébère, B. Tribollet, *Electrochim. Acta* **51** (2006) 1473-1479.
[76] G. G. Láng, M. Ujvári, T. A. Rokob, G. Inzelt, *Electrochim. Acta* **51** (2006) 1680-1694.
[77] D. D. Macdonald, *Electrochim. Acta* **51** (2006) 1376-1388.
[78] M. Ujvári, G. G. Láng, Investigation of the electrochemical reduction of chlorate and perchlorate ions on rhodium, *2nd Regional Symp. on Electrochemistry South-East Europe*, Belgrade, Serbia, June 6-10, 2010, Book of Abstracts, PEA-O-03.
[79] W. J. Lorenz, K. E. Heusler in *Corrosion Mechanisms,* (F. Mansfeld Ed.) Marcel Dekker, New York, 1987, pp 1-83.
[80] S. Y. Zhao, S. H. Chen, H. Y. Ma, D. G. Li, F. J. Kong, *J. Appl. Electrochem.* **32** (2002) 231-235.
[81] H. Ma, G. Li, S. Chen, S. Zhao, X. Cheng, *Corr. Sci.* **44** (2002) 1177-1191.
[82] F. Zucchi, M. Fonsati, G. Trabanelli, *J. Appl. Electrochem*. **28** (1998) 441-447.
[83] M. Ujvári, G. Láng, G. Horányi, *J. Appl. Electrochem.* **31** (2001) 1171-1173.
[84] M. Ujvári, G. Láng, G. Horányi, *J. Appl. Electrochem*. **32** (2002) 581-582.
[85] G. Láng, M. Ujvári, G. Horányi, *Corr. Sci.* **45** (2003) 1-5.
[86] M. Pagitsas, M. Pavlidou, D. Sazou, *Electrochim. Acta* **53** (2008) 4784-4795.
[87] M. A. Amin, *Electrochim. Acta* **54** (2009) 1857-1863.
[88] L. Li, S. H. Chen, X. G. Yang, C. Wang, W. J. Guo, *J. Electroanal. Chem*. **572** (2004) 41-49.
[89] J. Lei, S. Rudenja, N. Magtoto, J. A. Kelber, *Thin Solid Films* **497** (2006) 121 – 129.
[90] H. H. Hassan, *Electrochim. Acta* **51** (2006) 5966-5972.
[91] H. H. Hassan, M. A. Amin, S. Gubbala, M. K. Sunkara, *Electrochim. Acta* **52** (2007) 6929-6937.
[92] G. Láng, G. Inzelt, A. Vrabecz, G. Horányi, *J. Electroanal. Chem.* **582** (2005) 249-257.
[93] H. Göhr, *Electrochim*. Acta **11** (1966) 827-834.
[94] H. Göhr, H. Krüger, *Electrochim. Acta* **11** (1966) 835-847.
[95] A. M. Lecco, V. D. Canić, *Glasnik Hemijskog Društva Beograd* **14** (1949) 249-251.
[96] V. C. Canić, *Glasnik Hemijskog Društva Beograd*, **16** (1951) 13-18.
[97] G. G. Láng, A. Vrabecz, G. Horányi, *Electrochem. Commun*. **5** (2003) 609-612.
[98] M. Ujvári, G. Láng, G. Horányi, *J. Appl. Electrochem.* **32** (2002) 1403-1406.
[99] M. Y. Rusanova, P. Polaskova, M. Muzikar, W. R. Fawcett, *Electrochim. Acta* **51** (2006) 3097-3101.
[100] G. Horányi, *Corr. Sci.* **46** (2004) 1741-1749.
[101] G.G. Láng, M. Ujvári in *Perchlorates: Production, Uses and Health Effects,* (L.E. Matthews, Ed.) Nova Publishers, in press, ISBN: 978-1-61122-857-1

J. Electrochem. Sci. Eng. **1(1)** (2011) 27-37; doi: **10.5599/jese.2011.0005**

Open Access : : ISSN 1847-9286
www.jESE-online.org

Original scientific paper

Effective numbers of electrons as a criterion of carbon suitability as a hemosorbent

MOGELY KHUBUTIYA, BORIS GRAFOV*, MIKHAIL GOLDIN**✉, ALEXEI DAVYDOV*, VLADIMIR KOLESNIKOV*** and MARK GOLDIN

N.V. Sklifosovsky Research Institute of Emergency Medicine, Sukharevskaya pl. 3, Moscow, 129010, Russia
**A. N. Frumkin Institute of Physical Chemistry and Electrochemistry, Russian Academy of Sciences, Leninskii pr. 31, Moscow, 119991, Russia*
***Liberty University, 1971 University Blvd., Lynchburg, VA 24502-2213, USA*
****D.I. Mendeleev University of Chemical Technology of Russia, Miusskaya pl. 9, Moscow, 125047, Russia*

✉Corresponding Author: E-mail: mgoldin@liberty.edu; Tel.: +1-434-582-2210; Fax: +1-434-582-2488

Received: May 20, 2011; Revised: August 01, 2011; Published: August 20, 2011

Abstract

The number of medical applications of electrochemistry has grown in recent years due to the increased applications of electrochemical concepts to various systems of the organism. This includes electrochemically controlled hemosorption detoxification, where the removal of toxicants is controlled by changing the potential of the hemosorbent. It is important to avoid Faradaic processes in the course of hemosorption, which can lead to the addition of electrochemically modified toxicants to blood. The probability of their occurrence should depend on the open-circuit potential of the activated carbon. In order to elucidate the identification of Faradaic reactions, a model system was investigated. The adsorption of copper ions, tert-butanol and acetone on samples of electrochemically modified AG-3 activated carbon hemosorbent with various open-circuit potentials was used as a model of the detoxification processes. The effective number of electrons transferred in the elementary act of adsorption was shown to be a non-zero quantity for all three cases, which corroborates an electrochemical mechanism of hemosorption. For the cupric ions, ranges of open-circuit potentials were identified corresponding to different mechanisms of adsorption and Faradaic processes.

Keywords

Activated carbon; Thermally expanded graphite; Hemosorption; Open-circuit potential; Effective number of electrons

Introduction

A continual increase of the number of applications of electrochemistry in modern medical technologies is primarily due to the broader use made of theoretical electrochemical concepts in the functioning of various systems of the human organism. Of note here are the works of Sawyer *et al*. [1-2] on electrochemically induced intravascular thrombosis (blood clotting) by introducing anodically polarized metal conductors into damaged blood vessels in order to attract negatively charged blood components to the electrode and stop the hemorrhage. These investigations were continued by Guglielmi, et al. and applied for the treatment of aneurisms [3-6].

At the present time, one of the leading applications of electrochemical concepts in medicine is the ideas of Nordenström and his model of homeostasis as a biologically closed electric circuit [7], in which blood flowing through the blood vessels is treated as a conductor of electrical signals. Vascular walls and other tissues possess electrochemical potentials whose values depend on the state of the tissue (i.e., normal, inflamed, damaged, etc.). Potentials measured with platinum electrodes implanted into the tissue can serve as a source of information about the presence or absence of certain pathological states in the vicinity of the implanted electrode. Based on the above model, Nordenström proposed and realized an electrochemical method of treatment for malignant carcinomas by passing DC current through the affected areas of tissue in order to impose certain potentials upon it [8,9].

Another novel medical treatment also has electrochemical basis, *viz.*, detoxification by means of electrochemically controlled hemosorption [10,11]. In this electrochemical model, the hemosorbent was considered to be a porous electrode immersed in aqueous 0.15 M sodium chloride solution. Based on such an approach, an important conclusion was reached as to the mechanism of interaction between the negatively charged formed elements of blood and the activated carbon hemosorbent. The sign and magnitude of the charge of the hemosorbent surface is determined by its potential. The latter, in turn, depends on the nature of the activated carbon material, since the composition of the electrolyte (blood) remains virtually unchanged.

The electrochemical model of hemosorption has made it possible to find a new approach to identifying new promising materials suitable as potential hemosorbents. This is important, since the requirements towards “good” hemosorbents are quite rigorous and somewhat self-contradictory: on the one hand, such a material must be indifferent towards blood, while on the other it should maintain high adsorption activity towards the toxicants being removed from blood. By treating the hemosorbent/blood interface as an electrochemical system, authors [10,11] were able to assert the possibility of controlling the removal of toxicants from blood via polarization of the hemosorbent (which is usually a porous carbon material). An important aspect of this, however, is the mechanism of interaction between the carbon material and the electrolyte (blood), since adsorption on activated carbon may include the occurrence of Faradaic processes. Such processes may occur in cases where the potential of the hemosorbent in blood is comparable to the reduction or oxidation potential of the toxicant.

It is well known that Faradaic processes (especially electrooxidation) can lead to highly undesirable effects in blood. For example, anodic oxidation of proteins leads to their denaturation [12]. At the same time, Frumkin showed [13] that the potential of an electrode depends on the adsorption of organic and inorganic substances on it.

Unfortunately, electrochemical data are rarely given or utilized in carbon adsorption research. For instance, authors of [14] considered the properties of the carbon/electrolyte interface when certain cations are adsorbed; however, while the authors [14] recounted Frumkin’s conception of

activated carbon as an oxygen electrode, they considered chromene-like groups that generate resonance-stabilized carbonium ions to be the initiators of adsorption activity of carbons [15].

Thus, consideration of carbon potential may help elucidate the mechanism of adsorption on carbons and reveal the presence or absence of Faradaic processes during it. For this purpose the mathematical expressions given in [16] can be used, which are based on Frumkin's conception of activated carbon as a perfectly polarizable electrode, i.e. an electrode whose state is fully dependent on the amount of electrical charge consumed [13]. The total charge q of a perfectly polarizable electrode is a function of both electrode potential E and the amount Γ of adsorbed electrochemically indifferent surface-active substance. Since the measurements are being made in an open circuit, an assumption can be made that the total charge of the carbon q is constant

$$q = q(E,\Gamma) = const \quad (1)$$

and therefore its total differential is equal to zero:

$$\mathrm{d}q = \left(\frac{\partial q}{\partial E}\right)_{\Gamma} \mathrm{d}E + \left(\frac{\partial q}{\partial \Gamma}\right)_{E} \mathrm{d}\Gamma = 0 \quad (2)$$

In line with [16,17], $(\partial q/\partial E)_{\Gamma} = C_{\infty}$, i.e. the capacitance of the electrode at a sufficiently high frequency; and $-(\partial q/\partial \Gamma)_{E} = nF$. Therefore:

$$C_{\infty}\,\mathrm{d}E - nF\,\mathrm{d}\Gamma = 0$$

which can be rearranged as

$$C_{\infty}\,\mathrm{d}E = nF\,\mathrm{d}\Gamma$$

Isolating n, one would obtain:

$$n = \frac{C_{\infty}}{F}\frac{\mathrm{d}E}{\mathrm{d}\Gamma} \quad (3)$$

Finally, if the assumption is made that the ratio $dE/d\Gamma \approx \Delta E/\Delta\Gamma$, i.e., replacing the first derivative of potential with respect to adsorption by the finite ratio of changes in E and Γ, the following expression is obtained, from which the effective number of electrons can be estimated:

$$n = (C_{\infty}\cdot\Delta E)/(F\cdot\Delta\Gamma), \quad (4)$$

where n – effective number of electrons needed for the elementary act of adsorption and/or Faradaic process, C_{∞} (F) – differential capacitance of the adsorbent, ΔE / V – OCP shift corresponding to a relatively short period of time t, F (= 96500 C mol^{-1}) – Faraday's constant, $\Delta\Gamma$ / mol – change in the adsorption (Gibbs' surface excess) of the adsorbate during time t. Equation (3) can be used for computations of the effective number of electrons. Thus, the empirical data needed to calculate the value of n are the open-circuit potentials of activated carbon and corresponding values of adsorption. The value of differential capacitance C_{∞} = 100 F was used for 1 g of activated carbon according to the data in [18]. An approximation was made that the capacitance C_{∞} of the adsorbent is weakly dependent on the electrode potential and Gibbs' adsorption of the adsorbate.

With the above considerations, the effective number of electrons transferred in the elementary act of adsorption process or Faradaic process was chosen as the criterion of suitability of carbon materials for use as hemosorbents: *viz.*, the virtual absence of Faradaic processes points to the suitability of such hemosorbents. The adsorption of certain undissociated organic toxicants and

cupric ions was chosen for a model-based investigation of the applicability of the concept of effective charge transfer for hemosorption.

Experimental

An IPC-Pro L potentiostat (Volta Co. Ltd, Russia) was used for measurements of polarization curves; it was also utilized for OCP measurements. A saturated silver/silver chloride electrode was used as the reference electrode in all measurements. Adsorption of acetone and 2-methyl-2-propanol (*tert*-butanol, TB) was investigated using gas chromatography. An SRI 310C chromatograph (SRI Instruments, USA) with a 1 m HayeSep-D packed column and a catalytic combustion detector, as well as a Shimadzu GC17 chromatograph with a CarboWAX 20M phase, were used. 0.150 M NaCl or 0.200 M Na_2SO_4 solutions were used as a supporting electrolyte in adsorption and potential measurements of the organic compounds and in measurements of the initial carbon potentials.

Adsorption of organic compounds and cupric ions was investigated on AG-3 activated carbon; the OCP value of the initial sample measured in 0.200 M Na_2SO_4 was 50 mV (*vs.* Ag/AgCl). Modification of the AG-3 carbon was carried out according to [10,11] in the cell shown in Fig. 1. The granules of initial activated carbon were placed in the anode (1) and cathode (2) chambers separated by perforated discs made from a dielectric material (8), with the granules subsequently compressed by the current-carrying discs (6) by turning the bolts (7). A peristaltic pump was used to pass an aqueous sodium chloride solution through the assembled cell at a flow rate of 50 mL/min. Carbon was modified galvanostatically with a current of 0.75 A for 10 to 90 min, with subsequent washing of the cathodically and anodically modified carbons to a pH = 7. As a result of the modification, carbons with OCP values in the range between +475 mV and –775 mV (*vs.* Ag/AgCl) were obtained and used for further experiments.

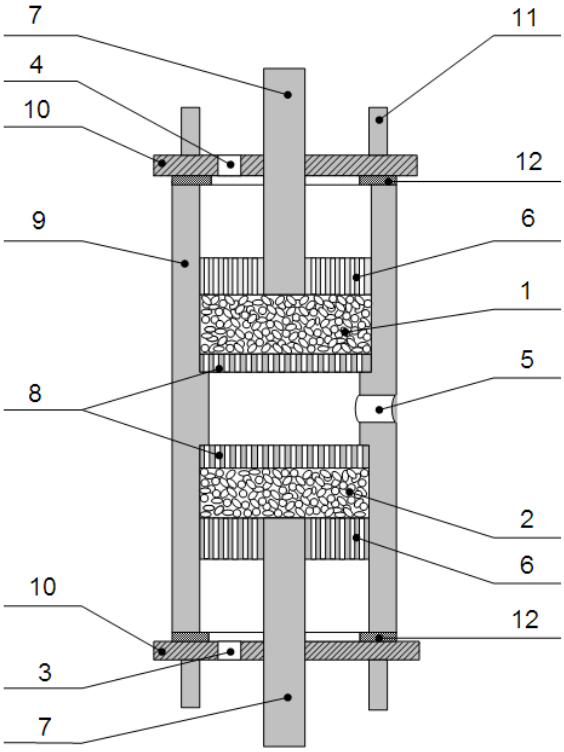

Figure 1. *Flow-through cell for the electrochemical modification of activated carbon: 1 – anodic chamber, 2 – cathodic chamber, 3 – electrolyte inlet, 4 – electrolyte outlet, 5 – alternative inlet for solution or reference electrode, 6 – stainless steel perforated current-carrying disc, 7 – stainless steel bolt, 8 – perforated polymer disc, 9 – housing, 10 – covers, 11 – screw, 12 – rubber gasket.*

The amount of copper adsorbed on activated carbon was determined spectrometrically by measuring the concentration change of Cu^{2+} ions in aqueous 0.100 M $CuSO_4$ solution on scanning UV/visible spectrophotometers Genesys 10uv (Thermo Scientific, USA) at λ_{max} = 808 nm in the form of copper sulfate and Beckman-Coulter DU 800 at λ_{max} = 607 nm in the form of an amino complex. Carbon OCP was recorded simultaneously with solution sampling. Contact time of the activated carbon with the solution was 30 min.

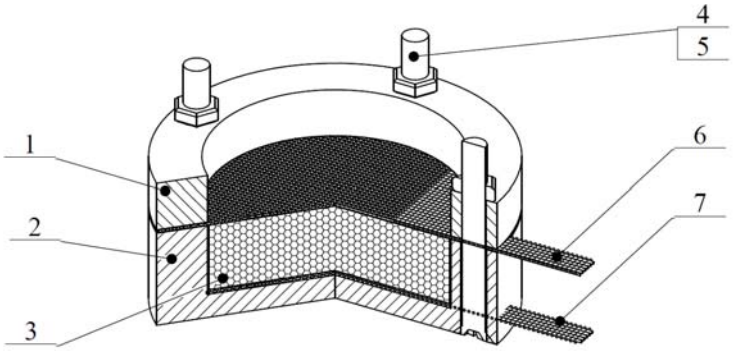

Figure 2. Non-flow-through cell for measurement of granulated carbon OCP: 1 – clamp cover, 2 – housing,3 – cylindrical chamber, 4,5 – Teflon bolts and nuts, 6,7 – current-carrying stainless steel meshes.

Carbon OCP was measured in a non-flow-through apparatus described in [19], shown in Fig. 2. This apparatus was immersed in solution with constant stirring at 100 rpm using a magnetic stirrer. Carbon granules were placed in the cylindrical chamber (3) of the apparatus and compressed against the stainless steel meshes (6,7) by the cover (1). The current-carrying meshes and the reference electrode were connected to the potentiostat, and the time dependence of OCP values was recorded. Since the surface area of the carbon is 1000 m^2/g, while the surface area of the steel mesh is on the order of 10^{-4} – 10^{-5} m^2, the potential measured is that of the carbon and not of the current-carrying steel.

Cyclic voltammetry was used to obtain a potentiodynamic charging curve for computation of differential capacitance of AG-3 activated carbon. A single granule of AG-3 carbon was placed in a three-electrode cell. Thermally expanded graphite was used as the current collector and the auxiliary electrode. The cyclic voltammogram was collected at a scan rate of 0.5 mV/s in the range between –800 mV and +600 mV.

Results and Discussion

As noted above, carbon modification in the present work was performed according to the method previously developed in [10,11]. It was shown in [11] that anodic and cathodic treatment of carbon led to significant changes in the composition of its surface functional groups (Table 1).

As seen from the data shown in Table 1, cathodic treatment of activated carbon drastically reduced the amount of acidic functional groups on carbon surface, while anodic treatment increases their amount. This trend is observed regardless of the acidity of the electrolyte used for modification. Thus, cathodic treatment results in the reduction of oxygenated surface functional groups, while anodic treatment leads to the oxidation of carbon atoms.

OCP data for unmodified and electrochemically modified AG-3 carbon samples during contact with solutions of acetone (in 0.150 M NaCl) and TB (in 0.20 M Na_2SO_4) were obtained as a time dependence, with corresponding concentration changes of the organic compounds in solution. A typical graph of OCP and adsorption, calculated from chromatographic data, is shown in Fig. 3 (for TB on unmodified AG-3); similar dependences were obtained for all other samples. Zero

adsorption corresponds to the initial potential of AG-3 in the experiment in the investigated solution.

Table 1. *Influence of electrochemical modification of activated carbon on its surface functional groups [11].*

Type of treatment	Amount of functional group, mmol g^{-1}		
	Carboxyl	Lactone	Phenol
Initial untreated carbon	0.47	0.10	0.18
NaCl solution (pH = 11.5)			
cathodic	0	0	0
anodic	0.41	0.30	0.32
NaCl solution (pH = 1.4)			
cathodic	0.15	0.04	0.20
anodic	0.51	0.16	0.20

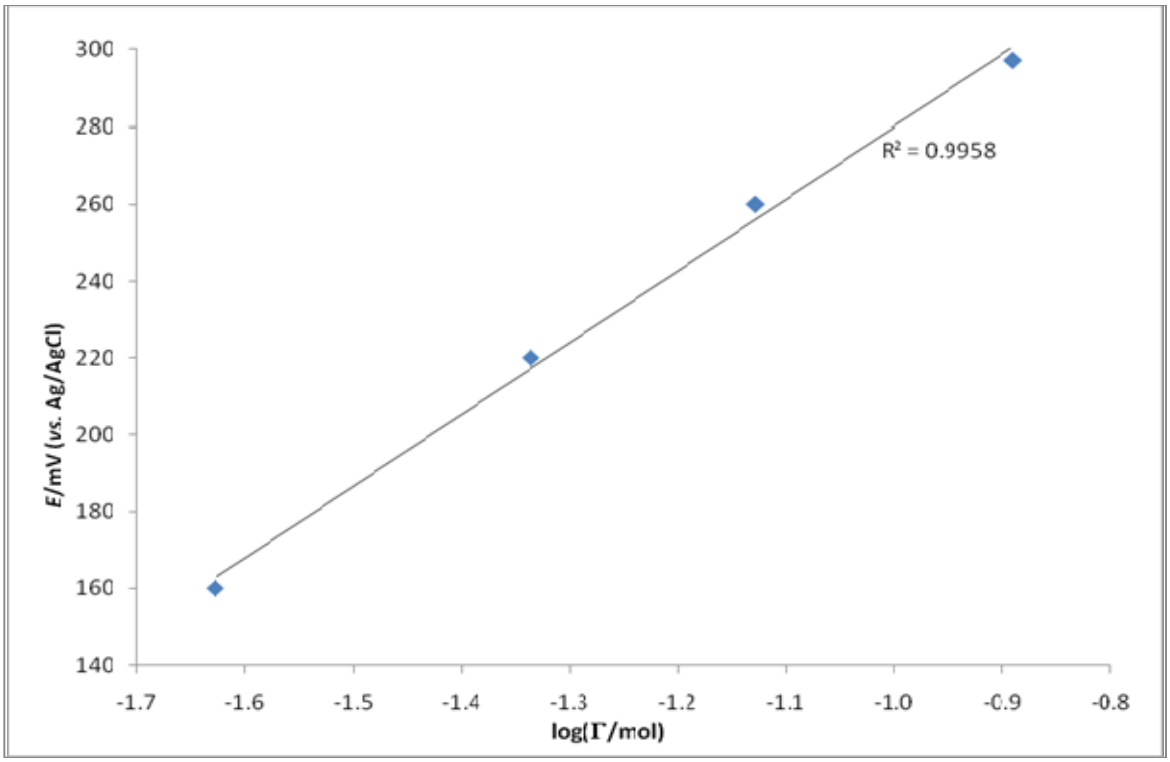

Figure 3. *Dependence of the OCP of AG-3 carbon on TB adsorption from 0.20 M Na_2SO_4. Initial TB concentration: 77 g/L.*

Differential Capacitance

The differential capacitance of the AG-3 activated carbon was computed based on the potentiodynamic data. An 8.0 mg carbon sample was used, and potentials were scanned in the range between –700 mV and +500 mV at a scan rate of 0.5 mV/s. The resulting dependence of potential on differential capacitance is shown in Fig. 4.

A minimum at C_{min} = 78.7 F per gram and a maximum at C_{max} = 121 F per gram were observed. The average value of differential capacitance from the calculated results was C_{avg} = 95.4 F per gram of carbon, which closely matches the literature data [18]. Thus, the value of capacitance C_{∞} = 100 F per gram of carbon was used in all further computations.

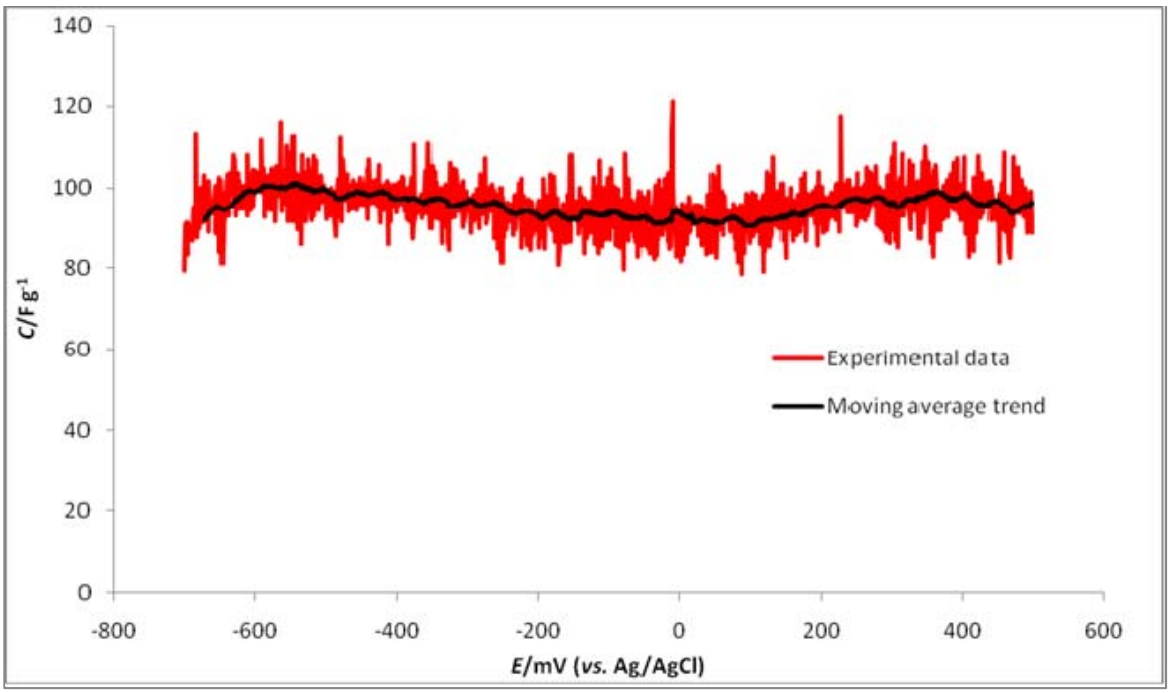

Figure 4. *Differential capacitance per gram of AG-3 activated carbon as a function of potential.*

Adsorption of Organic Molecules

Based on the final OCP and adsorption values for unmodified and electrochemically modified AG-3 carbon samples, effective numbers of electrons were calculated for acetone and TB adsorption. The results are summarized in Tables 2-3. It should be noted that these calculations reflect the integral character of effective charge transfer in the range from $E_{initial}$ to E_{final}.

Table 2. *Adsorption of* tert-*butanol on AG-3 carbon. Potentials reported vs. Ag/AgCl.*

m_{carbon}/g	$E_{initial}$/mV	E_{final}/mV	ΔE/mV	ΔΓ/mmol	n
2.0157	-670	-590	+80	12	0.014
1.8550	-267	-8	+259	12	0.043
2.0461	0	+165	+165	11	0.046
1.9979	+35	+280	+245	9.7	0.046
1.9763	+85	+300	+215	9.9	0.035
2.1517	+280	+450	+170	13	0.034
1.6763	+380	+575	+195	11	0.018
1.6747	+425	+540	+115	10.	0.014

Table 3. *Adsorption of acetone on AG-3 carbon. Carbon mass* m = 10.00 g. *(Potentials vs. Ag/AgCl).*

$E_{initial}$/mV	E_{final}/mV	ΔE/mV	ΔΓ/mmol	n
+440	+580	+140	72	0.020
+310	+460	+150	88	0.018
+190	+290	+100	95	0.011
+102	+190	+88	110	0.0084
-96	+45	+141	110	0.013
-144	-10	+134	98	0.014

Calculated values for the effective number of electrons in the course of adsorption of organic molecules on AG-3 carbon were quite small (0.0084 to 0.046). This may indicate that Faradaic processes do not contribute significantly to the adsorption process of these substances. Importantly, adsorption of all of these compounds on AG-3 carbon is accompanied by a positive shift in carbon OCP, which points to an electrochemical mechanism of adsorption (since changes in an electrochemical parameter are observed).

Adsorption of Cupric Ions

Similar adsorption experiments were performed on AG-3 carbon samples in aqueous $CuSO_4$. The most important results of these experiments are summarized in Table 4. A typical time dependence of the OCP and concentration (for unmodified AG-3) is shown in Fig. 5. Fig. 6 shows the dependence of the "local" effective number of electrons (calculated between data points) on potential in the course of the experiment described in Fig. 6. Discrete values of (E, n) correspond to the elapsed time, as shown next to each point in the figure. It can be seen from Fig. 6 that the process of adsorption reaches equilibrium after about 30 min, as the "local" effective number of electrons transferred reaches zero (within the precision of the experimental data).

Table 4. *Integral values of the effective numbers of electrons* n *in the course of* Cu^{2+} *ion adsorption on AG-3 carbon with various initial potentials. Carbon masses (*m_{carbon}*) as shown below. (Potentials* vs. *Ag/AgCl)*

m_{carbon}/g	E_{init}/mV	E_{final}/mV	ΔE/mV	Γ/mmol	n
5.022	–775	40	815	2.1	2.07
4.990	–700	40	740	1.8	2.13
5.007	–580	40	620	1.5	2.15
5.001	–470	47	517	1.4	1.91

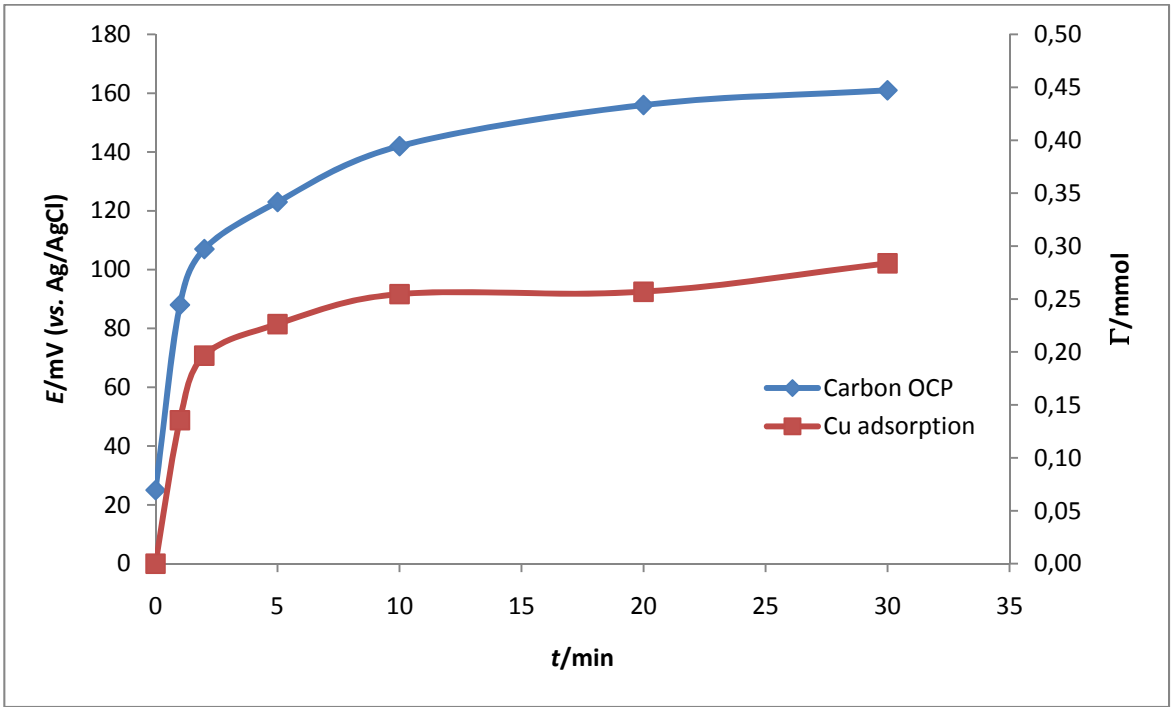

Figure 5. *Time dependence of the OCP of unmodified AG-3 carbon and the adsorption of cupric ions from solution.*

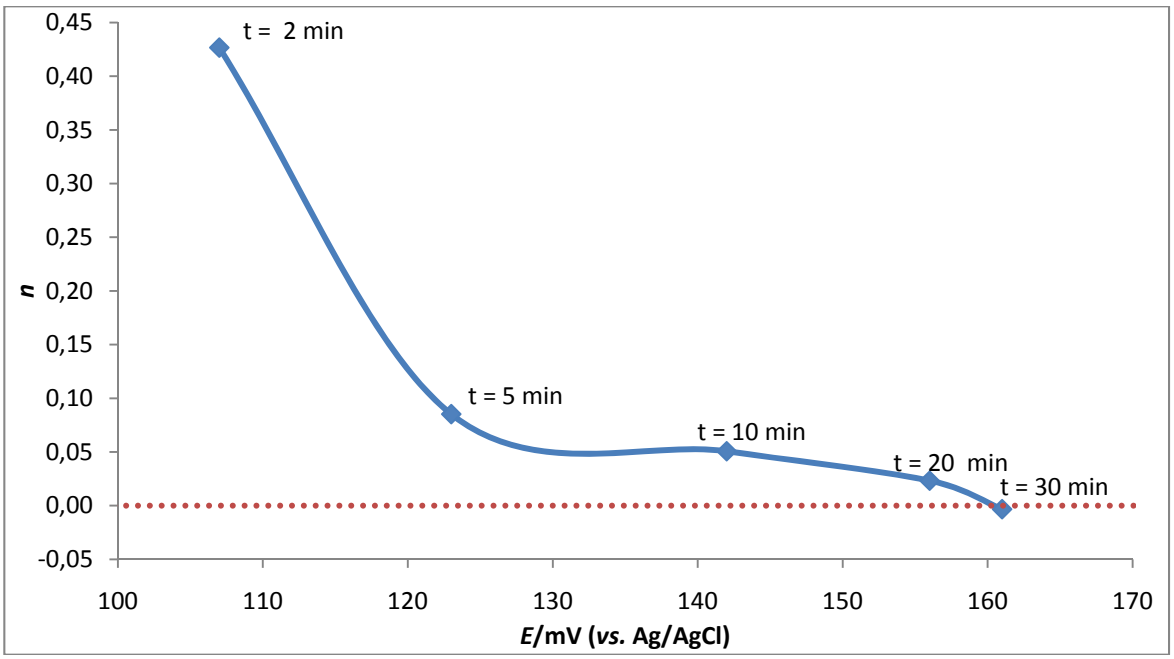

Figure 6. *Dependence of the effective number of electrons on the OCP of unmodified AG-3 carbon during Cu^{2+} adsorption.*

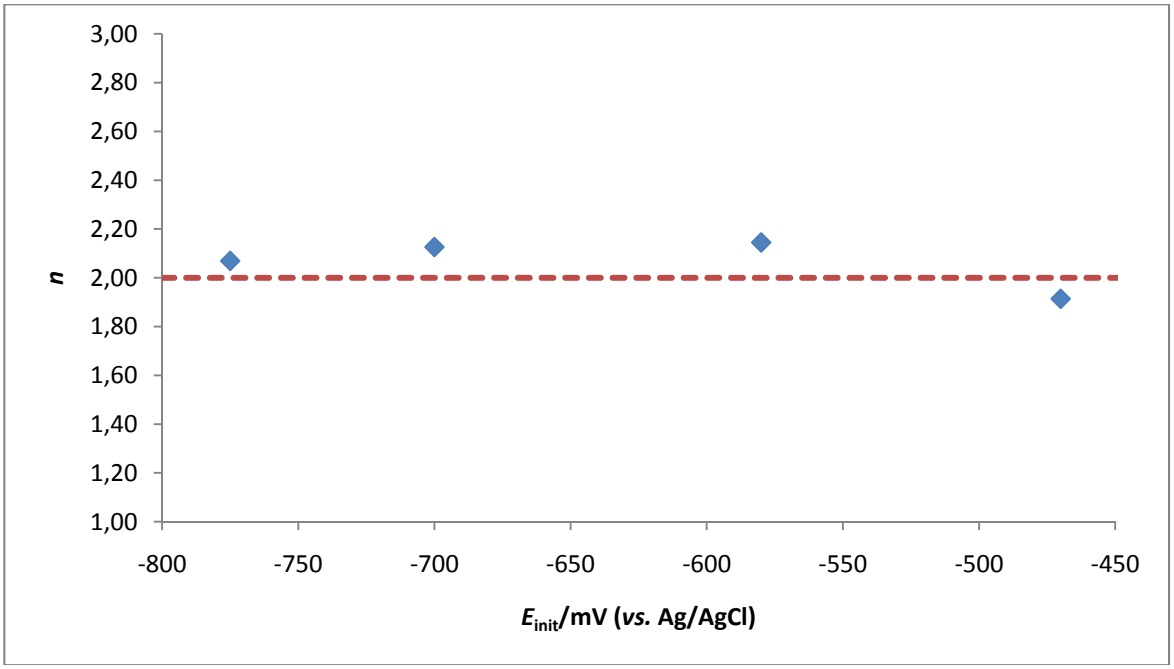

Figure 7. *Dependence of the integral effective number of electrons on the initial open-circuit potential of carbon for Cu^{2+} cation adsorption on AG-3 carbon.*

For initial carbon potentials in the range between –775 and –470 mV (vs. Ag/AgCl), the data obtained (Table 4 and Fig. 7) shows effective numbers of electrons $n \approx 2$. This corresponds to the two-electron Faradaic open-circuit process of copper electroreduction on the carbon:

$$R'—C + Cu^{2+} + H_2O \rightarrow R'—C{=}O + Cu^0 + 2H^+ \quad (5)$$

This is also corroborated by the appearance of a characteristic reddish-colored copper deposit on the carbon granules after cathodically modified AG-3 is immersed in aqueous $CuSO_4$. Thus, it is possible to detect the presence of Faradaic processes in the course of adsorption by measuring OCP and calculating the effective number of electrons. (It should also be noted that, while noble

metals are known to deposit onto carbons [20], the literature does not relate this to the OCP of carbon.)

Probability of One-Electron Copper Reduction

Importantly, one should consider the probability of the one-electron reduction process in the course of adsorption (as a competing process, with possible further transformation of Cu^{+}):

$$Cu^{2+} + e^{-} \rightarrow Cu^{+} \quad (6)$$

$$Cu^{+} + e^{-} \rightarrow Cu^{0} \quad (7)$$

The determination of Cu^{+} in solution is rather difficult, since it quickly disproportionates in solution:

$$2Cu^{+} \rightarrow Cu^{2+} + Cu^{0} \quad (8)$$

In electrolytic refining of copper [21], bulk $[Cu^{+}]$ concentration for aqueous $CuSO_4$ in equilibrium with metallic copper was *ca*. three orders of magnitude below $[Cu^{2+}]$, *i.e.* virtually negligible. Other investigations [22-26], however, suggest a stepwise mechanism for the deposition of cupric ions/ionization of metallic copper, with excess Cu^{+} in the interphase region as an intermediate between Cu^{0} and Cu^{2+}.

While a polarographic method of Cu^{+} determination in solution has been proposed [27], it involves the addition of organic ligands that might interact with activated carbon, making this method impractical for the present work. In addition, if Cu^{+} only exists in excess near the interface, as suggested by [22-26], it would be difficult to detect it at an additional electrode removed from the vicinity of the carbon surface. Thus, it is not possible to elucidate the involvement of Cu^{+} in the investigated processes. However, regardless of mechanistic details, Faradaic reduction of Cu^{2+} to metallic Cu^{0} undoubtedly occurs in the above experiments; this is also corroborated by the calculated values of *n*.

Conclusions

Thus, experimental data on the effective number of electrons unequivocally confirm an electrochemical mechanism of hemosorption. All effective numbers of electrons were calculated assuming that the electric double layer capacitance remained constant despite significant potential changes of the carbon. For the model processes of acetone and TB adsorption it was shown that the adsorption of an organic toxicant on AG-3 activated carbon took place virtually without any electron transfer, *i.e.* Faradaic processes did not occur, while the carbon potential did change in the course of adsorption. The interaction of copper cations with the surface of activated carbon depended on carbon potential: for potentials more negative than –470 mV (*vs.* Ag/AgCl), the two-electron Faradaic process of copper deposition $Cu^{2+} + 2e^{-} \rightarrow Cu^{0}$ occurred, as reflected by calculated values of the effective number of electrons.

Therefore, it is possible to determine the mechanism of adsorbate interaction with an activated carbon hemosorbent by performing open-circuit potential and adsorption measurements. The effective number of electrons can be calculated and utilized as a criterion of hemosorbent suitability, since it allows the detection of Faradaic processes between the hemosorbent and adsorbate. It is important that the phenomenon of partial transfer of charge allows working hemosorbens to be reclassified according to their electric effectiveness.

Acknowledgements*: This study is supported by funds from the Center for Research and Scholarship Fund of Liberty University. Grant # 021_030110. We wish to thank the anonymous referee for a thorough reading of and valuable suggestions for the present paper.*

References

[1] P.N. Sawyer, J.W. Pate, *Am. J. Physiol.* **175** (1953) 113–117
[2] P.N. Sawyer, J.W. Pate, C.S. Weldon, *Am. J. Physiol.* **175** (1953) 108–112
[3] G. Guglielmi, F. Viñuela, I. Sepetka, V. Macellari, *J. Neurosurg.* **75** (1991) 1–7
[4] G. Guglielmi, F. Viñuela, J. Dion, G. Duckwiler, *J. Neurosurg.* **75** (1991) 8–14
[5] G. Guglielmi, F. Viñuela, in *Neurosurgery Clinics of North America: Endovascular Approach to Central Nervous System Disease,* L.N. Hopkins, Ed., Saunders, Philadelphia, PA, 1994, vol. 5, p. 427–435
[6] G. Guglielmi, in: *Neuroimaging Clinics of North America: Interventional Neuroradiology,* F. Viñuela, J. Dion, G. Duckwiler, Eds., Saunders, Philadelphia, PA, 1992, vol.2, p. 269–278.
[7] B.E.W. Nordenström, *Biologically closed electrical circuits*, Nordic medical publication, Stockholm, 1983, p. 358.
[8] B.E.W. Nordenström, in *New radiologic imaging and intervention in general surgery*, G. Ussia , F. Bassi, J.T. Feirucci, Eds., Masson, Milano, 1989, p. 143-159
[9] B.E.W. Nordenström, *Electromagnetic Biology and Medicine* **3** (1984) 137 – 154
[10] Mark M. Goldin, A.G. Volkov, Yu.S. Goldfarb, Mikhail M. Goldin, *J. Electrochem. Soc.* **153** (2006) J91-J99
[11] M.R. Tarasevich, Mark M. Goldin, Ye.A. Luzhnikov, V.A. Bogdanovskaya, in *Itogi Nauki i Tekhniki:Electrochemistry*, Yu.M. Polukarov, Ed., VINITI, Moscow, 1990, vol.31, p. 127-150 [in Russian]
[12] asilyev Yu.B., Sergienko V. I., *Elektrokhimiya*, **23** (1987) 661-662 [in Russian]
[13] A. N. Frumkin, E. A. Ponomarenko, R. H. Burshtein, *Doklady Acad. Sci. USSR* **149** (1963) 1123-1126
[14] *Chemistry and physics of carbon*, L.R.Radovich, Ed., vol. **27**, Marcel Dekker, NY, 2001
[15] V.A. Garten, D.E. Weiss, *Rev. Pure and Applied Chem* **7** (1957) 69-122
[16] A.N. Frumkin, V.I. Melik-Gaykazyan, *Doklady Acad. Sci. USSR* **77** (1951) 855-858
[17] B.M. Grafov, V.V. Elkin, *J. Electroanal. Chem.* **304** (1991) 31-40
[18] A.Yu. Rychagov, N.A. Urisson and Yu.M. Volfkovich, *Russ. J. Electrochem.* **37** (2001) 1172–1179
[19] Mikhail M. Goldin, V.A. Kolesnikov, M.Sh. Khubutiya, A.G. Volkov, G.J. Blanchard, A.K. Evseev, Mark M. Goldin, *J. Appl. Electrochem.* **38** (2008) 1369–1374
[20] M.P. Yunusov, I.V. Perezdrienko, Sh.N. Namazbaev, T.B. Molodozhenyuk, *Khimicheskaya promyshlennost* **8** (2003) 382-385 [in Russian]
[21] N.P. Fedotyev, A.F. Alabyshev, A.P. Rotinyan, P.M. Vyacheslavov, P.B. Zhivotinskiy, A.A. Galnbek, *Prikladnaya elektrokhimiya*, 2nd ed., Khimiya, Leningrad, 1967, 600 p [in Russian]
[22] A.I. Molodov, G.N. Markosyan, I.R. Lyumkis, V.V. Losev, *Elektrokhimiya* **9** (1973) 1460-1467 [in Russian]
[23] A.I. Molodov, G.N. Markosyan, V.V. Losev, *Elektrokhimiya* **7** (1972) 263-267 [in Russian]
[24] A.I. Molodov, *Elektrokhimiya* **6** (1970) 365-369 [in Russian]
[25] V.V. Losev, L.E. Sribnyi, A.I. Molodov, *Elektrokhimiya* **2** (1966) 1431-1437 [in Russian]
[26] Yu.S. Dmitriev, A.A. Murtazina, A.S. Kolosov, *Elektrokhimiya* **5** (1969) 106-108 [in Russian]
[27] J.A. Altermatt, S.E. Manahan, *Anal. Chem.* **40** (1968) 655-657

J. Electrochem. Sci. Eng. **1(1)** (2011) 39-54; doi: **10.5599/jese.2011.0004**

Open Access : : ISSN 1847-9286
www.jESE-online.org

Original scientific paper

External control of anodic dissolution mechanisms of 100Cr6 in nitrate/chloride mixed electrolytes

ANDREAS LESCH, GUNTHER WITTSTOCK✉, CHRIS BURGER*, BENJAMIN WALTHER* and JÜRGEN HACKENBERG*

Department of Pure and Applied Chemistry, CIS - Center of Interface Science, Faculty of Mathematics and Natural Sciences, Carl von Ossietzky University of Oldenburg, D–26111 Oldenburg, Germany
**Robert Bosch GmbH, Stuttgart, Germany*

✉Corresponding Author: gunther.wittstock@uni-oldenburg.de; Tel.: +49 441 7983971; Fax: +49 441 7983979

Received: June 17, 2011; Published: August 20, 2011

Abstract

The anodic dissolution of 100Cr6 steel in neutral electrolytes containing sodium chloride and sodium nitrate was investigated potentiodynamically and galvanodynamically with a rotating disc electrode at room temperature. The total concentration of the mixed electrolyte was 3 mol L^{-1} with variation of chloride/nitrate mole ratios. The potentiodynamic linear sweep voltammograms (LSVs) in mixed electrolytes are similar to the LSVs in pure chloride electrolyte at lower current densities and switch to behaviour observed in pure nitrate electrolytes at higher current densities. Provided that both anions are present, it seems that the dissolution reactions at the steel anode are determined by the interface layer only. The effect of these layers on surface quality and current efficiency was also investigated in a flow channel applying galvanostatic pulses. An evidence for different dissolution mechanisms can be seen with an important influence of duty cycle and flow conditions. This allows external control of the desired dissolution mechanism in mixed electrolytes.

Keywords

Electrochemical machining; Mixed electrolyte; Anodic dissolution; Rotating disc electrode; Flow channel; Galvanostatic pulses

1. Introduction

Electrochemical machining (ECM) is often applied to deburring and shaping components made of e.g. iron and steels in aqueous inorganic salt electrolytes[1,2]. Shape and surface of work pieces are modified by high rate anodic dissolution at high current densities (10-150 A cm^{-2}) with a special

designed cathode as tool. The resulting gap width is usually below one millimetre. High electrolyte flow velocities (5-50 m s^{-1}) are required to remove reaction products and Joule heat. The precision of pulsed ECM is higher compared to direct current ECM because reaction products can be removed during pulse off time [3]. Sodium chloride and sodium nitrate are often used as electrolytes in industrial ECM because of low costs and labour safety aspects. Anodic dissolution of iron and many steels in pure sodium chloride and in pure sodium nitrate electrolytes has been investigated in great detail [4-9]. The dissolution mechanisms in both electrolytes differ strongly and result in very different features of the machined work piece. In chloride media an active anodic dissolution takes place whereas nitrate anions cause a passivation of the substrate surface and transpassive dissolution can be observed. Methods of characterizing the dissolution mechanism are anodic polarization curves, analysis of the resulting surface quality and weight-loss measurements in order to determine the current efficiency. The anodic dissolution of pure iron in chloride electrolyte is divalent over a wide range of current density and the current efficiency is closely to 100 % [5]. Hydrogen is developed in the counter reaction at the cathode [10]. In nitrate media the evolution of oxygen takes place as a second import anodic reaction and the anodic dissolution of iron leads simultaneously to Fe^{2+} ions and Fe^{3+} ions [8,11,12]. At low current densities the iron dissolution efficiency is close to zero because the anodic current originates from oxygen evolution. With increasing current density the current efficiency of the anodic iron dissolution increases up to 90 % but oxygen evolution is still present [11]. The reduction of nitrate anions takes place at the cathode [1].

The anodic dissolution of iron and many steels is mass transport-controlled and reaction products enrich at the anode interface [5,6]. Electrochemically inert metal carbides cause an apparent higher current efficiency for carbide-containing steels because the measured weight-loss includes the mass of carbide particles that were detached but not dissolved during the ECM treatment [13,14]. Qualitative anodic dissolution models explain the observed dissolution behaviour and the resulting surfaces. A two-layer model explains the dissolution in nitrate electrolyte [8,15,16]. Because of the current density-dependent divalent/trivalent dissolution of iron, different iron oxides (Fe_2O_3 and Fe_3O_4) are formed and cover the steel surface as a thin film. An adherent liquid polishing film consisting of supersaturated iron nitrate hydrates is built at the oxide/electrolyte interface and causes a decreasing oxygen evolution rate [11,16]. In chloride media a weakly attached, easily removable black, carbide-rich solid surface film and a thin polishing film consisting of $FeCl_2$, $Fe(OH)_2$ and FeO ($Fe_xO_yCl_z$) are formed at the active-steel-anode/electrolyte interface [14]. In NaCl electrolyte the dissolution rate is higher than in $NaNO_3$ electrolyte due to active dissolution and high current efficiency while in $NaNO_3$ electrolyte a much better dimensional control can be reached.

The anodic dissolution of mild steel in chloride/nitrate mixed electrolytes has been described by Hoare, LaBoda and Mao [17,18]. From their steady-state anodic polarization curves, film stripping and current efficiency measurements, they concluded that chloride anions cause only a localized attack of passive films formed in the presence of nitrate anions on the steel surface. Depending on the chloride/nitrate ratio, the chloride anions lower the oxidation power of the nitrate anions, prevent the formation of a compact, protective film and only a non-protective salt film is present and the resulting surfaces are severe cratered. At lower potentials an active dissolution caused by the chloride anions takes place while passivation and transpassive dissolution dominates the behaviour at more positive potentials. With increasing chloride/nitrate ratio, the work piece surface is passivated at higher potentials [18]. Chloride/nitrate mixed electrolyte have been used

in pulse and pulse reverse through-mask ECM of channels for flow field in stainless steel bipolar plates for PEM fuel cells [19], where the process improved the surface roughness of the channels at the expense of the process time and the rib/channel width uniformity compared to the process in pure chloride electrolyte.

According to the reported results from Mao et al [18] we describe in this paper more detailed insights and process conditions under which the dissolution mechanism of soft annealed steel in chloride/nitrate mixed electrolytes can be externally controlled, i.e. switched between two mechanisms. The influence of varying flow conditions at a rotating disc electrode and in a flow channel as well as the influence of applied potentiodynamic, galvanodynamic and galvanostatic pulse series show clearly the possibility to switch in one and the same electrolyte exclusively by external control (current or voltage, hydrodynamics) between both dissolution mechanisms allowing fast machining rates using the chloride mechanism and high precision by the nitrate mechanism in order to obtain crater-free surfaces.

Experimental

Specimens

Spheroidization-annealed 100Cr6 cylinders (annealed to globular cementite, 5 mm diameter) were used as specimens from which the cross sectional surfaces were investigated. The 100Cr6 steel is mainly composed of approximately 96 wt. % iron, 1.5 wt. % chromium and 1 wt. % carbon. Carbon is contained as C in the steel matrix (20 % of total C content), as globular Fe_3C (40 % of total C content) with diameters of approximately 1-3 µm and as 100 nm-slices $Fe_{2.5}C$ (40 % of total C content). The metal carbides were considered to be electrochemically inert under the applied conditions. Directly before and after the experiments the specimens were washed with distilled water and isopropanol.

Electrolytes

Aqueous solutions of sodium chloride and sodium nitrate served as electrolytes. The total salt concentration c_{tot} was set to 3 mol L^{-1} with variation of chloride/nitrate mole ratio. The chloride/nitrate concentration ratio is given as the relative chloride concentration θ (Eq. 1).

$$\Theta = \frac{c_{Cl^-}}{c_{tot}} \tag{1}$$

The electrolyte temperature was (23±1) °C. With increasing θ the measured conductivity increases from 156 mS cm^{-1} (θ = 0) up to 194 mS cm^{-1} (θ = 1).

Rotating disc electrode (RDE)

The measurements of potentiodynamic and galvanodynamic scans or cyclic voltammograms (CVs) were performed with a rotating disc electrode and potentiostat VoltaLab 80 PGZ402 & VoltaMaster4 Software (Radiometer Analytical SAS). The front surfaces of the 100Cr6 specimens were ground mechanically with SiC papers and the cylinder barrels were masked with an insulating galvanic polyester tape before each measurement. These samples were used as working electrodes (WE) in a three electrode cell completed by a platinized titanium net as counter electrode (CE) and an Ag/AgCl/sat. KCl reference electrode (RE). WE and CE had an electrode distance of approximately 1 cm. The scan rate for potentiodynamic experiments was set to 50 mV s^{-1}. In this paper all potentials *E* are referred to the standard hydrogen electrode (SHE). Under the

typical rotation rate of 3000 rpm laminar flow conditions are expected. Incipient turbulences must, however, be expected because of grinding marks at the work piece surface, roughness due to anodic dissolution and recess of the surface below the galvanic polyester tape used to mask the side walls of the sample cylinders.

Flow channel

A flow channel in form of a parallel plate reactor was used. The flow velocity was set to 7 m s^{-1} assuming turbulent flow conditions [20]. Mechanical grinding was done for preparation of the specimens. A steel cathode with 5 mm diameter was positioned directly opposite to the 100Cr6 specimen with a gap of 0.75 mm before start of anodic dissolution. The electrodes were fixed and, therefore, the gap width increased during experiments. With this two-electrode configuration galvanostatic pulses up to 40 A cm^{-2} were applied with a custom made galvanostat (plating electronic GmbH, Germany). No current was applied during pulse off time. The pulse times were in the range of milliseconds. The duty cycle γ is

$$\gamma = \frac{t_{on}}{t_{on} + t_{off}} \tag{2}$$

t_{on} is the pulse on time and t_{off} is the pulse off time. An averaged current i_d can be calculated with γ and pulse current i_p (Eq. 3 [21]).

$$i_d = i_p \cdot \frac{t_{on}}{t_{on} + t_{off}} = i_p \cdot \gamma \tag{3}$$

Multiplying i_d with measuring time t_{tot} gives flowing charge Q (Eq. 4):

$$Q = i_d \cdot t_{tot} \tag{4}$$

The theoretical weight loss Δm_{theo} was calculated by the Faraday law (Eq. 5):

$$\Delta m_{theo} = \frac{i_d \cdot t_{tot} \cdot M}{z \cdot F} = \frac{Q \cdot M}{z \cdot F} \tag{5}$$

where M is the molar mass of iron and F is the Faraday constant. The dissolution valence z was taken as 2 in all calculations knowing that the valence is between 2 and 3 in $NaNO_3$ electrolyte depending on current density [11]. Current efficiency η is then given by equation 6:

$$\eta = \frac{\Delta m_{tot}}{\Delta m_{theo}} \cdot 100\%. \tag{6}$$

where Δm_{tot} is the total experimental mass loss of the specimens which was obtained as mass difference before and after the dissolution. Duty cylces γ of 0.625, 0.5 and 0.167 were applied with charges Q between 50 and 300 C.

Surface characterisation

Observation with optical microscopes was used for rough classification of the dissolution mechanisms. The topography of the surface was measured with confocal microscope nanofocus µsurf (NanoFocus AG), for which regions in the middle of the surface were chosen at which minor streaming artefacts occur. The 3D average roughness S_a was then calculated with software nanoExplorer XT. The topography was filtered in waviness and roughness by a robust Gauss-filter

with a cut-off wavelength of 0.25 mm. S_a is the arithmetic mean of the absolute distances of the surface points from the mean plane and is given by equation 7:

$$S_a = \frac{1}{NL}\sum_{j}^{N}\sum_{i}^{L}|Z|\left(x_j, y_i\right) \quad (7)$$

N and *L* are the indexes of measured points in *x*- and *y*-direction. This method facilitates a relative comparison of the resulting surface roughnesses. Additionally, the resulting surfaces were examined with scanning electron microscope (SEM) EVO 50 VPX (Carl Zeiss AG). An Everhart-Thornley-detector and an acceleration voltage of 20 kV were used for 1000× enlargement with a work distance of 10 mm.

Results and Discussion

Sharp transition from active to transpassive dissolution at resting electrode

Linear sweep voltammograms (LSV) were recorded between -0.5 V and 7.2 V. Figure 1 shows the LSVs in pure NaCl electrolyte (θ = 1), in pure $NaNO_3$ electrolyte (θ = 0) and in mixed electrolytes with θ = 0.67, 0.5 and 0.33 at a resting electrode.

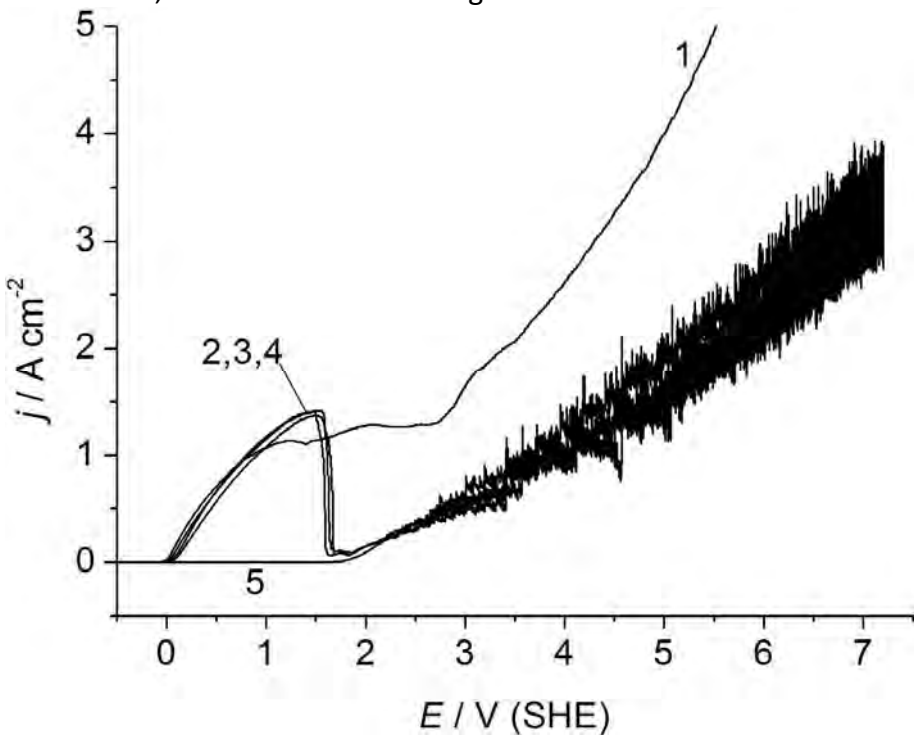

Figure 1. *LSVs in 3 M NaCl, 3 M $NaNO_3$ and in three chloride/nitrate mixed electrolytes; static WE; Scan rate 50 mV s^{-1}; relative chloride concentrations θ: 1 (1), 0.67 (2), 0.5 (3), 0.33 (4), 0 (5).*

The curves of the pure electrolytes show the well known behaviour of active (NaCl) and transpassive dissolution ($NaNO_3$) [1]. In NaCl electrolyte a limiting current is reached because the concentration of reaction products increases to saturation. Thus a limiting current plateau is built until the overlimiting current is reached and the current increases again. In $NaNO_3$ electrolyte fluctuating current densities are caused by the evolution of oxygen at the WE which sets in at 1.8 V. The curves that were measured in the three mixed electrolytes overlap with each other. They agree qualitatively with earlier reports about anodic dissolution in mixed electrolytes [18]. Surprisingly, there is no strong influence of the relative chloride ion concentration on the anodic dissolution at the resting WE in Figure 1. At low potentials active dissolution takes place, indicated

by an increasing current density from 0 V on. The surface is suddenly passivated at approximately 1.6 V and the current density decreases to nearly 0 A cm^{-2}, oxygen evolution starts at 1.8 V and transpassive dissolution sets in at higher current densities. With respect to the models of metal/electrolyte interface [11,14,16] the following mechanistic model can be proposed. At lower current densities which occur at potentials below 1.6 V at the resting electrode, the dissolution mechanism must be dominated by the chloride anions and the LSV is very similar to the curve in pure chloride solution. In this paper this section of LSVs will be called "chloride curve". Due to active dissolution, the chloride polishing film is formed. The nitrate anions are larger than chloride anions. Most likely their incorporation in the polishing film changes the structure of the polishing film so that no diffusion controlled current regime (plateau in the pure NaCl electrolyte) is observed in mixed electrolytes. The higher the current density, the higher is the active dissolution rate of the steel. Chloride anions have to diffuse from the bulk of the electrolyte through the diffusion layer to the steel surface. When the current density becomes higher than approximately 1.4 A cm^{-2} not enough chloride anions reach the steel surface. Therefore, the nitrate polishing film composed of iron nitrate hydrates is formed. This film could withdraw the water from the chloride polishing layer. Hence, iron chloride could be precipitated and could be displaced by the nitrate polishing film and the anodic dissolution is dominated by the nitrate anions at potentials higher than 1.8 V. Hence, the transpassive dissolution sets in at higher current densities at E > 1.8 V and this section of LSVs is called "nitrate curve" below. The transition from active to transpassive dissolution can also be observed visually (see Figure SM-11 in Supporting Information). During active dissolution the assumed reaction products creep down as a green viscose film. After passivation, the evolution of oxygen breaks off the visible flakes of the black carbide-containing layer from the anode surface. It is suggested that this surface layer is equal to the one in pure NaCl electrolyte. Haisch et al. [7] investigated the surface layer obtained in pure NaCl electrolyte by energy dispersive X-ray microanalysis. They reported that the particles of this layer mainly consist of Fe, Cr and C and suggested that they originate from the carbides in the steel matrix [7]. Transpassive dissolution can be observed by the formation of oxygen bubbles and yellow-brown colouration of the solution.

Influence of anion transport on the transition from active to transpassive dissolution at RDE

For further experiments the WE was operated as RDE in order to improve the removal of oxidation products and simulate the electrolyte flow under technical ECM conditions. This leads to an increasing of limiting current in NaCl electrolyte [22] and to a less fluctuating current density in $NaNO_3$ electrolyte in corresponding LSVs at 3000 rpm (Figure 2).

In pure 3 M NaCl electrolyte no limiting current plateau is observed within the resulting current density range (curve 1). The electrolyte changes its colour from colourless to green and green precipitation occurs. In pure $NaNO_3$ electrolyte the current density rises linearly at 1.8 V (curve 14). Because transpassive dissolution sets in at even higher current densities, the colourless electrolyte changes to yellow-brown and yellow-brown precipitations are observed. With decreasing θ, the activation potential for the chloride dominating activation potential is shifted to more anodic potentials. The nitrate anions disturb the activation [23]. With respect to the proposed mechanistic model, increasing θ leads to higher current densities at which the change of dominating mechanism occurs due to the transport of chloride anions from the bulk of the electrolyte through the diffusion layer to the steel surface. With increasing θ formation of the chloride polishing film can be maintained to higher current densities until replacement by

the nitrate polishing film and commencement of transpassive dissolution. In this paper the term passivation is not used for this phenomenon because the current density does not fall to nearly zero for $\theta \geq 0.07$. Transpassive dissolution sets in directly. The LSVs in mixed electrolytes with $\theta > 0.83$ indicate no sharp decrease in current density. Both mechanisms compete and the relatively small concentration of nitrate anions cannot create an abrupt change of the dominating mechanism. Curve 13 shows that for $\theta = 0.03$ the flux of chloride ions is too small to induce and maintain active anodic dissolution in comparison with $\theta = 0.05$ (curve 12). The insert in Figure 2 shows separate forward and backward LSV in mixed electrolyte with $\theta = 0.5$ arranged like a CV. The backward LSV corresponds completely to the backward LSVs which are obtained in pure $NaNO_3$ electrolyte due to stable transpassive dissolution.

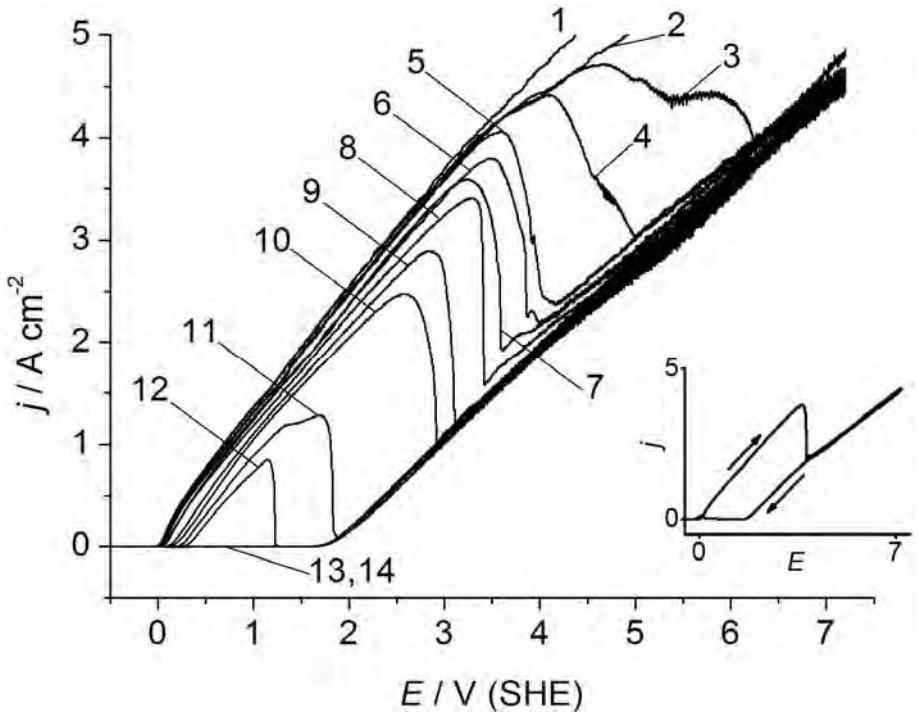

Figure 2. *LSVs; rotation rate of WE 3000 rpm; scan rate 50 mV s^{-1}; relative chloride concentrations* θ*: 1 (1); 0.9 (2); 0.87 (3); 0.83 (4); 0.77 (5); 0.67 (6); 0.5 (7); 0.33 (8); 0.13 (9); 0.1 (10); 0.07 (11); 0.05 (12); 0.03 (13); 0 (14). Insert: forward and backward LSV in mixed electrolyte with* θ *= 0.5.*

The transport of chloride anions and, therefore, the transition from chloride curve to nitrate curve can also be controlled by rotation rate. Increasing the rotation rate for a given $\theta = 0.5$ increases the current density at which the dissolution mechanism changes (Figure 3) due to a higher flux of chloride ions to the surface.

This is in agreement with the proposed mechanistic model. The mass flux of chloride anions J_{Cl^-} to the disc surface can be estimated by using equation 8 [24]:

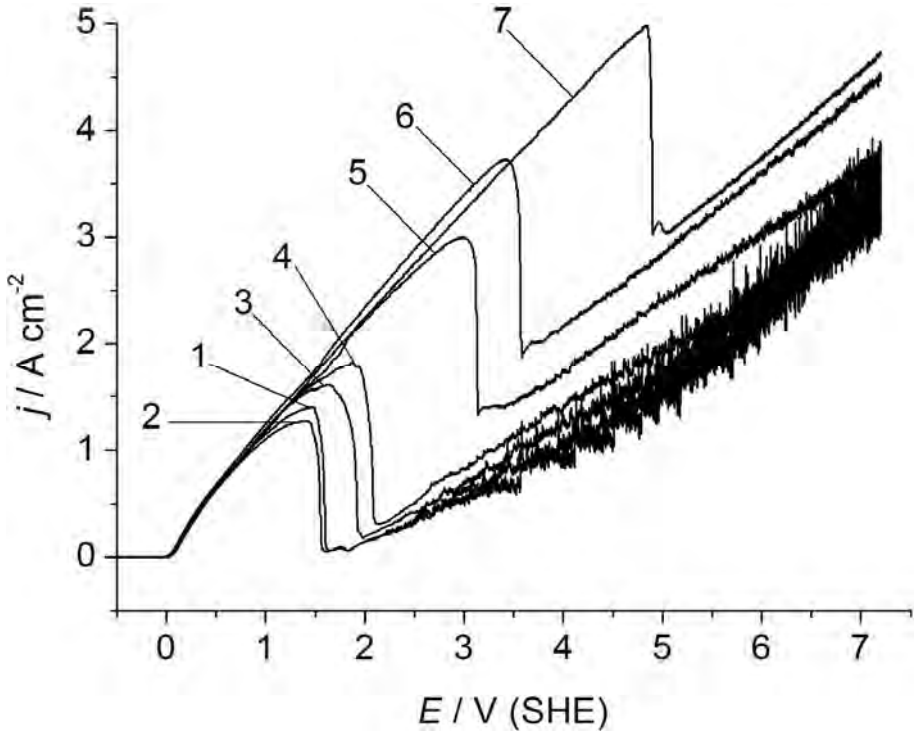

Figure 3. *LSVs in chloride/nitrate mixed electrolyte; θ = 0.5; scan rate 50 mV s^{-1}; rotation rates: 0 rpm (1); 100 rpm (2); 500 rpm (3); 1000 rpm (4); 2000 rpm (5); 3000 rpm (6), 4000 rpm (7).*

$$J_{Cl^-} = 0.62 \cdot D_{Cl^-}{}^{2/3} \cdot \nu^{-1/6} \cdot \omega^{1/2} \cdot c_{Cl^-} \quad (8)$$

where D_{Cl^-} = 2.032·10^{-5} cm^2 s^{-1} [25] is the diffusion coefficient of Cl^- anions at infinite dilution in water. The cinematic viscosity ν = 1·10^{-2} cm^2 s^{-1} [24] is assumed to be the one of water. ω is the angular velocity of the RDE and c_{Cl^-} the bulk concentration of chloride anions. With equation 8 only the diffusion is considered whereas migration is neglected. In the mixed electrolyte with θ = 0.5 the concentration of chloride is 1.5 mol L^{-1}. With rotation rate 3000 rpm and ω = 2·π·3000 rpm = 314.2 s^{-1}, J_{Cl^-} is 2.64·10^{-5} mol cm^{-2} s^{-1} calculated from equation 8. This calculation does not consider the larger existing nitrate anions in the solution. The nitrate anions could act as obstacles for the chloride anions flux but migration could lead to an increase of J_{Cl^-}. Therefore, the calculated mass flux of chloride anions is only an approximation. The dissolution rate of iron J_{Fe2+} at the surface can be calculated by using equation 9, which is derived from Faraday law (Eq. 5):

$$J_{Fe^{2+}} = \frac{j_{Cl^-,lim}}{F \cdot z} \quad (9)$$

where $j_{Cl^-,lim}$ = 3.6 A cm^{-2} is the current density at which the active dissolution mechanism cannot be maintained any longer. The calculated value J_{Fe2+} = 1.87·10^{-5} mol cm^{-2} s^{-1} is in agreement with the proposed model considering that a Fe^{2+} flux of 1.87·10^{-5} mol cm^{-2} s^{-1} would require a Cl^- flux of 2·1.87·10^{-5} mol cm^{-2} s^{-1} to form stoichiometrically $FeCl_2$.

The active dissolution in mixed electrolytes is mass transport-controlled with respect to chloride ions. From the LSV experiments it is concluded that under RDE conditions a sharp distinction is possible between active (chloride anion-dominated mechanism) and transpassive (nitrate anion-dominated mechanism) anodic dissolution mechanisms.

Switching between both mechanisms by potential control at RDE

Sequential LSVs which means in this paper that several LSVs are applied directly one after the other show that switching between the two dominating dissolution mechanisms is easily possible by potential control. The start potential can be chosen in the area of the chloride or the nitrate curve.

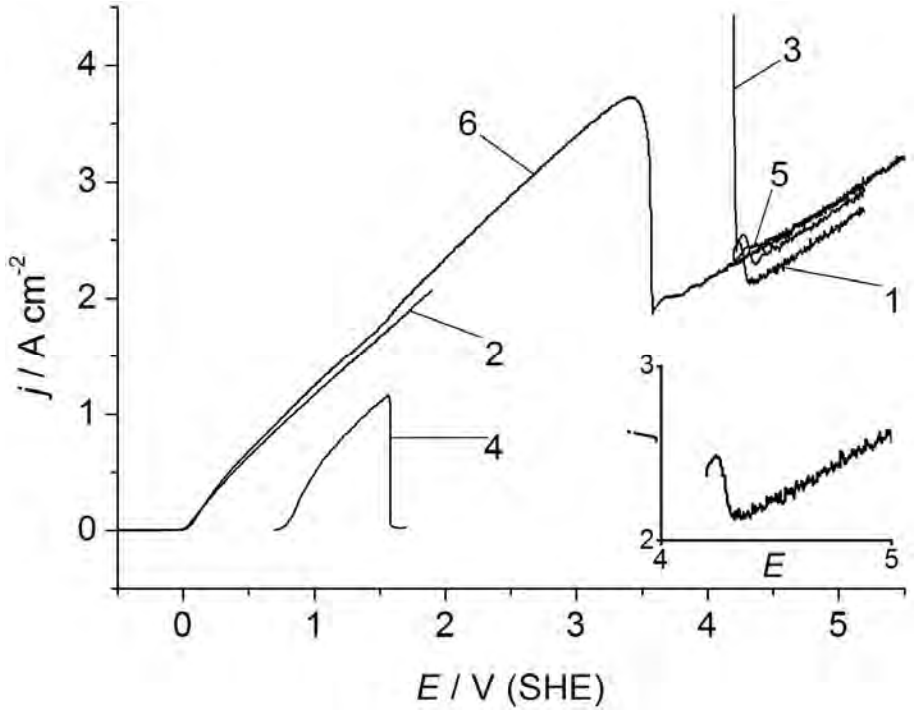

Figure 4. *In sequence (1) to (5) directly successive measured LSVs with potential limits 4.2 V to 5.2 V (1); -0.5 V to 1.9 V (2); 4.2 V to 5.2 V (3); 0.7 V to 1.7 V (4); 4.2 V to 5.2 V (5); complete LSV (6);* $\theta = 0.5$*; rotation rate 3000 rpm; scan rate 50 mV* s^{-1}*. Insert: sequence (1) enlarged.*

Curve 1 of Figure 4 starts in the potential region of the nitrate curve. After a short initial rise of the current density *j* (Figure 4 insert), *j* decreases and the curve follows the nitrate curve. The initial rise of *j* after switching from active to transpassive dissolution is reproducibly observed (curves 3, 6 in Figure 4). The reason of this effect is still unknown. Maybe chloride anions and nitrate anions which are initially present at the anode cause a situation where both mechanisms take place simultaneously. After the chloride anions are consumed, the dissolution follows the nitrate curve. Curve 2, initiated at 0 V, was applied directly after curve 1 and follows exactly the chloride curve. The surface is activated. Stepping the potential to 4.2 V, i.e. to a section of the LSV dominated by the transpassive dissolution, causes a change of dominating mechanism indicated by the large decrease of current density within a very short transition time (curve 3). The resulting current density after that switch is so high that the consumption of chloride ions cannot be maintained by mass transport and active dissolution ceases. Curve 4 starts within the section of the chloride curve (at 0.7 V). An instantaneous slope can be seen before the current density increases linearly with increasing potential. This slope fits to the chloride curve in the complete LSV but the current density is approximately 1 A cm^{-2} lower. It seems that the chloride curve is shifted to more anodic potentials for presently unknown reasons. One explanation could be that an acidification caused by oxygen evolution at anode/electrolyte interface influences the processes and shifts the chloride curve. A passivation is observed at approximately 1.5 V in this curve. So the next linear sweep in section of nitrate curve is following the expected behaviour of transpassive dissolution (curve 5).

Switching between both mechanisms by current density control at RDE

Programmed current chronopotentiometry (PCC) [26], i.e. the linear variation of the current in a galvanodynamic sweep experiment gave similar results like LSVs (see Figure SM-12). At low current densities active dissolution takes place in mixed electrolytes and the potential increases linearly with increasing current density. This section of PCC fits to the PCC in pure NaCl electrolyte. When a certain current density (depending on chloride mass transport) is reached the mechanism switches to transpassive dissolution which is indicated by an abrupt potential increase. From then on, the potential increases linearly with current density like the PCC in pure $NaNO_3$ electrolyte. This is in agreement with the proposed mechanistic model. An example for switching between both dominating mechanisms by current density control is shown in Figure 5.

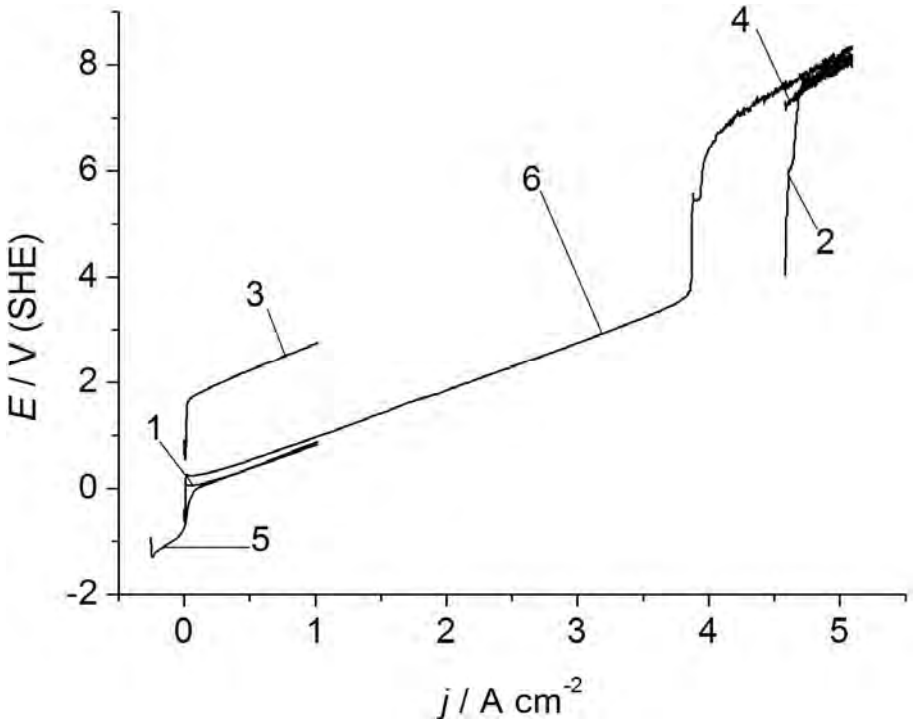

Figure 5. *In sequence (1) to (5) directly successive measured PCCs with current density limits from 0 A cm^{-2} to 1 A cm^{-2} (1); 4.6 A cm^{-2} to 5.1 A cm^{-2} (2); 0 A cm^{-2} to 1 A cm^{-2} (3); 4.6 A cm^{-2} to 5.1 A cm^{-2} (4); 0.3 A cm^{-2} to 1 A cm^{-2} (5); complete PCC (6); θ = 0.5; rotation rate 3000 rpm; scan rate 51 mA cm^{-2} s^{-1}.*

Curve 1 starts at current density of 0 A cm^{-2} and active dissolution sets in immediately. A current density step to 4.6 A cm^{-2} leads to a change of the dominating mechanism to transpassive as expected (curve 2). This is indicated by an abrupt increase of potential. Stepping back to 0 A cm^{-2} (curve 3) leads to a surprising effect. Passivity of the surface does not break down and transpassive dissolution sets in. After a current density ramp in the range of transpassive dissolution (curve 4) a slight cathodic current density of 0.3 A cm^{-2} leads to an activation of the steel surface (curve 5). Curve 6 shows a complete PCC.

From the LSV experiments it is concluded that not only a sharp transition from active to transpassive anodic dissolution due to mass transfer rate of chloride anions occurs, but switching between the dominating mechanisms by potential and current density control is possible as well.

Flow channel experiments

Flow channel experiments permit a more realistic modelling of ECM experiments under various flow conditions using galvanostatic pulses. The anodic dissolution in pure NaCl electroylte, in pure

$NaNO_3$ electrolyte and in mixed chloride/nitrate electrolytes was investigated. It was assumed that flow conditions in flow channel are more turbulent than in RDE experiments. The more turbulent flow causes a thinner diffusion layer and better mass transfer of chloride ions. Therefore, the chloride-dominated mechanism can be maintained at higher current densities, or the chloride-dominated mechanism at a given current density should be sustained by an electrolyte with a lower θ. This hypothesis was tested with relative low values of θ of 0.07, 0.17 and 0.33 by determining the current efficiencies according to equation 6. The dissolution valence *z* was set to 2. Because of other probable reactions, such as the formation of trivalent iron and the formation of trivalent chromium species, the experimental results are useful only for relative comparisons between similar experiments of the same material.

Experiments were performed for pulse current densities *j* of 5, 10, 20 and 40 A cm^{-2} (Figure 6).

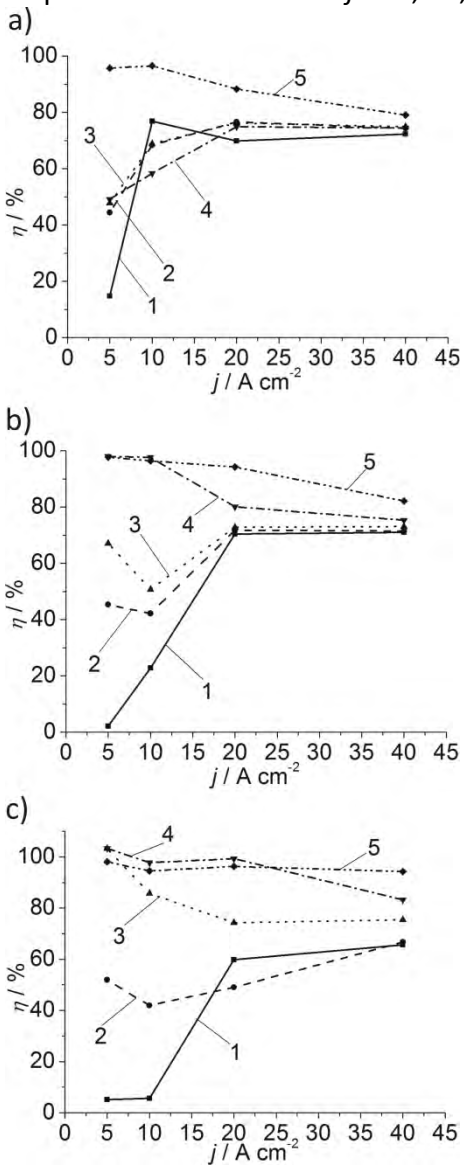

Figure 6. *Current efficiencies* η *with* γ *= 0.625 (**(a)**, 300 C), 0.5 (**(b)**, 100 C) and 0.167 (**(c)**, 100 C); relative chloride concentrations* θ*: 0 (1); 0.07 (2); 0.17 (3); 0.33 (4); 1 (5);* j *= 5 A cm^{-2}, 10 A cm^{-2}, 20 A cm^{-2} and 40 A cm^{-2}; Lines of all styles are guides to the eye.*

The current efficiencies in pure NaCl electrolyte (curves 5) and in pure $NaNO_3$ electrolyte (curves 1) correspond to literature values [11,14,15,20]. In pure NaCl electrolyte η is about 100 %. Decreasing η at higher *j* could be caused by additional formation of trivalent iron. In pure $NaNO_3$ electrolyte it can be distinguished between passivation of the surface, transition zone and

transpassive dissolution. The region of the transition zone is shifted to higher current densities with lower γ. Total experimental mass loss Δm_{tot} includes the erosion of electrochemically inert metal carbides. Often the ratio $\Delta m_{tot}/\Delta m_{theo}$ is quoted as current efficiency that might exceed 100 %. From known carbon content and its compounds Δm_{tot} can be corrected by subtracting the mass of electrochemical inert components Δm_C in order to obtain the carbide-free weight loss Δm by equation 10 (Details in SM-3):

$$\eta_{corr} = \frac{\Delta m_{tot} - \Delta m_{inert}}{\Delta m_{theo}} \cdot 100\% = \frac{\Delta m}{\Delta m_{theo}} \cdot 100\%. \quad (10)$$

For example in pure NaCl electrolyte with γ = 0.625 and 0.167 at 5 A cm^{-2} a $\eta = \Delta m_{tot}/\Delta m_{theo}$ of 112 % and 115 % are measured and yields a corrected η_{corr} of 100 % and 102 %. There is still a trend of η_{corr} being slightly larger than 100 % indicating a more complex dissolution mechanism for 100Cr6.

With γ = 0.625, the current efficiencies in the mixed electrolytes are rather uniform (curves 2 and 4, Figure 6a). At 20 A cm^{-2} and 40 A cm^{-2} η is about 87 % and is approximately the same as in pure $NaNO_3$ electrolyte. This is in agreement with the results of a microscopic inspection of the resulting surfaces at 40 A cm^{-2} with θ = 1, 0.33 and 0 (Figure 7a-c).

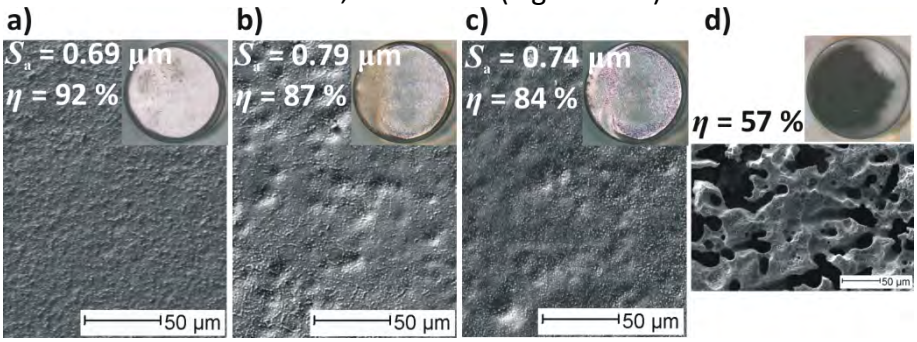

Figure 7. *Optical and SEM micrographs of the resulting surfaces with γ = 0.625. Electrolyte flow direction in optical micrographs and in SEM micrographs is from left to right.* ***(a)*** *j = 40 A cm^{-2}; θ = 1.* ***(b)*** *j = 40 A cm^{-2}; θ = 0.33.* ***(c)*** *j = 40 A cm^{-2}; θ = 0.* ***(b)*** *j = 5 A cm^{-2}; θ = 0.33.*

A very similar appearance of the surfaces is obtained in mixed electrolyte (θ = 0.33, Figure 7b) and in pure $NaNO_3$ electrolyte (Figure 7c). The current efficiencies in the mixed electrolyte and in pure $NaNO_3$ electrolyte (87 % and 84 %, respectively) and the surface roughnesses S_a (0.79 µm and 0.74 µm, respectively) are approximately the same (Figure 7b-c). Moreover, the SEM micrographs appear equal and are distinctly different from those obtained in pure NaCl electrolyte (θ = 1, Figure 7a). These are all indications of a nitrate anion-dominated dissolution mechanism at high current densities which is in line with the RDE results. Embedded small globular carbides can be seen clearly in the SEM micrographs in Figure 7a-c. The influence of additional turbulent flow due to the emerging edge can be seen in the optical micrographs, especially in Figure 7c for θ = 0. The higher material removal at the edge of the samples can be explained by higher current density which can be calculated by secondary current distribution. Applying 5 A cm^{-2} in mixed electrolyte with θ = 0.33 leads to a very porous, black surface structure with deep holes (Figure 7d). The porosity is so high that S_a cannot be measured with confocal microscopy. Instead of a dominating chloride dissolution mechanism it is proposed that both mechanisms proceed simultaneously at different regions of the surface. The current efficiency of 57 % is an indication for that. Active dissolution produces deep holes while the transition zone from passive to transpassive dissolution obtained in pure $NaNO_3$ electrolyte produces the black surface film in between. This black surface

film could correspond to the surface films described by Haisch in direct current experiments in pure $NaNO_3$ [15]. Described simultaneous dissolution by both mechanisms was not seen in RDE experiments. These observations illustrate the importance of flow conditions for the electrochemical dissolution reaction and the turbulence increasing from RDE to flow channel.

With γ = 0.5 the influence of γ becomes apparent. For θ = 0.07 (curve 2, Figure 6b) and 0.17 (curve 3, Figure 6b) there are current efficiencies measured at 5 A cm^{-2} and 10 A cm^{-2} which indicates a simultaneous chloride-dominated and nitrate-dominated dissolution. The current efficiencies at 20 A cm^{-2} and 40 A cm^{-2} approach those in pure $NaNO_3$ electrolyte. With θ = 0.33 (curve 4, Figure 6b) a minor influence of chloride anions is obtained at 20 A cm^{-2} and 40 A cm^{-2} because of little higher current efficiencies than in pure $NaNO_3$ electrolyte (93 % and 88 % compared to 82 % and 83 %). In this mixed electrolyte at 5 A cm^{-2} and 10 A cm^{-2} the anodic dissolution is dominated by chloride anions indicated by current efficiencies, surface roughnesses and the optical impression (Figure 8a-d).

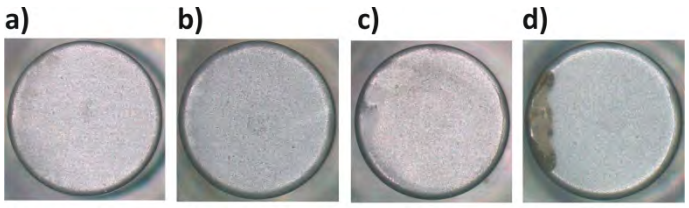

Figure 8. *Comparison of resulting surfaces with* θ *= 0.33 and 1 at 5 A* cm^{-2} *und 10 A* cm^{-2}*;* γ *= 0.5. Electrolyte flow direction in optical micrographs and in SEM micrographs is from left to right.* ***(a)*** j *= 5 A* cm^{-2}*,* θ *= 1.* ***(b)*** j *= 5 A* cm^{-2}*,* θ *= 0.33.* ***(c)*** j *= 10 A* cm^{-2}*,* θ *= 1.* ***(d)*** j *= 10 A* cm^{-2}*,* θ *= 0.33.*

This result is in agreement with the proposed mechanism which is based on the idea of chloride-dominated dissolution mechanism at lower and nitrate-dominated dissolution mechanism at higher *j*. The more pronounced edge effect due to the additional flow effect at the emerging edge can be seen at the surface in mixed electrolyte with θ = 0.33 at 10 A cm^{-2} as well (Figure 8d). Here the surface has a completely different appearance. This is another hint for the importance of flow conditions.

For the duty cycle γ of 0.167 the current efficiencies in the mixed electrolytes approaches η in pure NaCl electrolyte (Figure 6c). The current efficiencies with θ = 0.33 are equal to the ones in pure NaCl electrolyte except for the current density of 40 A cm^{-2}. At this current density, the current efficiency is η = 97 % in mixed electrolyte with θ = 0.33. This value is in between the values obtained in the pure chloride and nitrate electrolytes.

Also the surface quality obtained in the mixed electrolyte (Figure 9e and g) appears similar to those obtained in pure NaCl electrolyte (Figure 9d and f) at 10 A cm^{-2} and 20 A cm^{-2}. The S_a values indicate that the chloride dissolution mechanism dominates. Lower current densities show a slightly different behaviour. Figure 9b shows the surface obtained at 5 A cm^{-2} in mixed electrolyte with θ = 0.33 and γ = 0.167. It is rougher than those obtained in pure NaCl with the same γ (Figure 9a) and in mixed electrolyte with the same mixing ratio and larger duty cycle of γ = 0.5 (Figure 8b). A value S_a > 1 µm indicates that under these specific conditions a higher roughness is obtained in the presence of both anions. Perhaps the chloride ion flux towards the surface is insufficient with respect to competing nitrate anions. At higher current densities of 40 A cm^{-2} in a mixed electrolyte with θ = 0.33 (Figure 9i) the surface show features found on surfaces obtained

in both pure NaCl and $NaNO_3$ electrolytes (Figures 9h and 9j). It is concluded that both mechanisms proceed simultaneously at the same regions of a surface (in contrast to the situation found in Figure 7d). Applying different duty cycles in series was tested with γ = 0.625 (Q = 200 C), 0.5 (50 C) and 0.167 (50 C) at 5 A cm^{-2} with θ = 0.33 in order to assess the surface quality after each step.

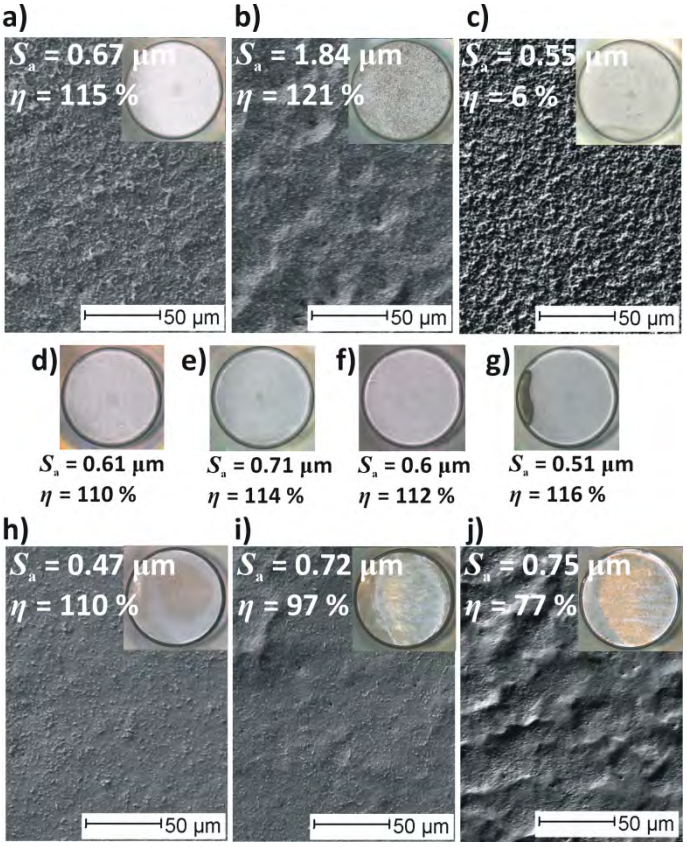

Figure 9. *Comparison of resulting surfaces with γ = 0.167. Electrolyte flow direction in optical micrographs and in SEM micrographs is from left to right.* ***(a)*** *j = 5 A cm^{-2}, θ = 1.* ***(b)*** *j = 5 A cm^{-2}, θ = 0.33.* ***(c)*** *j = 5 A cm^{-2}, θ = 0.* ***(d)*** *j = 10 A cm^{-2}, θ = 1.* ***(e)*** *j = 10 A cm^{-2}, θ = 0.33.* ***(f)*** *j = 20 A cm^{-2}, θ = 1.* ***(g)*** *j = 20 A cm^{-2}, θ = 0.33.* ***(g)*** *j = 40 A cm^{-2}, θ = 1.* ***(i)*** *j = 40 A cm^{-2}, θ = 0.33.* ***(j)*** *j = 40 A cm^{-2},θ = 0.*

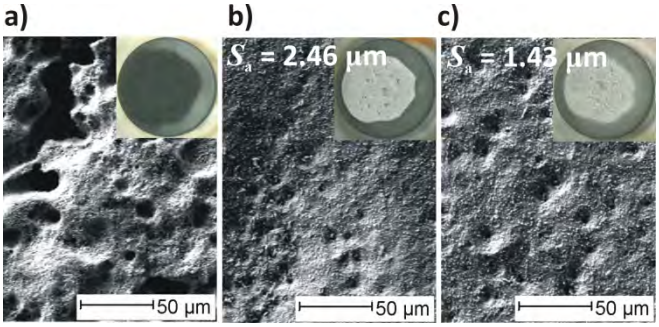

Figure 10. *Comparison of resulting surfaces after anodic dissolution in series with variation of duty cycle*; j = *5 A cm^{-2},* θ = 0.33. ***(a)*** *γ = 0.625; Q = 200 C;* ***(b)*** *i. γ = 0.625; Q = 200 C, ii. γ = 0.5; Q = 50 C;* ***(c)*** *i. γ = 0.625; Q = 200 C, ii. γ = 0.5; Q = 50 C, iii. γ = 0.167; Q = 50 C. Electrolyte flow direction in optical micrographs and in SEM micrographs is from left to right.*

In Figure 10, three specimens are shown, one processed just with the first step (Figure 10a), the second processed with the first two steps (Figure 10b) and the third processed with all three steps

(Figure 10c). The conditions in Figure 10a were identical to Figure 7d except for the use of a lower charge (200 C instead of 300 C). Because both dissolution mechanisms take place simultaneously, a black porous surface is observed (Figure 10a). However, less material is removed in Figure 10a than in Figure 7b causing a less distinctive porosity. S_a is still larger than the measurable range. The next step (γ = 0.5) in which the dissolution is dominated by chloride anions efficiently removes the black surface (Figure 10b). Only a few pits and an edge at transition from flat plateau to the rim of specimen remain. Applying all three steps decreases the roughness in the last step (Figure 10c). The last step in which chloride anions dominate the dissolution flattens the surface and a smooth transition to the rim of the specimen is achieved. A look at the SEM micrograph shows that the surface is equal to the one in Figure 9b with the same duty cycle and chloride anion ratio (γ = 0.167, θ = 0.33).

Conclusions

The anodic dissolution of 100Cr6 in chloride/nitrate mixed electrolytes was investigated. LSV at RDE assuming mainly laminar flow conditions showed that either active or transpassive dissolution can be achieved by controllable mass transport conditions (bulk chloride concentration and rotation rate). This is indicated by an abrupt decrease in current density with increasing anodic potential. While active dissolution due to chloride-dominated mechanism takes place at lower current densities, transpassive dissolution due to nitrate-anion dominated mechanism is observed at higher current densities. By changing the potential or current density, it is possible to switch reversibly between both dissolution mechanisms.

The following dissolution mechanism is proposed. If the flux of chloride ions relative to the current density is too small, the chloride anion mechanism cannot be maintained and transpassive dissolution due to nitrate-dominated dissolution commences. This transpassive dissolution is then stable in the observed current density ranges. The anodic dissolution is mass transport-controlled and depends on the anode/electrolyte interface layer.

Flow channel experiments applying galvanostatic pulses showed that under assumed turbulent flow conditions a separation of dominating dissolution mechanisms can be observed under specific conditions while both mechanisms may also proceed simultaneously under other conditions. There is not only an influence of anion ratio but also on current density, pulse parameters and flow conditions.

Acknowledgements: *The technical assistance by Ms. Carmen Pritsch is acknowledged.*

References

[1] A. D. Davydov, V. M. Volgin in *Encyclopedia of Electrochemistry* (D.D. Macdonalds, P. Schmuki Eds.) Wiley, Vol. **5,** 2007pp. 809-854.
[2] J. A. McGeough, M. B. Barker, *Chemtech* **21** (1991) 536-542.
[3] M. Datta, D. Landolt, *Electrochim. Acta* **26** (1981) 899-907.
[4] D. T. Chin, K. W. Mao, *J. Appl. Electrochem.* **4** (1974, 155-161.
[5] M. Datta, D. Landolt, *Electrochim. Acta* **25** (1980) 1255-1262.
[6] M. Datta, D. Landolt, *Electrochim. Acta* **25** (1980) 1263-1271.
[7] T. Haisch, E. Mittemeijer, J. W. Schultze, *Electrochim. Acta* **47** (2001) 235-241.
[8] M. M. Lohrengel, *Mater. Manuf. Process.* **20** (2005) 1-8.
[9] K.-W. Mao, M. A. LaBoda, J. P. Hoare, *J. Electrochem. Soc.* **119** (1972) 419-427.
[10] K.-W. Mao, *J. Electrochem. Soc.* **118** (1971) 1876-1879.
[11] M. M. Lohrengel, C. Rosenkranz, D. Rohrbeck, *Microchim. Acta* **156** (2006) 163-166.

[12] C. Rosenkranz, M. M. Lohrengel, J. W. Schultze, *Electrochim. Acta* **50** (2005) 2009-2016.
[13] T. Haisch, E. J. Mittemeijer, *Jom* **54** (2002) 38-41.
[14] T. Haisch, E. J. Mittemeijer, J. W. Schultze, *Mater. Corros.* **53** (2002) 740-755.
[15] T. Haisch, E. J. Mittemeijer, J. W. Schultze, *J. Appl. Electrochem.* **34** (2004) 997-1005.
[16] M. M. Lohrengel, I. Kluppel, C. Rosenkranz, H. Bettermann, J. W. Schultze, *Electrochim. Acta* **48** (2003) 3203-3211.
[17] J. P. Hoare, M. A. LaBoda, *Comprehensive Treatise of Electrochemistry,* Plenum Press, New York, 1981, pp. 806.
[18] K.-W. Mao, J. P. Hoare, *Corr. Sci.* **13** (1973) 799-803.
[19] H. McCrabb, A. Lozano-Morales, S. Snyder, L. Gebhart, E. J. Taylor, *T.Electrochem. Soc.* **19** (2009) 19-33.
[20] S. Moser, Thesis, Heinrich-Heine-University of Düsseldorf (2004).
[21] M. Datta, *IBM J. Res. Dev.* **37** (1993) 207-226.
[22] H. C. Kuo, D. Landolt, *Electrochim. Acta* **20** (1975) 393-399.
[23] A. D. Davydov, A. N. Kamkin, *Elektrokhimiya* **14** (1978) 979-992.
[24] V. G. Levich, *Physicochemical Hydrodynamics*, Prentice Hall, 1962.
[25] D. R. Lide, *CRC handbook of chemistry and physics*, CRC Press, Boca Raton, Fla., 2006.
[26] A. J. Bard, L. R. Faulkner, *Electrochemical Methods: Fundamentals and Applications*, John Wiley & Sons, New York, 2001, p. 347.

J. Electrochem. Sci. Eng. **1(1)** (2011) S1-S2

Open Access : : ISSN 1847-9286
www.jESE-online.org

SUPPLEMENTARY MATERIAL TO

Anodic dissolution of 100Cr6 in nitrate/chloride mixed electrolytes

ANDREAS LESCH, GUNTHER WITTSTOCK, CHRIS BURGER, BENJAMIN WALTHER and JÜRGEN HACKENBERG

J. Electrochem. Sci. Eng. **1(1)** (2011) 39-54; doi: **10.5599/jese.2011.0004**

SM-1 Photographs of formed films during LSV in mixed electrolyte at resting disc electrode

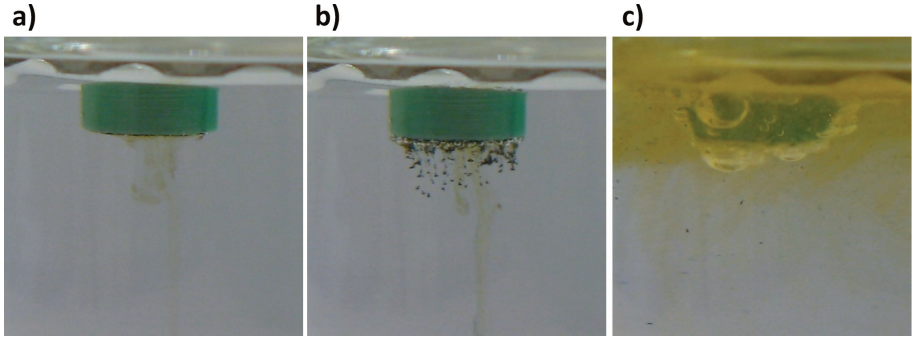

Figure SM-1. *Reaction products in mixed electrolytes at static anode;* ***(a)*** *green viscous film in section of "chloride curve";* ***(b)*** *Evolution of oxygen after passivation;* ***(c)*** *Evolution of oxygen and yellow-green colored solution in section of "nitrate curve".*

Figure SM-1 shows photographs of the transition from active to passive dissolution. During active dissolution the assumed reaction products creep down as a green viscose film (Figure SM-1a). After passivation, the evolution of oxygen breaks off the visible flakes of the black carbide-containing surface layer from the anode surface (Figure SI-1b) and transpassive dissolution can be observed by the formation of oxygen bubbles and yellow-brown colouration of the solution (Figure SM-1c).

SM-2 Programmed Current Chronopotentiometry

Active dissolution in pure NaCl electrolyte and transpassive dissolution in pure $NaNO_3$ electrolyte are indicated by curves 1 and 7. The PCCs in mixed electrolytes show active dissolution at low current densities. The transition from active to transpassive is indicated by the increase in potential. The current density at transition depends on the relative chloride anion concentration.

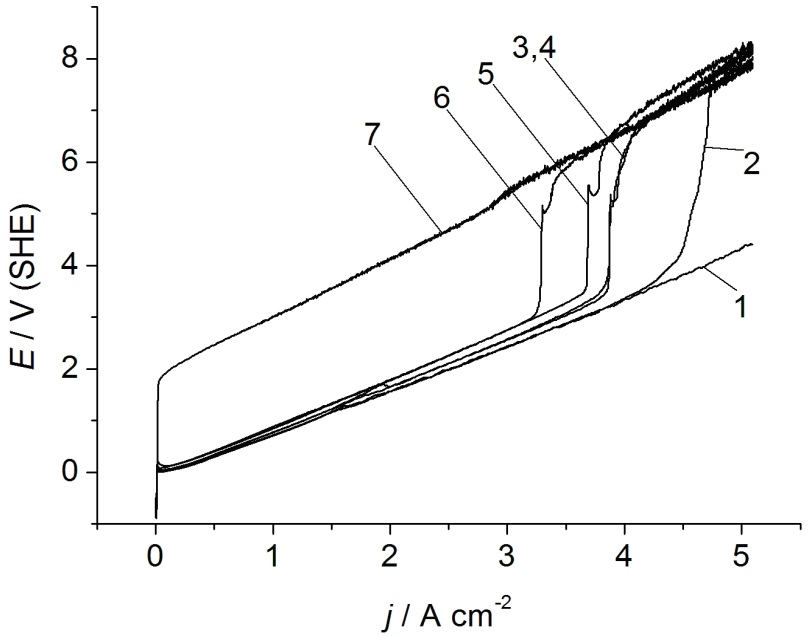

Figure SM-2. *PCCs in 3 M NaCl (1), 3 M $NaNO_3$ (7) and in mixed electrolytes with relative chloride concentrations θ: 0.83 (2), 0.67 (3), 0.5 (4), 0.33 (5), 0.17 (6); rotation rate 3000 rpm; Scan rate 50.9 mA cm^{-2} s^{-1}.*

SM-3: Correction of current efficiency of inactive carbides

A correction of current efficiency considering the elementary carbon and the metal carbides which are assumed to be electrochemically inert can be done by using the equations SM-3-1 to SM-3-3.

$$m_{\text{inert}} = m_{\text{tot}} \cdot p_{\text{C}} \cdot \left(p_{\text{C,elementary}} \cdot \frac{M_{\text{C,elementary}}}{M_{\text{C,elementary}}} + p_{\text{C,Fe3C}} \cdot \frac{M_{\text{Fe3C}}}{M_{\text{C,elementary}}} + p_{\text{C,Fe2.5C}} \cdot \frac{M_{\text{Fe2.5C}}}{M_{\text{C,elementary}}} \right) \quad (1)$$

$$m_{\text{inert}} = m_{\text{tot}} \cdot 0.01 \cdot \left(0.2 \cdot 1 + 0.4 \cdot \frac{179.5457}{12.0107} + 0.4 \cdot \frac{151.6232}{12.0107} \right) = m_{\text{tot}} \cdot 0.1123 \quad (2)$$

$$m_{\text{inert}} = m_{\text{C,elementary}} + m_{\text{Fe3C}} + m_{\text{Fe2.5C}} \quad (3)$$

m_{inert} – total mass of assumed inert carbon compounds in annealed to globular cementite 100Cr6
$m_{\text{C,elementary}}$ – mass of elementary carbon
m_{Fe3C} – mass of Fe_3C
$m_{\text{Fe2.5C}}$ – mass of $Fe_{2.5}C$
m_{tot} – experimental weight mass loss of annealed to globular cementite 100Cr6 specimen
p_{C} – weight percentage of total carbon in 100Cr6
$p_{\text{C,elementary}}$ – percentage of elementary carbon of total carbon
$M_{\text{C,elementary}}$ – molar mass of carbon
$p_{\text{C,Fe3C}}$ – percentage of carbon, bound in Fe_3C, of total carbon
M_{Fe3C} – molar mass of Fe_3C
$p_{\text{C,Fe2.5C}}$ – percentage of carbon, bound in of $Fe_{2.5}C$, of total carbon
$M_{\text{Fe2.5C}}$ – molar mass of $Fe_{2.5}C$

J. Electrochem. Sci. Eng. **1(1)** (2011) 55-65; doi: **10.5599/jese.2011.0002**

Open Access : : ISSN 1847-9286
www.jESE-online.org

Original scientific paper

Removal of arsenic and COD from industrial wastewaters by electrocoagulation

S. ZODI, O. POTIER, C. MICHON, H. POIROT, G. VALENTIN, J. P. LECLERC and F. LAPICQUE✉

Laboratoire Réactions et Génie des Procédés, CNRS – Nancy Université , ENSIC- BP 20451, F-54001 Nancy, France

✉Corresponding Author: +33 0 383 175 266, francois.lapicque@ensic.inpl-nancy.fr

Received: March 21, 2011; Revised: May 09, 2011; Published: August 20, 2011

Abstract

The paper deals with the treatment of arsenic-containing industrial wastewaters by electrocoagulation. The waste issued from a paper mill industry downstream of the biological treatment by activated sludge was enriched with arsenic salts for the purpose of investigation of the treatment of mixed pollution. First, the treatment of single polluted waters, i.e. containing either the regular organic charge from the industrial waste or arsenic salts only, was studied. In the case of arsenic-containing waters, a broad selection of experimental data available in the literature was compiled and interpreted using an adsorption model developed previously. The same technique was used in the case of industrial waste. Arsenic-enriched paper mill wastewaters with various amounts of As salts were then treated by electrocoagulation with Fe electrodes. The set of data obtained were interpreted by a model developed on the basis of the separate models. The agreement between predicted and experimental variations of the As concentrations ranging from 0.3 µg/L to 730 µg/L showed that both the organic matter and As salt can be removed from the liquid independently from each other.

Keywords

Electrocoagulation; industrial wastewaters; arsenic; adsorption model

Introduction

Arsenic (As) is one of the most toxic elements that can be present in wastewaters and environment in general. Therefore, the treatment of groundwater has been investigated for decades for the possible use of existing water stocks with appreciable As contents [1], in particular of those close to the mines, as reported by Leist et al. [2].

Treatment of As-containing solutions, being of natural origin or prepared by dissolving chemicals in pure water, has been tackled for years. It seems that As compounds - particularly those in the pentavalent form - exhibit interesting sorption capacities on Fe(III) hydroxides. Adsorption also occurs on Al(III) hydroxides, although not as strongly as on Fe(III) species [1,3,4]. Coagulation and electrocoagulation, therefore, seem interesting and suitable methods for the treatment of arsenic-containing species. The two treatment techniques do not differ very much. In both cases, the treatment consists of two steps: (i) supply of the liquid to be treated with Fe(III) species, either by Fe electrode dissolution to Fe(II) and subsequent oxidation to Fe(III) upon air oxidation or by addition of Fe salts, (ii) complexation-adsorption of As species on Fe(III) species. Since the treatment is often carried out at pH above 3, trivalent Fe species are in the form of solid hydroxide $Fe(OH)_3$.

The largest part of research on this subject has been focused on potabilization of water [2,3,5,6]. Although the content of As-salts in the analyzed waters was as large as 100 mg/L, the chemical oxygen demand (COD) content of the solutions to be treated was very low and the presence of other species could be disregarded. In this study, we investigated the electrocoagulation treatment of As-containing industrial wastes for abatement of the COD and As species by using dissolution of iron anodes. Electrocoagulation technique relies on the destabilization of suspended matter by reduction of the absolute value of the zeta potential by the presence of electrogenerated trivalent metals. This technique has been used in and investigated for the treatment of various wastewaters [1,3,5,7,8]. The waste generated from paper mill industry has a slight arsenic content at ppb level. The addition of arsenic salts to the original waste makes it possible to investigate the treatment of mixed wastewaters. For this purpose, the published data on the treatment of single solutions of arsenic salts were compiled and analyzed using a simple model for electrocoagulation published previously [9] and relying upon two parameters. Moreover, the treatment of the industrial wastewater with negligible concentrations of As allowed for the estimation of the two parameters related to the COD abatement. Numerous electrocoagulation tests with the waste after the addition of various amount of As species were conducted. The interpretation of the data was made taking into account the presence of the two pollutants to examine whether the presence of As could affect COD removal in the electrocoagulation process, as it has been observed in the case of Cr-containing industrial solutions [7].

Experimental

Wastewater samples and chemicals

The wastewater was collected from a local paper mill industry (Clairefontaine, France) downstream of a primary settling stage and biological treatment by activated sludge. The waste already used in the previous investigation [10] had pH=7.7, COD=285 mg O_2/L, turbidity = 35 NTU, and a very low As content near 3.8 μg/L. The COD level was mainly due to the presence of dissolved or suspended organic matters. Because of the relatively high conductivity of the wastewater, 1.22 mS cm^{-1}, no supporting electrolyte, such as sodium chloride, had to be added.

The concentration of arsenic species was enhanced by adding small amounts of arsenic acid disodium salt, Na_2HAsO_3 (Purissimum, Fluka), to the wastewater. Arsenic concentration in the wastewater obtained was below 1 mg/L. The moderate COD of the industrial waste allows to have a reasonable organic pollution to As pollution ratio, so that interactions between As and the organic pollution could be investigated.

Electrochemical reactor

Treatment runs have been carried out batchwise by recirculation of 2.5 liters wastewater in the flow rig consisting of a reservoir tank, peristaltic pump, flow meter, and an electrochemical cell

[9,10]. The electrochemical cell had a rectangular cross-section and was provided with two flat facing Fe electrodes, being 15x7 cm^2. The electrode gap was maintained at 2 cm and the liquid was circulated at 300 cm^3 min^{-1}.

Runs were carried out for periods of time ranging from 45 to 90 minutes, depending on the current density applied, which ranged between 5 and 20 mA cm^{-2}. The cell voltage was monitored along the run..

Pollutants analysis and quantification

Liquid fractions of 10 cm^3 were collected at regular intervals along the runs. The concentration values of the various species were corrected for the change in the liquid volume caused by the regular sampling. Conductivity and pH were monitored using a multi-parameter instrument (Consort C931). A small volume of each sample was acidified by nitric acid in order to determine the Fe and As concentrations by ICP-MS (Series X7, Thermo) after suitable dilution of the acidic solution. For arsenic species, a small liquid volume was submitted to microwave digestion using a START-D instrument prior to injection to the ICP-MS instrument.

The rest of each sample was allowed to settle for at least twelve hours before the analysis of the clear fraction was carried out. The turbidity was measured using an IR beam at 890 nm and detection of the light dispersion using a Hanna Ins. LP2000 spectrophotometer, and COD was determined by the standardized colorimetric method after high temperature oxidation with excess chromic acid and subsequent measurement of the optical density at 530 nm using a HACH 2400 spectrophotometer. The estimated accuracy in the COD measurement was 25 ppm.

Electrocoagulation of the industrial waste

The industrial waste with a low content of As species was submitted to electrocoagulation at two levels of the current density. As expected, the COD level was observed to decrease regularly with time in spite of the slight scattering of the data due to the uncertainty in the assay. Moreover, electrocoagulation did not allow the entire removal of the organic charge since the final COD level was usually at approximately 50% of the initial value, even upon longer electrocoagulation runs. The concentration of dissolved iron increased regularly during the run. The overall current yield of the dissolution at time t was calculated as follows:

$$\Phi_{\mathrm{Fe}} = \frac{[\mathrm{Fe(III)}]_t \, V n_{\mathrm{Fe}} F}{M_{\mathrm{Fe}} A i t} \qquad (1)$$

where V is the volume of the wastewater under treatment, n_{Fe} the number of electrons involved in the dissolution, taken as 2 because the anode dissolution leads to Fe(II) species, which rapidly oxidizes to Fe(III) in the presence of air oxygen. In equation (1), M_{Fe} is the molecular weight of iron, i the current density applied, and A the geometrical area (105 cm^2). The current yield was observed to increase slightly over time, from 0.5 in the first minutes and reaching 0.8-0.85 after 30-40 minutes. This could be caused by partial inhibition of the iron electrode immersed in the liquid in the early stage of the run, as the electrode probably exhibited only moderate corrosive properties.

As often reported, the reduction in COD level is mainly governed by the amount of coagulant generated at the anode surface (Fig. 1). The experimental variation was modeled using a previous overall model [11] relying upon the instantaneous adsorption or complexation of the pollutant charge – expressed by the COD – with Fe(III) hydroxide. The presence of As species below 4 µg/L was neglected here.

Fe(III) complexes organic matter, expressed by the COD level, S, as follows:

$$\mathrm{Fe(III)} + n_1 \, \mathrm{S} \leftrightarrow \mathrm{FeS} \qquad (2)$$

where coefficient n_1 is expressed in mg/L O_2 per mg/L Fe species, since S is expressed by the COD level. For the sake of simplicity, the complex formed in the treatment is written FeS, regardless of n_1 value. In this section, Fe(III) and S represent free species. It can be observed at this level that numerous unknown elementary processes are involved in the overall treatment. Moreover, it is not clear whether the abatement of the pollutant is governed only by absorption and what are the molecular structures of coagulants and pollutants. Because of this, we defined a simplified apparent equilibrium constant K_1 simply written as:

$$K_1 = \frac{[\mathrm{FeS}]}{[\mathrm{Fe}][\mathrm{S}]} \quad (\text{in L/mg}) \tag{3}$$

where coefficient n_1 is expressed in mg/L O_2 per mg/L Fe species, since S is expressed by the COD level. For the sake of simplicity, the complex formed in the treatment is written FeS, regardless of n_1 value. In this section, Fe(III) and S represent free species. It can be observed at this level that numerous unknown elementary processes are involved in the overall treatment. Moreover, it is not clear whether the abatement of the pollutant is governed only by absorption and what are the molecular structures of coagulants and pollutants. Because of this, we defined a simplified apparent equilibrium constant K_1 simply written as:

$$[\mathrm{S}]_0 = [\mathrm{S}] + \frac{[\mathrm{FeS}]}{n_1} \tag{4}$$

$$[\mathrm{Fe}]_t = [\mathrm{Fe}] + [\mathrm{FeS}] \tag{5}$$

where $[S]_0$ expresses the initial COD level, and $[Fe]_t$ represents the concentration of the generated Fe(III) covering both free and complexed Fe(III) forms. As a matter of fact, a fraction of the pollutant matter with the concentration $[S]_f$ cannot be treated, so only fraction ($[S]-[S]_f$) has to be considered in the adsorption equilibrium constant. Equations (2)-(5) led to the expression for the untreated S concentration:

$$[\mathrm{S}] = [\mathrm{S}]_f + \frac{-\left(\frac{[\mathrm{Fe}]_t}{n_1} - \left([\mathrm{S}]_0 - [\mathrm{S}]_f\right) + \frac{1}{K_1}\right) + \sqrt{\left(\frac{[\mathrm{Fe}]_t}{n_1} - \left([\mathrm{S}]_0 - [\mathrm{S}]_f\right) + \frac{1}{K_1}\right)^2 + \frac{4\left([\mathrm{S}]_0 - [\mathrm{S}]_f\right)}{K_1}}}{2} \tag{6}$$

Fitting of the experimental variation of the COD led to the estimates for K_1 and n_1, even though a narrow-valley situation in the optimization procedure was encountered. As formerly observed in the treatment of other industrial wastes [12], moderate COD levels in relation to ratio (K_1/n_1) resulted in the higher accuracy obtained in determination of the ratio. Nevertheless, the two parameters could be estimated at n_1 = 2.1 mg O_2 per mg Fe, and K_1 = 0.029 L/mg (Fig. 1).

Electrocoagulation of pure solutions of arsenic salts

Before the compilation of published experimental data on As removal by electrocoagulation from waters possessing very low COD or turbidity levels, physicochemical properties of arsenic salts are briefly discussed.

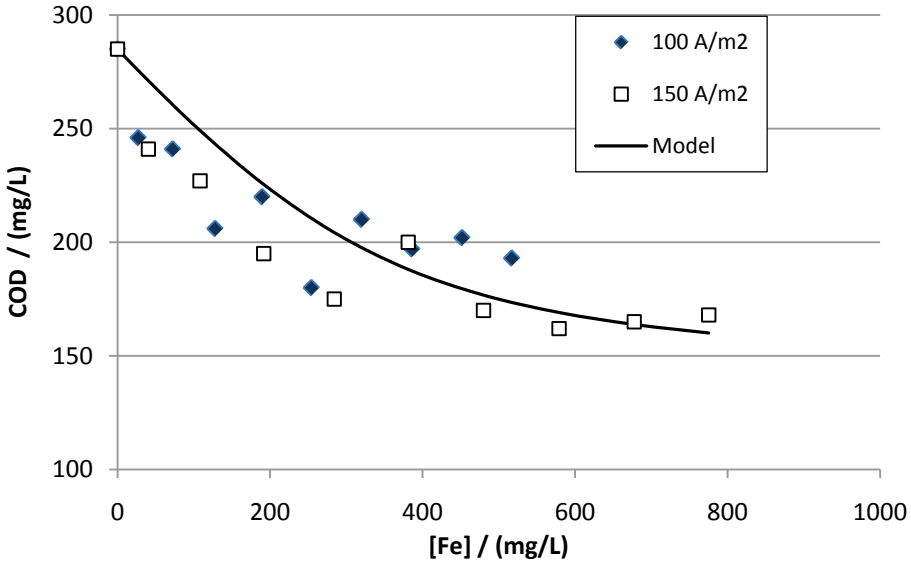

Figure 1. *COD abatement from the industrial waste. The model considered is expressed by rel. (4)*

General features of As species in wastewaters

Arsenic can be encountered in the form of either organic compounds with methyl groups or inorganic species. The most stable forms in ores or waste are arsenious salts (the trivalent form) and arsenate salts (pentavalent form). As(III) form is obtained from arsenious acid, $HAsO_2$, or its hydrated form, H_3AsO_3 [13]. The two acids exhibit weak acidity, with a pKa near 9.2. As(V) is obtained from arsenic acid, H_3AsO_4. The acidity constants of the triacid are near 2.25, 6.77, and 11.60 [8,14]. Therefore, for electrocoagulation of As-containing wastewater with an initial pH near 7 and increasing up to 9 in the course of the treatment, As mainly has the following forms: H_3AsO_3 with slight amounts of $H_2AsO_3^-$ for As(III) and $H_2AsO_4^-$ and $HAsO_4^{2-}$ ions for As(V). The latter two species are prone to adsorption on Fe(III) hydroxide [15,16].

Pentavalent salts might be considered as oxidants, i.e. existing at appreciable extent under oxidizing conditions. Pentavalent arsenic is in equilibrium with As(III) according to:

$$H_3AsO_4 + 2\,H^+ + 2\,e^- \leftrightarrow HAsO_2 + 2H_2O \quad E_0 = 0.560\ V \qquad (7)$$

Considering a solution with a pH 7, the equilibrium potential deduced from Nernst law is 0.147 V/NHE. From a thermodynamic point of view, As(V) and As(III) can be present in most aqueous media. It is generally admitted that As(V) is a predominant form in waters provided sufficient aeration.

The iron anode dissolves to Fe(II). This reducing species can oxidize to Fe(III) according to:

$$Fe^{2+} \leftrightarrow Fe^{3+} + e \qquad E_0 = 0.771\ V \qquad (8)$$

Comparison of the equilibrium potentials of the redox couples shows that As(V) cannot be reduced by Fe(II); the latter rapidly oxidizes to Fe(III) by air oxygen in aerated media.

Nevertheless, removal of As by adsorption or electrocoagulation is more efficient for As(V) than As(III). In addition to its lower intrinsic toxicity, As(V) is thus a less hazardous form of arsenic to be used for treatment or consumption purposes. For this reason, in most investigations, pretreatment of wastewaters includes the preliminary step of As(III) oxidation using hydrogen peroxide, Fe(III), or at the anode surface, as reported by Ratna Kumar et al. [4].

Application of the electrocoagulation model to As removal

The model was directly derived from that for COD abatement. Fe(III) complexes As species as follows:

$$Fe(III) + n_2\ As(V) \leftrightarrow FeAs \quad (9)$$

where coefficient n_2 is expressed in mg Fe(III) per mg As species. Equilibrium constant K_2 is simply written as:

$$K_2 = \frac{[FeAs]}{[Fe][As]} \quad (\text{in L/mg}) \quad (10)$$

Langmuir's model has been used in several investigations for modeling the adsorption equilibrium of As species on Fe(III) hydroxide. Mass balances on Fe and As species were also written:

$$[As]_0 = [As] + \frac{[FeAs]}{n_2} \quad (11)$$

From the equations (10-12), the concentration of complex FeAs can be expressed as follows:

$$[FeAs] = \frac{K_2[Fe]_t[As]}{1 + \frac{K_2}{n_2}[As]} \quad (13)$$

which appears perfectly similar to the conventional Langmuir's expression

$$q_{As} = \frac{K_L[As]}{1 + a_L[As]} \quad (14)$$

where q_{As} is the amount of As adsorbed on Fe hydroxides, the binding constant K_L can be related to product $K_2[Fe]_t$, and the sorbent capacity a_L to the ratio (K_2 / n_2).

As with S, the concentration of free, untreated arsenic species is obtained by solving the system formed byequations (10-13):

$$[As] = \frac{-\left(\frac{[Fe]_t}{n_2} - [As]_0 + \frac{1}{K_2}\right) + \sqrt{\left(\frac{[Fe]_t}{n_2} - [As]_0 + \frac{1}{K_2}\right)^2 + \frac{4[As]_0}{K_2}}}{2} \quad (15)$$

As relevant studies indicate, As(V) species can be totally removed by electrocoagulation; therefore, its final concentration $[As]_f$ was neglected here. The model was applied to various data reported in the literature [1,4,15,17]. Because the corresponding values for the concentration of generated iron species were rarely reported, it was assumed that iron anodes dissolved with a current efficiency equal to 0.8, as observed in previous investigations [9,10]. The postulated value is also in fair agreement with the value observed for the treatment of the industrial waste (see above section). The various data considered were approximately fitted to the model, yielding estimates for constants K_2 and n_2.

Fig. 2 shows the good correlation between theory and experimental data for As concentrations ranging from 100 μg/L to 30 mg/L within a factor 2, with

K_2 = 1.12 L/mg and n_2 = 1.82 mg Fe per mg As

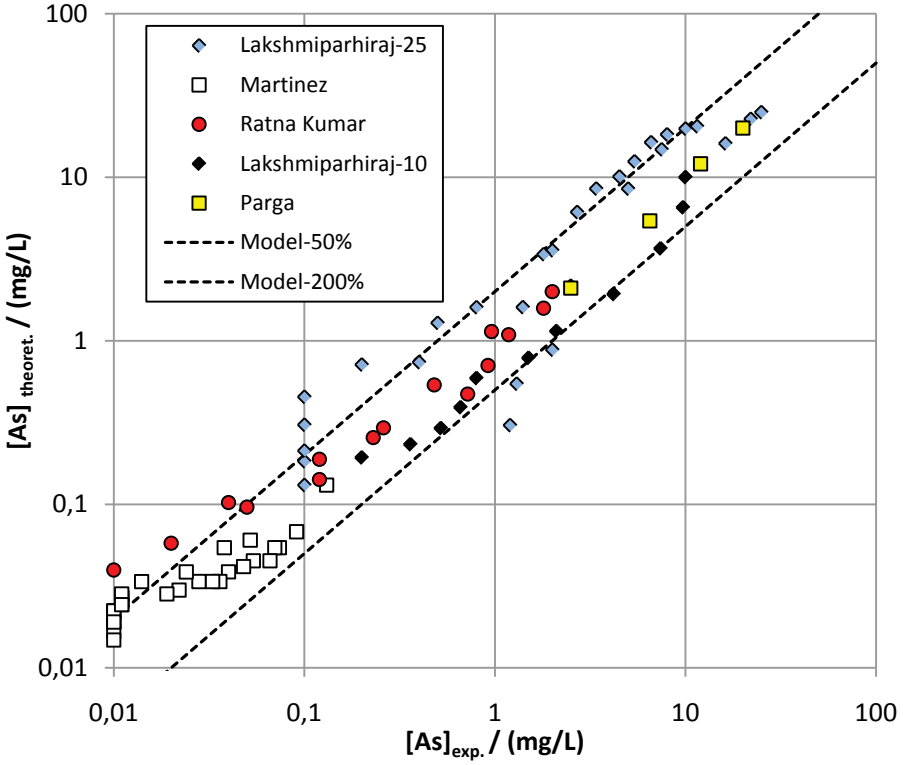

Figure 2. *Validation of the model for adsorption of As species onto Fe hydroxide (rel. 15): data issued from refs. [1], [4], [15] and [17] are related to treatment of synthetic As solutions or groundwater. The dotted lines correspond to 50% and 200% of the diagonal expressing perfect agreement between the model and experiments.*

The existing scattering of the data is probably due to the lack of accuracy in the estimation of coagulant concentration. Simulation tests actually showed that Fe(III) concentration had a noticeable impact on the predicted concentration of remaining As species. Besides, the value for n_2 could not be compared directly to the molar Fe/As ratio values reported in the literature and discussed by Hansen et al. [3], because the adsorption of As species, like other pollutants, obeys an adsorption isotherm law involving equilibrium between complexed and free species. Therefore, the parameter n_2 does not correspond to the Fe/As ratio, which is deduced by global assessment of As removal depending on the amount of Fe(III) generated.

Removal of As-containing industrial waste

Experimental observations

Numerous batch runs have been carried out with As concentrations up to 700 µg/L. In most cases, iron dissolution in the industrial waste was shown to be unaffected by the presence of the arsenic salt (Fig. 3). The concentration in Fe species in the liquid increased regularly with the electrical charge passed, although at a slower dissolution rate in the first minutes of the run. This corresponds to the increase in current yield mentioned in a previous section with the raw industrial waste. In addition, the concentration of arsenic salt decreased with time. As for the COD and other features of the wastewater under treatment, the abatement of the toxic As-additives is governed by the amount of Fe dissolved (Fig. 4). Nevertheless, removal of As(V) species is nearly complete with 150 mg/L Fe dissolved, whereas the removal of the organic matter requires more significant dissolution (Fig. 1).

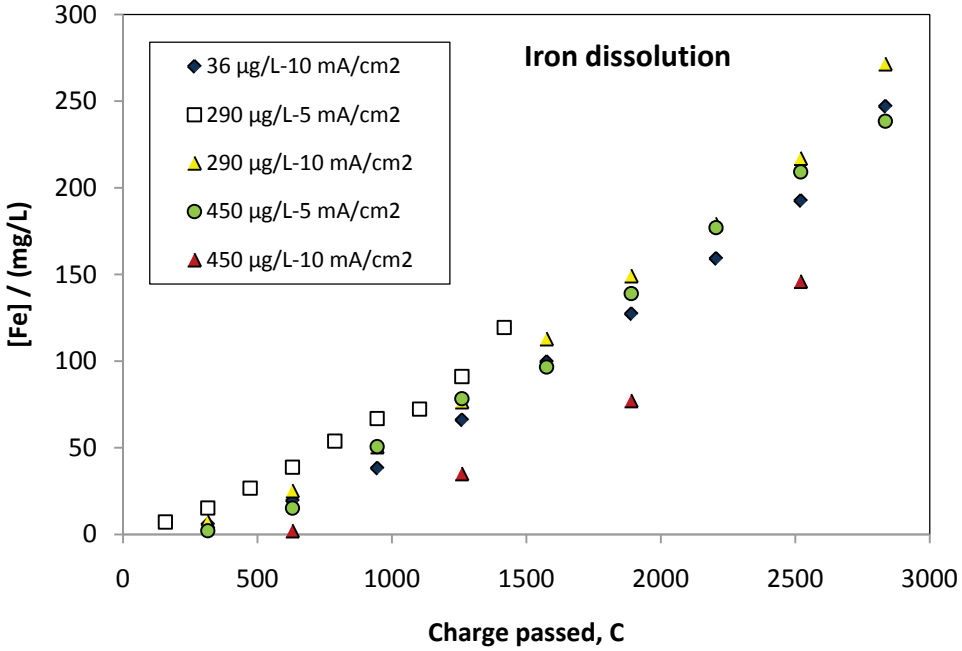

Figure 3. *Anode iron dissolution in the treatment runs for various concentrations of As in the enriched paper mill wastewater.*

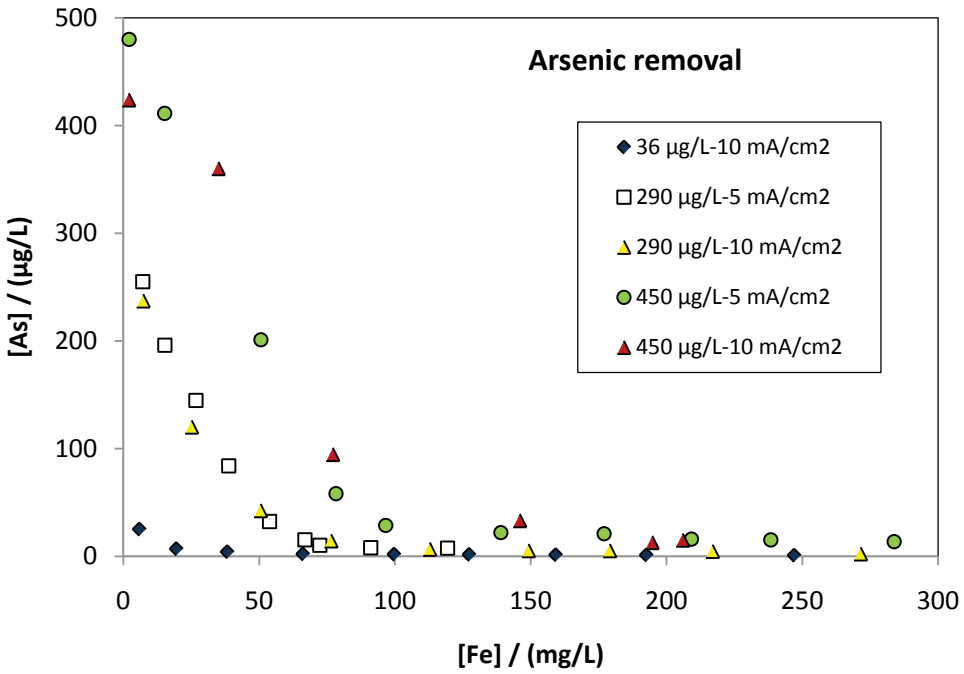

Figure 4. *Typical variations of As species concentrations with the amount of dissolved iron in treatment runs of the As-enriched paper mill wastewater depending of operating conditions.*

Modeling of As-removal from the industrial waste

Treatment of As-containing wastewaters was modeled assuming that the generated coagulant acts independently on the organic matter and As(V) species. S adsorbs on Fe(III) hydroxide according to parameters (K_1, n_1), whereas As(V) adsorbs on the solid coagulant with parameters (K_2, n_2). The model was, therefore, developed on the basis of equilibrium (2) and (8) with constants K_1 and K_2. Mass balances were written for the pollutant charge expressed by S, as well as for As(V) and Fe(III). The two first balances are given in equations (4) and (11), respectively, whereas the conservation of Fe species is written as:

$$[Fe]t = [Fe] + [FeS] + [FeAs] \quad (16)$$

Taking into account the expressions of constants K_1 and K_2, the three mass balances lead to the equation:

$$[Fe]_t = [Fe] + \frac{K_1\left([S]_0 - [S]_f\right)[Fe]}{1 + \frac{K_1}{n_1}[Fe]} + \frac{K_2[As]_0[Fe]}{1 + \frac{K_2}{n_2}[Fe]} \quad (17)$$

from which the concentration of free Fe(III) hydroxide, [Fe], can be obtained by numerical solution. The variation of concentration of arsenic species in time is deduced straightforwardly from [Fe] using:

$$[As] = \frac{n_2[As]_0}{n_2 + K_2[Fe]} \quad (18)$$

whereas the COD level is calculated according to:

$$[S] = [S]_f + \frac{n_1\left([S]_0 - [S]_f\right)}{n_1 + K_1[Fe]} \quad (19)$$

The model required the values for parameters K_1, K_2, n_1, and n_2. The above model, assuming no interactions between the abatement of COD and As species, was applied to the set of data. Fig. 5 establishes the acceptable validity of the model for As concentrations ranging from 0.3 µg/L to 700 µg/L.

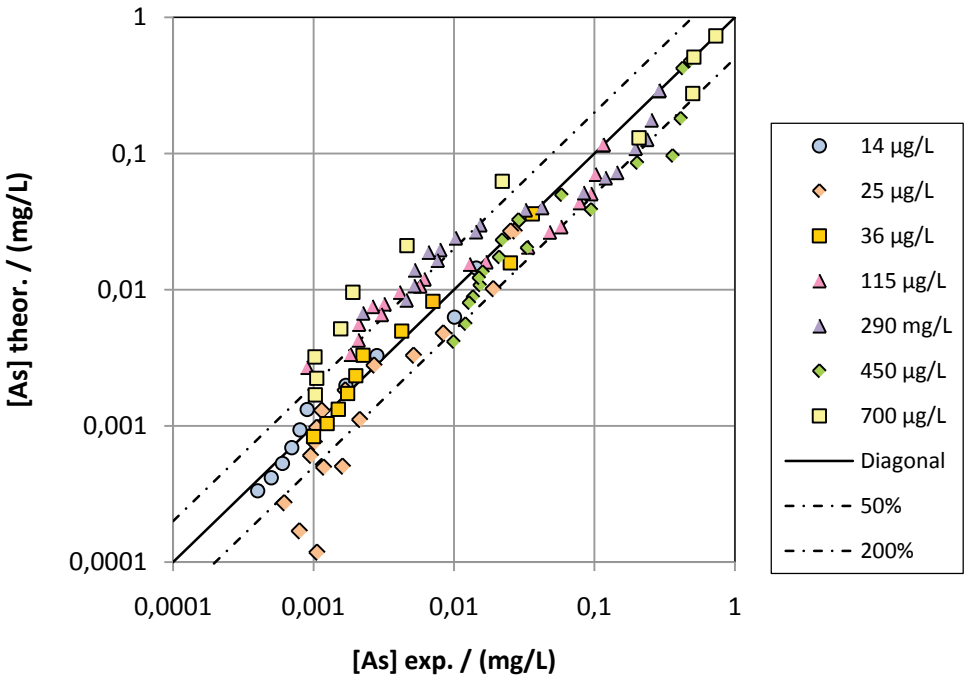

***Figure 5**. Validation of the model for As removal from As-enriched paper mill wastewater (rel. 12 and 13).*

Most predicted values for the concentration lie between 50 and 200% of the experimental value. Taking into account the uncertainty in the experiments, in particular in the chemical analysis of As in quite a large range of concentration and the existing uncertainty in the values for the parameters n_2 and K_2, the approach can be considered as successful. Therefore, for the sample of

industrial waste considered, the highly toxic salt added seems to be removed from the wastewater independently of the organic matter contained in the waste. In addition, the simple equations developed here are sufficient to model the waste treatment. Comparison of the experimental and predicted COD levels was not carried out since COD abatement was only slightly affected by the presence of As species, which was added in concentrations of nearly two orders below the COD level.

Conclusions

Arsenic species can be successfully removed from industrial waste by electrocoagulation using Fe electrodes. As(V) ions adsorb on Fe hydroxide in accordance with Langmuir-like adsorption isotherm. The parameters of the adsorption equilibrium could be estimated from previously published data dealing with the treatment of waters with low COD levels. This equilibrium could be incorporated into a more general model for the abatement of both As and COD, assuming no interaction in the treatment of the two pollution sources. In the example of industrial waste issued by a paper mill industry, the model was shown to hold, allowing a fairly accurate prediction of the As species. However, the approach may not be successful for industrial wastewaters containing oxidizing or reductive agents, which could change the chemical state of the arsenic salt and then affect its adsorption onto the Fe hydroxide particles. Whatever the model, a thorough characterization of the waste to be treated is required prior to designing the electrocoagulation process. For such reactive wastes, further characterization of their chemical behavior seems to be absolutely necessary.

***Acknowledgements**: The authors are indebted to S. Pontvianne for his thorough assistance in chemical analysis of the fractions collected.*

References

[1] J.R. Parga, D.L. Cocke, J.L. Valenzuela, J.A. Gomes, M. Kesmez, G. Irwin, H. Moreno, M. Weir, *J. Hazard. Mater.* **124** (2005) 247-254.
[2] M. Leist, R.J. Casey, D. Caridi, *J. Hazard. Mater.* **76** (2000) 125-138.
[3] H.K. Hansen, P. Nunez, D. Raboy, I. Schippacasse, R. Grandon, *Electrochim*. *Acta* **52** (2007) 3464-3470.
[4] P. Ranta Kumar, S. Chaudhari, K.C. Khilar, S.P. Mahajan, *Chemosphere* **55** (2004) 1245-1252.
[5] J.A.G. Gomes, P. Daida, M. Kesmez, M. Weir, H. Moreno, J.R. Parga, G. Irwin, H. McWhinney, T. Grady, E. Peterson, D.L. Cocke, *J. Hazard. Mater.* **139** (2007) 220-231.
[6] G. Dodbiba, T. Nukaya, Y. Kamioka, Y. Tanimura, T. Fujita, *Resour. Conserv. Recy.* **53** (2009) 688-697.
[7] P. Canizares, F. Martinez, C. Jimenez, C. Saez, M.A. Rodrigo, *J. Hazard. Mater.* **151** (2008) 44-51.
[8] B. Merzouk, B. Gourich, A. Sekki, J.K. Madani, M. Chibane, *J. Hazard. Mat.* **164** (2009) 215-222
[9] I. Zongo, J.P. Leclerc, H.A. Maiga, J. Wethe, F. Lapicque, *Sep. Purif. Technol.* **66** (2009) 159-166.
[10] S. Zodi, J.N. Louvet, C. Michon, O. Potier, M.N. Pons, F. Lapicque, J.P. Leclerc, accepted in *Chem. Eng. Proc. Proc. Intens.*
[11] M. Khemis, J.P. Leclerc, G. Tanguy, G. Valentin, F. Lapicque, *Chem. Eng. Sci*. **61** (2006) 3602-3609.
[12] I. Zongo, A.H. Maiga, J. Wéthé, G. Valentin, J-P. Leclerc, G. Paternotte, F. Lapicque *J. Hazard. Mater.* **169** (2009) 70-76.
[13] R.B. Heslop and P.L. Robinson, *Inorganic Chemistry*, Elsevier, Amsterdam (1967).

[14] R.C. Weast, *Handbook of Chemistry and Physics*, 76th Edition CRC Press, Boca Raton (2005-2006).
[15] J.F. Martinez-Villafane, C. Montero-Ocampo, A.M. Garcia Lara, *J. Hazard. Mater*. **B172** (2009) 1617-1622.
[16] A. Maldonado-Reyes, C. Montero-Ocampo, O. Solorio-Feria, *J. Environ. Monit.* **9** (2007) 1241-1247.
[17] P. Lakshmipathiraj, S. Prabhakar, G.B. Raju, *Sep. Purif. Technol.* **73** (2010) 114-121

J. Electrochem. Sci. Eng. **1(1)** (2011) 67-73; doi: **10.5599/jese.2011.0001**

Open Access : : ISSN 1847-9286
www.jESE-online.org

Original scientific paper

Preparation of mesoporous carbon/polypyrrole composite materials and their supercapacitive properties

WU-JUN ZOU, SHAN-SHAN MO, SHUANG-LI ZHOU, TIAN-XIANG ZHOU, NAN-NAN XIA and DING-SHENG YUAN✉

Department of Chemistry, Jinan University, Guangzhou 510632, China

✉Corresponding Author: E-mail: tydsh@jnu.edu.cn; Tel.: +86-20-85220597; fax: +86-20-85221697

Received: March 18, 2011; Revised: May 19, 2011; Published: August 20, 2011

Abstract

We synthesized mesoporous carbons/polypyrrole composites, using a chemical oxidative polymerization and calcium carbonate as a sacrificial template. N_2 adsorption-desorption method, Fourier infrared spectroscopy, and transmission electron microscopy were used to characterize the structure and morphology of the composites. The measurement results indicated that as-synthesized carbon with the disordered mesoporous structure and a pore size of approximately 5 nm was uniformly coated by polypyrrole. The electrochemical behavior of the resulting composite was examined by cyclic voltammetry and cycle life measurements, and the obtained results showed that the specific capacitance of the resulting composite electrode was as high as 313 F g^{-1}, nearly twice the capacitance of pure mesoporous carbon electrode (163 F g^{-1}). This reveals that the electrochemical performance of these materials is governed by a combination of the electric double layer capacitance of mesoporous carbon and pseudocapacitance of polypyrrole.

Keywords

Mesoporous carbon/polypyrrole composites; Chemical oxidation; Calcium carbonate; Sacrificial template; Specific capacitance; Pseudocapacitance

Introduction

Mesoporous carbon (MC) is one of the most important carbon materials with high surface area, uniform pore size, and good electric conductivity. During the past ten years, many efforts have been made to develop simple and efficient methods for the preparation of MC materials and to improve their properties for various applications. Recently, one-step soft template methods for MC preparation have gradually replaced time-consuming and tedious two-step hard mesoporous

silica templates, such as SBA-15, MCM-41, and MCM-48 [1,2]. The MCs and their composites are broadly applied to electrochemical capacitors [1,3], catalyst supports [4] and adsorbents [5,6], and magnetic separation [7]. Compared with mesopourous carbon materials, conducting polymers (CPs) possess pseudocapacitance, which is almost 10-100 times higher than the capacitance of electrochemical double-layer capacitors (EDLCs) [8]. Polypyrrole (PPy), one of CPs, has drawn a lot of attention for supercapacitor applications [9,10], mainly due to its oxidation-reduction properties, high conductivity in doped state, high specific capacitance, good environmental stability, and especially facile synthesis [11]. However, the shortcomings of CPs, such as low surface area and constrained power-output properties [12], markedly restrict their application to electrochemical capacitors. Hence, the most effective way is to use MC materials to improve the property of the CPs electrode. A new class of composite materials has originated from the combination of MCs and CPs [13]. Choi et al. introduced a conducting polymer layer into the pore surface of mesoporous carbon via vapor infiltration of a monomer and, by subsequent chemical oxidative polymerization, obtained mesoporous carbon-polypyrrole composites [14]. The maximum specific capacitance of these composites is 274.5 F g^{-1}. Pacheco-Catalán et al. synthesized mesoporous carbon/conducting polymer composites by adsorption of different monomers (aniline, pyrrole, thiophene, and 3-methyltiophene) in the gas phase onto the carbon surface, followed by oxidative chemical polymerization [15]. The electrochemical performance of carbon/polypyrrole composites electrode showed that it had a low specific capacitance (maximum value: 83.8 F g^{-1}) and stable cycle life in the potential range of 0 to 1V. However, all those materials showed low specific capacitance. Recently, we prepared mesoporous carbon by one-step method [16]. The obtained results revealed that MCs display good capacitive behavior with high reversibility and reproducibility due to their unique large mesopore size, which is favorable for fast ionic transport. However, the specific capacitance of MCs reaches only 163 F g^{-1}, which limits their application to electric vehicles and high power electronic devices. In this study, we used PPy growth on the surface of MC via simple chemical oxidative polymerization with calcium carbonate as the sacrificial template to improve the capacitance of carbon materials. The resulting composite material combined double layer capacitance of MC with pseudocapacitance of PPy.

Experimental

Chemicals

Pyrrole monomer (98%, Aldrich Chemical Co.) was distilled under reduced pressure, transferred into a refrigerator, and stored under nitrogen until further use. The diameter of nanoscale calcium carbonate was 80 nm and the BET surface area was 25 m^3 g^{-1}. Sodium 4-methyl benzene sulfonate (TsONa) was purchased from Sinopharm Chemical Reagent Co. Ltd, Shanghai, China. The other starting materials in this work were of analytical grade.

Synthesis of mesoporous carbons/polypyrrole composites

MCs were synthesized from F127/silica/butanol according to the procedure described previously [16]. Typically, 2 cm^3 sulfuric acid (98 wt%) and 9.3 cm^3 butanol (BuOH) were directly added into a clear solution containing 2.5 g F127 and 120 g deionized water at 318 K. After stirring for 1.5 h, 5 cm^3 tetraethyl orthosilicate (TEOS) was added, vigorously stirred at 318 K for 24 h, and aged at 373 K for 24 h. The F127/silica/butanol composites were collected by filtration and dried at room temperature for 12 h and at 433 K for 6 h. Finally, the obtained composites were transferred into a tube furnace and carbonized under pure N_2 atmosphere at 1123 K for 2 h, followed by the treatment with diluted HF solution. The chemical oxidative polymerization of pyrrole was performed using a modified procedure reported previously [17]. First, 0.3 g TsONa, 0.5 g $CaCO_3$, 25 g $CaCl_2$, 20 cm^3 C_2H_5OH, and 0.5 g Silica/Carbon were mixed into 40 cm^3 deionized water with magnetic stirring under N_2 atmosphere for 30 min; the nanoscale $CaCO_3$ served as a

core, and TsONa was used as anionic surfactant. Then 0.3 cm^3 pyrrole was added by a syringe. After 10 min, 40 cm^3 of 0.02 mol dm^{-3} $FeCl_3$ solution was slowly added as oxidant into the reaction vessel. The polymerization was carried out for 12 h in an ice-bath with magnetic stirring and maintained under N_2 atmosphere. The mesoporous carbon/polypyrrole composite was filtered and rinsed several times with distilled water and ethanol to remove retained pyrrole monomer and oxidant. The as-synthesized powder was transferred into HCl solution for $CaCO_3$ removal for 24 h. The mixture was filtered and rinsed several times again with distilled water. Then the silica/carbon/PPy composite was treated by diluted HF solution to remove the silica and dried in vacuum at 333 K for 12 h. The product was denoted as MP, containing an approximate MC:PPy weight ratio of 6:4. Under the influence of the Lewis acid $FeCl_3$ and inhibition by abundant $CaCl_2$, $CaCO_3$ was dissolved, slowly releasing CO_2, which contributed to the holes formation in the composite during the overflow process. Actually, $CaCO_3$ as a core was the sacrificial template.

Characterization

The morphologies of MC and as-synthesized composite were examined using a high-resolution transmission electron microscopy (TEM, JEOL JEM-2100, 200 kV). Nitrogen sorption isotherms of samples were measured by a Micromertics TriStar 3000 analyzer at 77 K. The FT-IR measurements on samples were performed using Nicolet 6700 FT-IR spectrometer. The electrochemical behavior of both MC and MP was investigated by cyclic voltammetry (CV) conducted on a CHI 660 B electrochemical workstation (ChenHua Instruments Co., Shanghai, China). The measurements were carried out in a standard three-electrode cell system. A Pt-foil modified by either MC or MP was used as the working electrode, saturated calomel electrode was used as the reference electrode, and a Pt-foil as the auxiliary electrode. The working electrodes were prepared by mixing active materials (8 mg), acetylene black as a conductive reagent, and 5%-Nafion as a binder (80:10:10 wt %) and dispersed in absolute ethanol in ultrasonic bath. The dispersion was coated onto Pt foil drop by drop and then dried at 353 K. The CV experiments were carried out in aqueous solution of 1 mol dm^{-3} H_2SO_4.

Results and Discussion

Fig. 1a and 1b show the N_2 adsorption-desorption isotherms and BJH pore size distribution of MC and MP. The two samples are found to yield a type IV isotherm with a type H2 hysteresis loop near relative pressure of 0.50 in the desorption branch, which is associated with sharp capillary condensation taking place in mesopores [18].

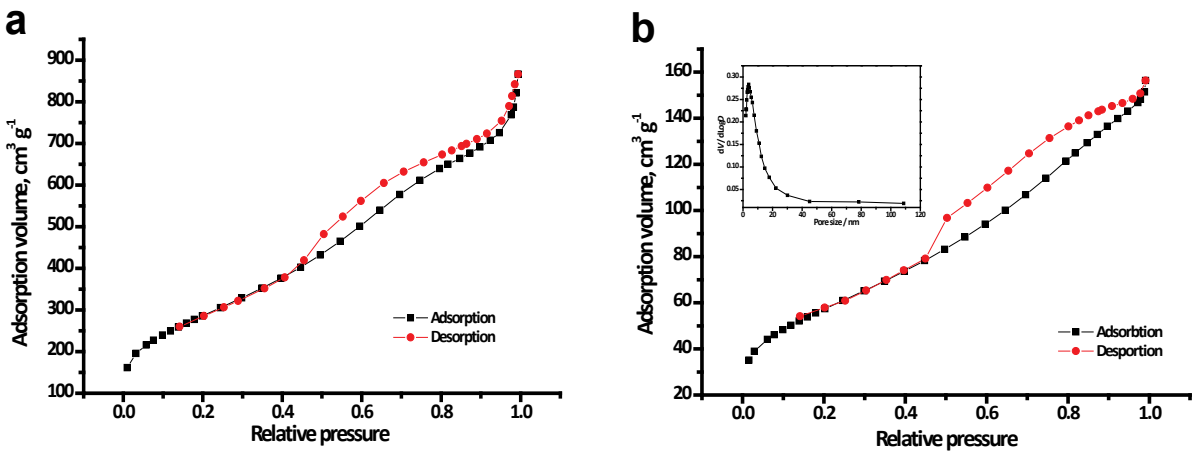

Figure 1. *Nitrogen adsorption-desorption isotherms and BJH pore size distribution (inset) of* ***a)*** *MC and* ***b)*** *MP.*

The results show that the mesoporous structure of MC was maintained after loading of PPy. However, BET surface area of MP was considerably lower. The specific surface areas of mesoporous carbon and MP were 1041 and 207 $m^2\ g^{-1}$, respectively (Table 1). The decrease of specific surface area is mainly attributed to the mesopores of the support being partially covered or filled by PPy. Therefore, pore volume and average pore size also decrease from 1.18 $cm^3\ g^{-1}$ and 5.2 nm to 0.22 $cm^3\ g^{-1}$ and 4.9 nm, respectively. This indicates that PPy was distributed evenly over the surface of MC.

In order to gain further insights into the structure of mesporous carbons, we investigated their appearance on the synthesized materials by TEM (Fig. 2). The disordered mesoporous size of MC with around 5 nm, which is clearly visible in Fig. 2a, is in agreement with the data of the adsorption-desorption measurements (Fig. 1). Fig. 2b clearly shows the mesoporous structure of MC covered over with transparent films. In comparison with Fig. 2a, we may draw a conclusion that the transparent film is PPy and that it has been successfully loaded on the MC.

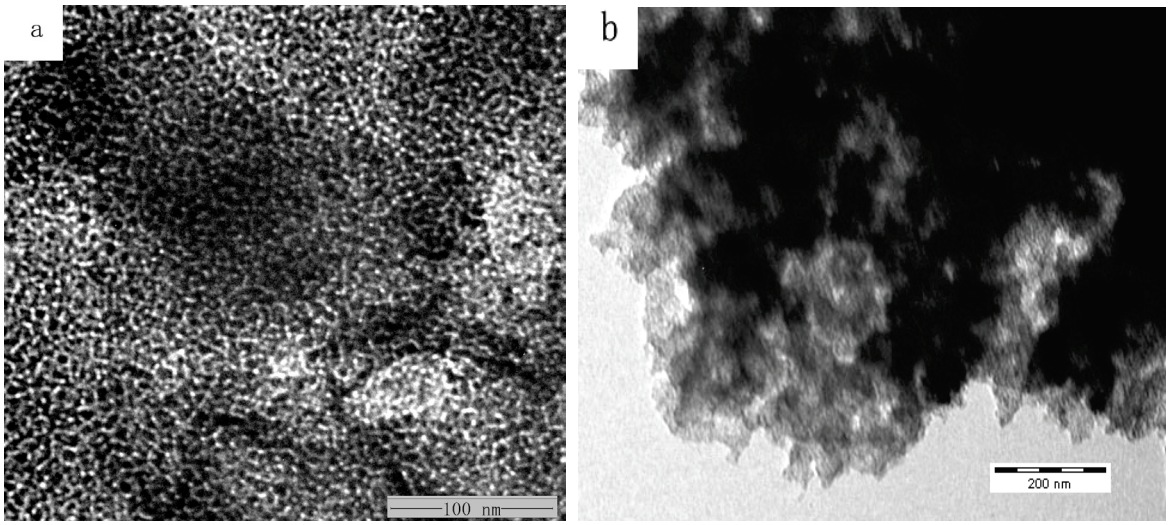

Figure 2. *TEM images of* ***a)*** *MC and* ***b)*** *MP.*

The functional groups of MC, PPy, and MP are characterized by FTIR spectroscopy (Fig. 3). The characteristic peak at 3423 cm^{-1} is observed in the IR spectrum of MC and ascribed to –OH. The small peaks at 2920 and 2850 cm^{-1} originate from the stretching vibrations of C–H bond. The peaks at 1731, 1632, and 1402 cm^{-1} could be assigned to the stretching vibration in carboxyl groups and C=O, C=C, and C–O bonds. The bands at 1537 and 1452 cm^{-1} in PPy and MP spectra are due to the typical pyrrole ring vibration of pure PPy and bands of =C–H in plane vibration at 1298, 1089, and 1032 cm^{-1} [19]. The peaks at 3434 and 1631 cm^{-1} correspond to N–H and C=C stretching vibrations, respectively. The spectrum of MP is very similar to that of PPy, verifying that PPy has been successfully applied onto MC. However, the peak at 1632 cm^{-1} for C=O disappeared due to the combination of MC and PPy. Similarly, the peak for N-H stretching exhibits a red-shift phenomenon due to the interaction with the reactive hydroxyl functional groups [20].

Fig. 4 shows CVs of MC and MP in 1 mol dm^{-3} H_2SO_4 at different scan rates. CVs of MC electrode contain redox peaks and deviate from the rectangular shape (Fig. 4a). With increasing scan rates, the redox current evidently increases, indicating that it has good rate capability. FTIR spectra confirm the existence of the abundant functional groups, for example C=O and O-H bonds, on the surface of MC. These groups are supposed to remarkably improve the hydrophilicity and wettability of the surface of MC and are beneficial for the aqueous electrochemical capacitors. The redox peaks might originate from the transformation of the O–H bond of MC into the C=O and *vice versa* during charge and discharge processes. In addition, the C=O bond of MC interacts with the H^+ to become –OH in the reduced state, which would be re-oxidized into C=O during the discharge.

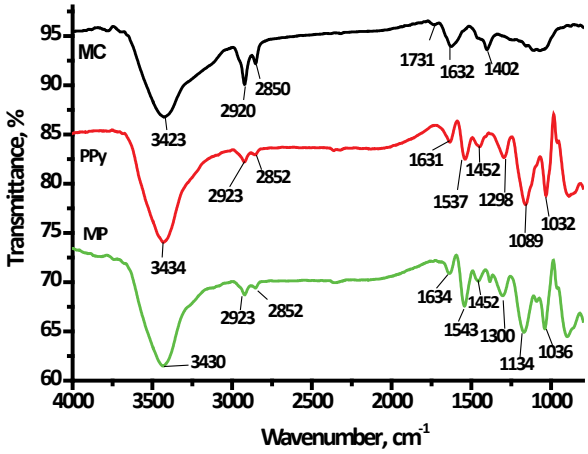

Figure 3. *FT-IR spectra of MC, PPy and MP.*

However, the CVs of MP present a steep increase in the current range from 0.0 to 0.1 V, which is an important behavior in supercapacitors [14], as shown in Fig. 4b. CV curves of the composites do not exhibit redox peaks as pronouncedly as in the case of MC. This is because the π-bonded surface of the MC may interact strongly with the conjugated structure of PPy, especially through the pyrrole ring [21], or N-H of PPy can interact with the reactive hydroxyl functional groups of MC [20].

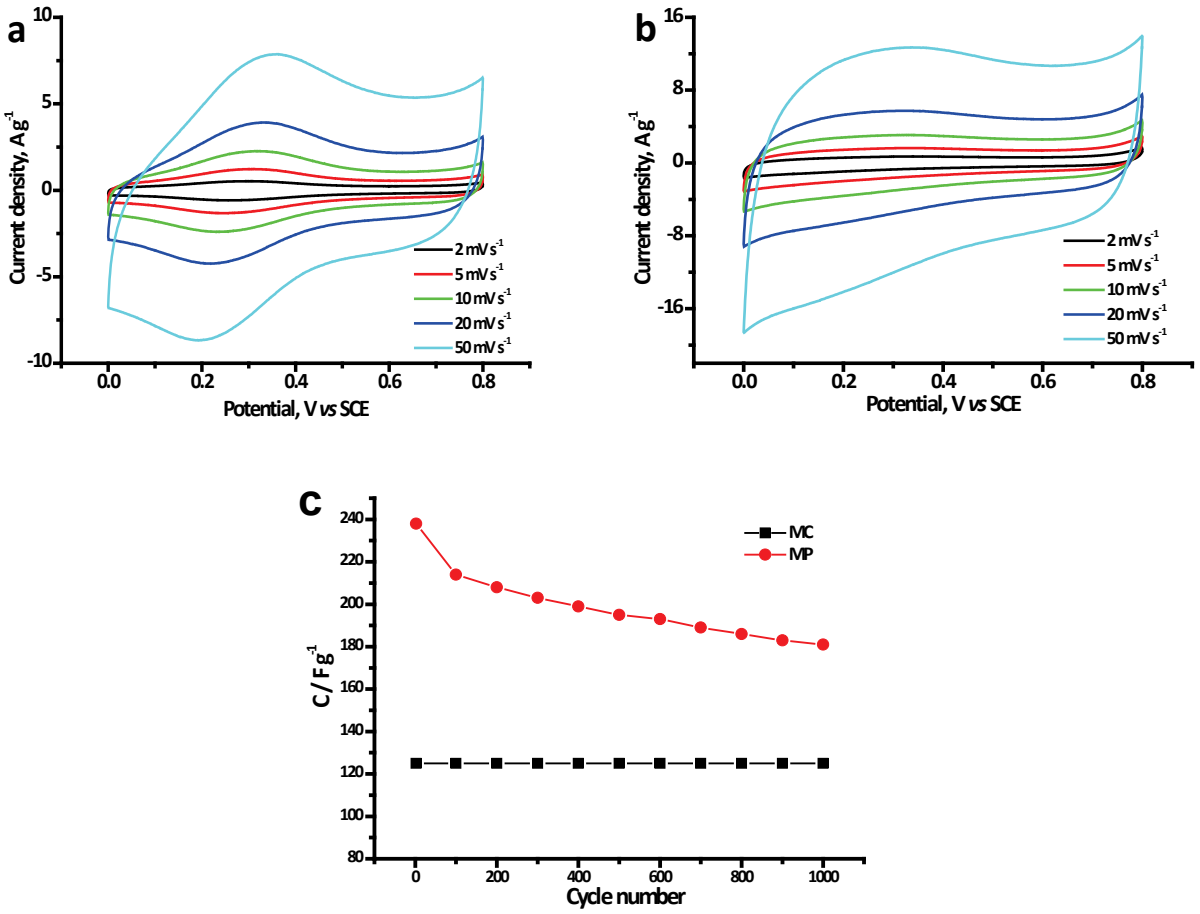

Figure 4. *CVs of* ***a)*** *MC and* ***b)*** *MP in 1 mol dm^{-3} H_2SO_4 electrolyte at different scan rates;* ***c)*** *cycle life of MC and MP in 1 mol dm^{-3} H_2SO_4 electrolyte at the scan rate of 20 mV s^{-1}.*

The gravimetric specific capacitance (*C*) of electrode is calculated according to the Eq. (1) from charge-discharge data of CVs:

$$C = \frac{Q}{WV} = \frac{\int i dt}{W \Delta V} \quad (1)$$

where *i*, *W* and *V* are the voltammetric current, the mass of active materials, and the total potential of electrochemical window, respectively. The calculated specific capacitances are listed in Table 1. The maximum specific capacitance of MP reaches as high as 313 F g^{-1} at the scan rate of 2 mV s^{-1}, which is nearly twice the specific capacitance of MC (163 F g^{-1}). Although the surface area of MC dramatically decreases due to the coverage of PPy, leading to the EDLC loss, the pseudocapacitance from the Faradic reaction on the PPy contributes much more to the total capacitance, leading to a higher specific capacitance of MP. Due to the different synthesis methods and electrolytes and measured potential windows, it is difficult to compare our results with those reported in the literatures. Therefore, for comparison purpose, we synthesized the PPy using the same method and measured the electrochemical properties in 1 mol dm^{-3} H_2SO_4. The specific capacitance of pure PPy was 328.4 F g^{-1} at a scan rate of 2mV s^{-1}. If the contribution of pure MC and pure PPy were calculated, the total was only 229 F g^{-1}. However, in this study, we obtained a higher result that reached 313 F g^{-1}, revealing the intensely synergetic effect between MC and PPy. Fig. 4c shows a cycle life of MC and MP in 1 mol dm^{-3} H_2SO_4 electrolyte at scan rate of 20 mV s^{-1}. The specific capacitance of MP drops from 238 F g^{-1} down to 181 F g^{-1} after 1000 cycles, corresponding to a 23.9% loss.

Table 1. *Pore structure parameters of the MC and MP and the specific capacitances of MC and MP electrodes calculated from CVs in 1 mol dm^{-3} H_2SO_4 electrolyte*

Sample	Surface area $m^2 g^{-1}$	Pore volume $cm^3 g^{-1}$	Pore size nm	*C* / F g^{-1}				
				2 mV s^{-1}	5 mV s^{-1}	10 mV s^{-1}	20 mV s^{-1}	50 mV s^{-1}
MC	1041	1.18	5.2	163	150	139	125	103
MP	207	0.22	4.9	313	281	261	238	203

Conclusions

MC/PPy composites were successfully synthesized using a chemical method of oxidative polymerization. The resulting modified electrode showed some properties similar to the combination of the double layer capacitance of MC and pseudocapacitance of PPy. The results obtained by cyclic voltammetry demonstrated that the specific capacitance of the MP electrode was as high as 313 F g^{-1} compared to 163 F g^{-1} of MC electrode. In conclusion, it seems that the MP is a promising electrode material in supercapacitor field.

Acknowledgements*: The study was financially supported by the National Natural Science Foundation of China (20876067 and 21031001) and the Fundamental Research Funds for the Central Universities (21609203).*

References

[1] J. Lee, S. Yoon, T. Hyeon, S.M. Oh and K.B. Kim, *Chem. Commun.* **21** (1999) 2177-2178
[2] K.T. Lee, X.L. Ji, M. Rault and L.F. Nazar, *Angew. Chem. Int. Ed.* **121** (2009) 5661-5665
[3] J.X. Chen, N.N. Xia, T.X. Zhou, S.X. Tan, F.P. Jiang and D.S. Yuan, *Int. J. Electrochem. Sci.* **4** (2009) 1063-1073
[4] S.H. Joo, S.J. Choi, I. Oh, J. Kwak, Z. Liu, O. Terasaki and R. Ryoo, *Nature* **412** (2001) 169-172
[5] A. Vinu, C. Streb, V. Murugesan and M. Hartmann, *J. Phys. Chem. B* **107** (2003) 8297-8299

[6] X.W. Liu, L. Zhou, J.W. Li, Y. Sun, W. Su and Y.P. Zhou, *Carbon* **44** (2006) 1386-1392
[7] J.W. Lee, S.M. Jin, Y.S. Hwang, J.G. Park, H.M. Park and T. Hyeon, *Carbon* **43** (2005) 2536-2543
[8] C. Peng, S.W. Zhang, D. Jewell and G.Z. Chen, *Prog. Nat. Sci.* **18** (2008) 777-788
[9] X.Q. Lin and Y.H. Xu, *Electrochim. Acta* **53** (2008) 4990-4997
[10] S.W. Woo, K. Dokko and K. Kanamura, *J. Power Sources* **185** (2008) 1589-1593
[11] J. Wang, Y.L. Xu, X. Chen and X.F. Sun, *Compos. Sci. Technol.* **67** (2007) 2981-2985
[12] W. Xing, X. Yuan, S.P. Zhuo and C.C. Huang, *Polym. Adv. Technol* .**20** (2009) 1179-1182
[13] W. Xing, S. P. Zhuo, H.Y. Cui and Z.F. Yan, *Mater. Letters* **61** (2007) 4627-4630
[14] M. Choi, B. Lim and J. Jang, *Macromol. Res.* **16** (2008) 200-203
[15] D.E. Pacheco-Catalán, M.A. Smit, E. Morales, *Int. J. Electrochem. Sci.* **6** (2011) 78-90
[16] X. Yan, H.H. Song and X.H. Chen, *J. Mater. Chem.* **19** (2009) 4491-4494
[17] F.P. Jiang, T.X. Zhou, S.X. Tan, Y. Zhu, Y.L. Liu and D.S. Yuan, *Int. J. Electrochem. Sci.* **4** (2009) 1541-1547
[18] K. S. W Sing, D. H. Everett, R. A. W. Haul, L. Moscou, R. A. Pierotti, J. Rouqoerol and T. Simieniewska, *Pure Appl. Chem.* **57** (1985) 603
[19] W. Chen, X.W. Li, G.Xue, Z.Q. Wang and W.Q. Zou, *Appl. Surf. Sci.* **218** (2003) 215-221
[20] L. Ding, C. Hao, X.J. Zhang and H.X. Ju, *Electrochem. Commun.* **11** (2009) 760-763
[21] Y.C. Zhao, X.L. Yang, J.N. Tian, F.Y. Wang and L. Zhan, *J. Power Sources* **195** (2010) 4634-4640